AFRL-SR-AR-TR-04-

0095

# REPORT DOCUMENTATION PAGE



| 1. AGENCY USE ONLY (Leave blank) | 2. REPORT DATE | 3. REPORT TYPE AND DATES COVERED |
|---|---|---|
| | 1 February 2004 | Final Report, 1 Jan 2001-31 Dec 2003 |

**4. TITLE AND SUBTITLE**
Structure Based Turbulence Modeling

**5. FUNDING NUMBERS**
AFOSR Grant F49620-01-1-0173

**6. AUTHOR(S)**
William C. Reynolds
Stavros Kassinos
Carlos A. Langer

**7. PERFORMING ORGANIZATION NAME(S) AND ADDRESS(ES)**
Stanford University
Department of Mechanical Engineering
Building 500
Stanford, CA 94305-3030

**8. PERFORMING ORGANIZATION REPORT NUMBER**
TF-85

**9. SPONSORING / MONITORING AGENCY NAME(S) AND ADDRESS(ES)**
Air Force Office of Scientific Research
AFOSR/NA
4015 Wilson Blvd., Rm 713
Arlington, VA 22203

**10. SPONSORING / MONITORING AGENCY REPORT NUMBER**

**11. SUPPLEMENTARY NOTES**

**12a. DISTRIBUTION / AVAILABILITY STATEMENT**
Unlimited

20040224 069

DISTRIBUTION STATEMENT A
Approved for Public Release
Distribution Unlimited

**13. ABSTRACT** ***(Maximum 200 Words)***
The Reynolds stresses alone are not sufficient to characterize complex turbulent flows adequately. Complementary information, contained in the structure dimensionality tensor, must also be included in one-point turbulence models. This work uses hypothetical turbulent eddies to bring awareness of turbulence structure into the turbulence model. Averaging over a large ensemble of eddies produces a set of one-point statistics, representative of the eddy field, and a set of equations of state relating the Reynolds stresses and the structure dimensionality to the eddy statistics. An algebraic model for the eddy statistics is constructed in terms of the local mean deformation and two turbulent scales; the turbulent kinetic energy and the large-scale enstrophy. The algebraic model is further sensitized to the presence of walls by a blocking scheme, which ensures proper asymptotic behavior for the Reynolds stresses in the vicinity of walls. Contrary to existing *ad-hoc* definitions of a second scale equation, the large-scale enstrophy equation has a fundamental background; it is derived from the large-scale vorticity equation. Its terms represent large-scale processes, and their exact form provides valuable guidance when making choices for their closure, and when matching their asymptotic behavior in the vicinity of walls. The algebraic model produces physically realistic Reynolds stresses and structure tensors for different combinations of mean strain and mean rotation, with and without frame rotation. The complete model, with evolution equations for the turbulent scales and algebraic equations for the turbulence structure, was successfully implemented. The full model was found to produce excellent results for a set of channel flows in fixed frames and in spanwise-rotating frames of reference.

| 14. SUBJECT TERMS | 15. NUMBER OF PAGES |
|---|---|
| Structure-based, algebraic two-equation model, large-scale enstrophy | 117 |
| | 16. PRICE CODE |

| 17. SECURITY CLASSIFICATION OF REPORT | 18. SECURITY CLASSIFICATION OF THIS PAGE | 19. SECURITY CLASSIFICATION OF ABSTRACT | 20. LIMITATION OF ABSTRACT |
|---|---|---|---|
| | | | |

# STRUCTURE-BASED TURBULENCE MODELING

## AFOSR grant F49620-01-1-0173

W. C. Reynolds and S. C. Kassinos
Department of Mechanical Engineering
Stanford University, California

## Executive Summary

### Overview

Turbulence modeling is a critical element of modern CFD codes for flow analysis. Models must be fairly simple and computationally affordable to be useful in repetitive engineering calculations, yet they must be sufficiently representative of the physics to capture the important flow features controlled by turbulence, such as flow separation, skin friction, and heat and mass transfer. There is particular need for improved models that are robust and accurate in rotating flows, which are important in aerospace propulsion systems. Advanced aerospace power and propulsion systems employing magnetohydrodynamics, and possible schemes for control of electrically conducting external flow on aerospace vehicles, also require turbulence models superior to those presently available. We have been developing a new, structure-based approach to turbulence modeling that seems well suited towards meeting these needs.

Under previous AFOSR support, a Structure-Based Model [1,2] was developed and shown to perform better than standard Reynolds Stress Transport models in many complex flows, such as flows with strong mean or frame rotation. Although the performance of the original SBM was considered quite satisfactory [3,4,5,6], it was deemed necessary to simplify the approach into an algebraic two-equation model for engineering use.

This final report describes the outcome of our work towards developing a new Algebraic Structure-Based model (ASBM) for engineering use that has been supported by AFSOR during the last three years.

### Stated Objectives

The stated objectives of this work program were the following:

- to complete the development of our two-equation algebraic structure-based turbulence model (ASBM) for complex engineering flows
- to evaluate the ASBM for canonical and complex flows using a wide range of experimental
- data and data from direct numerical simulations
- to incorporate the ASBM in a typical engineering CFD code and make it available for use in other CFD codes
- to extend our structure-based modeling ideas to MHD flows and other flows where structure information is essential for accurate flow predictions

### Work Team

The work was carried out by a team consisting of the Principal Investigator, Professor William C. Reynolds and Co-Investigator Dr. Stavros C. Kassinos. Drs. Scot Haire and Carlos Langer completed their PhD dissertations for work carried under this program.

### Results Obtained

As outlined in the attached technical report (Stanford TF-85) a new Algebraic Structure-Based Model (ASBM) has been developed. The ASBM has been evaluated in a wide range of canonical and complex flows using data from both experiments and direct numerical simulations. The ASBM has been found to produce excellent results for wall-bounded flows with strong rotation, a

class of flows with important engineering applications. The ASBM has been implemented in a simple in-house CFD code at Stanford, while at the writing of this report we have initiated implementation of the model in a major commercial CFD code. This implementation will enable the continued validation of the model for a wide range of complex flows and will facilitate its dissemination to the industry.

**Future Plans and Synergies**

At the writing of this final report, we have initiated a number of collaborations that aim at the wider dissemination and use of the results of this effort.

Under separate funding, one of us (Dr. Stavros Kassinos) has carried out a series of large-scale direct numerical simulations of homogeneous hydrodynamic and magnetohydrodynamic turbulence that is sheared in rotating frames [7]. Results from these simulations [8] have shown the importance of using the large-scale enstrophy equation as the second-scale equation in turbulence models used for the prediction of flows with strong frame rotation. These results generated interest in the astrophysical community in using structure-based modeling ideas in investigating a range of phenomena including accretion discs and the transport in solar convection zone [9]. We have also initiated a series of collaborations [10,11,12] that aim at the implementation of the structure-based model in codes used for the simulation of MHD turbulent flows and we hope to achieve dissemination of these ideas in that community as well. Finally, one of us (Dr. Stavros Kassinos) has initiated collaboration with Profs. John K. Eaton (Stanford University) and Damian Rouson (City College, New York) aiming at the development of structure-based models for the prediction of aerosol transport in turbulent atmospheres. Finally, Dr. Kassinos has established an ongoing collaboration with Dr. Datta Gaitonde at WPAFB aiming at the application of structure-based modeling ideas in the prediction of flow and heat transfer phenomena in advanced aerospace power and propulsion schemes employing magnetogasdynamics.

The remainder of this Final Report is in the form of a Technical Report prepared by the Department of Mechanical Engineering at Stanford University.

**Acknowledgment/Disclaimer**

This work was sponsored by the Air Force Office of Scientific Research under grant number F49620-01-1-0173. The views and conclusions contained herein are those of the authors and should not be interpreted as necessarily representing the official policies or endorsements, either expressed or implied, of the Air Force Office of Scientific Research or the U.S. Government.

**References**

1. S. C. Kassinos and W. C. Reynolds, A Structure-Based Model for the Rapid Distortion of Homogeneous Turbulence, Report TF-61, Mechanical Engineering Dept., Stanford University (1994).

2. W. C. Reynolds and S. C. Kassinos, One-point Modelling of Rapidly Deformed Homogeneous Turbulence, *Proc. R. Soc. Lond. A*, 451, pp. 87-104, (1995).

3. S. C. Kassinos, W. C. Reynolds and M. M. Rogers, One-Point Turbulence Tensors, *J. Fluid Mech.*, **428,** pp. 213-248, 2001.

4. S. C. Kassinos and W. C. Reynolds, Structure-Based Modeling for Homogeneous MHD Turbulence. *Annual Research Briefs 1999*, CTR, NASA Ames/Stanford, pp.301-315.

5. S. V. Poroseva, S. C. Kassinos, C. A. Langer and W. C. Reynolds, Simulation of Turbulent Flow in a Rotating Pipe Using the Structure-Based Model, In *Proc. of TSFP2*, vol. III, pp. 149-153, Stockholm, June 2001.

6. S. C. Kassinos, C. A. Langer, S. Haire, and W. C. Reynolds, "Structure-Based Modeling for Wall-Bounded Flows," *Int. J. Heat and Fluid Flow*, 21(5), 599-605, 2000.

7. S. C. Kassinos and W. C. Reynolds, "DNS and Structure-Based Modeling of Rotated Homogeneous Shear Flows," Proceedings of the *Third International Symposium on Turbulence and Shear Flow Phenomena*, Sendai, Japan, June 2003.

8. S. C. Kassinos, W. C. Reynolds, and C.A. Langer, "*The effect of the second turbulence scale equation on the prediction of rotated homogeneous shear flows,*" Bulletin of the American Physical Society, V-47, No. 10, p.29. (2002 Annual Meeting of the Division of Fluid Dynamics).

9. Mosqueira, I, Kassinos, S., Shariff, K., and Cuzzi, J. N., "Hydrodynamical Shear Instability in Accretion Disks?", *35th Annual Meeting of the Division for Planetary Sciences of the American Astrophysical Society,* Monterey California, USA, 1-6 September 2003.

10. B. Knaepen, S. Kassinos and D. Carati, "MHD Turbulence at Moderate Magnetic Reynolds Number," Submitted to *J. Fluid Mech.*, May 2003, under review.

11. J. Cho, A. Lazarian, A. Honein, B. Knaepen, S. Kassinos, and P. Moin, "Thermal Conduction in Magnetized Turbulent Gas," *The Astrophysical Journal*, **589,** L77-L80, June 1, 2003.

12. S. C. Kassinos, B. Knaepen, and D. Carati, "MHD Turbulence in the Presence of a Strong Magnetic Field," Proceeding of the 2002 Summer Program, Center for Turbulence Research, Stanford/NASA Ames Research Center, 2002.

**Personnel Supported**

| | |
|---|---|
| William C. Reynolds | Professor, Stanford University, California. |
| Stavros C. Kassinos | Research Associate, Stanford University, California. |
| Mr. Scot Haire | Graduate Student, Stanford University, California (PhD awarded). |
| Mr. Carlos Langer | Graduate Student, Stanford University, California (PhD awarded). |

# A NEW ALGEBRAIC STRUCTURE-BASED TURBULENCE MODEL FOR ROTATING WALL-BOUNDED FLOWS

By
Carlos A. Langer and William C. Reynolds

Prepared with support from the
Air Force Office of Scientific Research and the
National Council for Research and Development of Brazil

Report No. TF-85

Flow Physics and Computation Division
Department of Mechanical Engineering
Stanford University
Stanford, CA 94305-3030

December 2003

# Abstract

A primary goal of RANS based modeling is to determine the Reynolds stress tensor in order to close the turbulence problem at the mean velocity level. However, the Reynolds stresses alone are not sufficient to characterize complex turbulent flows adequately. More *independent* information on the turbulence is needed, especially in presence of rotation. For example, complementary information can be given by the one-point structure dimensionality tensor. It gives a measure of gradients in the turbulence — if the turbulence structures are preferentially aligned with one direction, then the dimensionality is smaller in that direction.

This work uses hypothetical turbulent eddies to bring awareness of turbulence structure into the turbulence model. Averaging over a large ensemble of eddies produces a set of one-point statistics, representative of the eddy field, and a set of equations of state relating the Reynolds stresses and the structure dimensionality to the eddy statistics. An algebraic model for the eddy statistics is constructed in terms of the local mean deformation and two turbulent scales; the turbulent kinetic energy and the large-scale enstrophy. The algebraic model is further sensitized to the presence of walls by a blocking scheme, which ensures proper asymptotic behavior for the Reynolds stresses in the vicinity of walls.

Contrary to existing *ad-hoc* definitions of a second scale equation, the large-scale enstrophy equation has a fundamental background; it is derived from the large-scale vorticity equation. Its terms represent large-scale processes, and their exact form provides valuable guidance when making choices for their closure. The exact forms also provide insight into making these model choices consistent with the asymptotic behavior of the exact terms in the vicinity of walls.

The algebraic model produces physically realistic Reynolds stresses and structure tensors for different combinations of mean strain and mean rotation, with and without frame rotation. The complete model, with evolution equations for the turbulent scales and algebraic equations for the turbulence structure, was successfully implemented. Although results for a channel in a streamwise rotating frame did overestimate stabilization, the full model was found to produce adequate results for a set of channel flows in fixed frames and in spanwise-rotating frames of reference.

# Acknowledgements

Financial support for this work was provided by the Air Force Office of Scientific Research, and by the National Council for Research and Development of Brazil (CNPq), the latter in the form of a scholarship for Carlos Langer.

The authors thank Professor Stavros Kassinos, Dr. Svetlana Poroseva, and Scot Haire for very helpful discussions and technical support on many aspects of this project. We also thank Professors Peter Bradshaw and Paul Durbin for their comments and suggestions on a draft of this report. We are grateful to Mrs. Deborah Michaels for her assistance with the production of the final document.

# Contents

# List of Tables

# List of Figures

# Nomenclature

## Acronyms

| | |
|---|---|
| ASBM | Algebraic Structure-Based Model |
| AXC | Axisymmetric Compression |
| AXE | Axisymmetric Expansion |
| DNS | Direct Numerical Simulation |
| PRM | Particle Representation Model |
| PS | Plane Strain |
| RDT | Rapid Distortion Theory |

## Universal Notations

| | |
|---|---|
| $\Upsilon$ | Any quantity or variable |
| $\overline{\Upsilon}$ | Ensemble average of $\Upsilon$ |
| $\Upsilon'$ | Turbulent fluctuation of $\Upsilon$ |
| $\tilde{\Upsilon}$ | Large-scale turbulent fluctuation of $\Upsilon$ |
| $\Upsilon''$ | Small-scale turbulent fluctuation of $\Upsilon$ |
| $\langle \Upsilon \vert \vec{a} \rangle$ | Ensemble average of $\Upsilon$ conditioned on vector quantity $\vec{a}$ |
| $\Upsilon_i$ | Denotes vector component $(i)$ |
| $\Upsilon_{ij}$ | Denotes tensor component $(i,j)$ |

## Roman Symbols

| | |
|---|---|
| $a_i$ | Normalized eddy-axis vector |
| $a_{ij}$ | Normalized eddy-axis tensor |
| $a^2$ | Second invariant of the normalized eddy-axis tensor |
| $a^s_{ij}$ | Normalized eddy-axis tensor resulting from mean strain only |
| $b_{ij}$ | Eddy-flattening tensor |
| $C_{ij}$ | Inhomogeneity tensor |

| | |
|---|---|
| $D_{ij}$ | Dimensionality tensor |
| $d_{ij}$ | Normalized dimensionality tensor |
| $F_{ij}$ | Circulicity tensor |
| $f_{ij}$ | Normalized circulicity tensor |
| $G_{ij}$ | Mean velocity gradient tensor |
| $H_{ij}$ | Eddy-axis rotational transformation tensor |
| $k$ | Turbulent kinetic energy |
| $l$ | Turbulent length scale |
| $l_h$ | Homogeneous turbulent length scale |
| $n_i$ | Normalized PRM gradient vector |
| $\mathcal{P}$ | Production of turbulent kinetic energy |
| $P_k$ | Production rate of turbulent kinetic energy |
| $q^2$ | Twice the turbulent kinetic energy, $R_{kk}$ |
| $R_{ij}$ | Componentality tensor, also Reynolds stress tensor |
| $r_{ij}$ | Normalized componentality tensor |
| $R_{ij}^{\vert\vec{a}}$ | $R_{ij}$ conditioned on vector $\vec{a}$ |
| $s_i$ | Normalized PRM stream function vector |
| $S_{ij}$ | Mean strain rate tensor |
| $S_{ij}^*$ | Anisotropic mean strain rate tensor |
| $\hat{S}^2$ | Invariant of eddy-axis tensor and mean strain rate tensor |
| $U_i$ | Mean velocity vector |
| $u_i$ | Instantaneous velocity vector |
| $U$ | Mean velocity component in $x_1$-direction |
| $u_i'$ | Fluctuating velocity vector |
| $v_i$ | Normalized PRM velocity vector |
| $V$ | Magnitude of PRM velocity vector |
| $v$ | Mean velocity component in $x_2$-direction |
| $x_i$ | Coordinate direction vector |

## Greek Symbols

| | |
|---|---|
| $\alpha$ | Turbulent diffusion coefficient |

| | |
|---|---|
| $\gamma_k$ | Eddy-helical vector |
| $\Gamma$ | Mean shear rate |
| $\delta_{ij}$ | Kronecker delta tensor |
| $\epsilon_{ijk}$ | Levi-Civita alternating tensor |
| $\varepsilon$ | Turbulent dissipation rate |
| $\eta_f$ | Eddy-axis-weighted ratio of frame rotation to mean strain |
| $\eta_m$ | Eddy-axis-weighted ratio of mean rotation to mean strain |
| $\tilde{\omega}^2$ | Large-scale turbulent enstrophy |
| $\nu_T$ | Turbulent eddy viscosity |
| $\tau$ | Turbulent time scale |
| $\phi$ | Eddy-jetal parameter |
| $\chi$ | Eddy-flattening scalar |
| $\Psi_i$ | Instantaneous vector stream function |
| $\psi_i$ | Mean vector stream function |
| $\psi_i'$ | Fluctuating vector stream function |
| $\Omega_{ij}$ | Mean rotation rate tensor |
| $\Omega_{ij}^T$ | Total (mean and frame) rotation rate tensor |
| $\Omega_i$ | Mean vorticity vector |
| $\Omega_i^f$ | Frame vorticity vector |
| $\Omega_i^T$ | Total (mean and frame) vorticity vector |
| $\hat{\Omega}^2$ | Invariant of eddy-axis tensor and mean rotation rate tensor |

# Chapter 1

# Introduction

## 1.1 Motivation

Turbulent flows are present everywhere, from naturally occurring flows to flows in and around mechanical devices. Turbulence is complex because of the wide range of temporal and spatial scales involved. The motion of a simple viscous fluid at all scales is completely described by the Navier-Stokes equations. However, simulation of all scales poses a considerable challenge for computational resources now and for the foreseeable future.

The alternative to costly or even currently out-of-reach simulations is to perform some form of averaging on the turbulent flow, drastically reducing the number of turbulent scales. Historically this started with Osborne Reynolds and is the engineering tool for mathematical analysis of turbulent flows. The effect of the discarded information is crucial in the development of the averaged flow. It enters the equations for the mean momentum through a new unknown, the Reynolds stress tensor, resulting in the familiar closure problem.

Turbulence models aim to capture the effect of the discarded information, on the mean flow, by providing a representation for the unknown terms in the averaged equations in terms of known quantities. Traditional turbulent models rely only on the Reynolds stresses for bringing turbulence anisotropy information for closure.

However the Reynolds stresses only characterize the componentality of the turbulence, *i.e.*, which velocity components are more energetic. The turbulent field has much more information than that contained in the Reynolds stresses. The question then is: what is the relevant information which should be extracted from the original turbulent field? Kassinos and Reynolds (1994) demonstrate that for rotating fluid turbulence knowledge about the turbulence structure is also crucial. Among other properties, the dimensionality of the flow is important. This carries information about which directions are favored by the more energetic turbulent eddies: if the turbulent eddies are preferentially aligned with a given direction, then the dimensionality is smaller along that direction.

The message repeatedly delivered by Reynolds and coworkers (1991, 1994, and 2001) is that models based solely on the Reynolds stresses are not complete. Key illustrations of

the importance of structure to capture flow physics are as follows:

- axisymmetric expansion anomaly (Kassinos, Reynolds, and Rogers 2001), which is beyond the reach of an equilibrium algebraic model and hence not addressed here. Homogeneous turbulence subjected to axisymmetric expansion develops a larger Reynolds stress anisotropy under slow deformation than under rapid deformation. Moreover, when the mean straining is removed, the stress anisotropy may continue to increase. This is counter to the idea of "return to isotropy" built into current day turbulence models, and can be explained resorting to the structure models;

- damped Reynolds-stress oscillations for rapidly rotating, unstrained, initially anisotropic homogeneous turbulence (Mansour, Shih, and Reynolds 1991), which is beyond the reach of an equilibrium algebraic model and hence not addressed here. One-point turbulence models based solely on the Reynolds stresses for its closure are unable to predict the decay in the Reynolds stress anisotropy in rapidly-rotating, unstrained turbulence;

- material indifference of two-dimensional (2D) turbulence to rotation (Speziale 1981), which the proposed algebraic model does address. 2D turbulence rotated around its axis of independence is materially insensitive to the rotation (2DMIR). There are only kinematic effects, so an observer rotating with the frame or mean motion is completely unaware of the rotation. Matching the 2D material indifference limit may not be as important as an awareness of the dimensionality and its degree of alignment with the rotation vector. Note that a model needs to be aware of the dimensionality of the turbulence in order to capture the 2DMIR effect. Reynolds stress models are only aware of the componentality of the turbulence. They may be built to satisfy properties of two-component turbulence, *e.g.* near-wall turbulence. However, they will not, in general, meet properties of two-dimensional turbulence, *e.g.* the 2DMIR condition. Ristorcelli, Lumley, and Abid (1995) proposed a pressure-strain model which is consistent with the 2DMIR property under certain conditions. However, their model does not satisfy the 2DMIR property in general.

The development of a structure-based turbulence model is a formidable task. Haire (2003) summarizes the efforts of the structure-based turbulence modeling group at Stanford over the past few years. Recently the effort has shifted towards the development of an

algebraic structure-based turbulence model (ASBM). Reynolds, Kassinos, Langer, and Haire (2000) and Haire (2003) built an ASBM based on Kassinos and Reynolds (1994). It is based on an axisymmetric eddy-axis model, where the energy-normalized Reynolds stress tensor is based on "axisymmetric" eddies, computed as in Kassinos and Reynolds. Eddy flattening was introduced in the algebraic model as a way of considering more general energy distributions around the conceptual eddies that constitute the basis of the model. The homogeneous model developed was found to produce realizable and physically realistic turbulent states for diverse normalized deformation rates, with and without frame rotation. Haire explored that ASBM in free shear flows, along with a set of scale equations (*e.g.* $k$ and $\varepsilon$), and found it produced adequate results.

Flows of general engineering interest are likely to be bounded by walls. The ASBM would not be complete unless it incorporates some near-wall physics, allowing it to produce sensible solutions near walls. Reynolds *et al.* (2000) did propose an extension of the ASBM for wall-bounded flows. However coupling the complete model (with scale equations) to the mean flow did not produce satisfactory results near walls.

The specification of an ASBM is not complete without reference to a set of evolution equations for appropriate turbulence scales. Reynolds, Langer, and Kassinos (2002) proposed a set of scale equations based on the large-scale energy-bearing motion. The development of the second scale equation (accompanying the turbulence kinetic energy equation) is based on the large-scale vorticity equation, and its source terms are representative of large-scale motion. It is expected that coupling this equations with an ASBM can produce a model with superior predictive capabilities.

## 1.2 Objective

This work sets out to develop and assess a complete ASBM for wall bounded flows, in fixed and rotating frames of reference, revisiting and extending earlier formulations of an algebraic structure-based model with accompanying scale equations.

## 1.3 Contributions

The most significant contributions of this work are

- the development of a revised version of a (homogeneous) ASBM with improved physical content, regarding eddy flattening and the specification of scalar parameters representative of the hypothetical eddy field;
- the modification of the ASBM and the scale equations for compatibility with expected near wall asymptotic behavior, ensuring the relative magnitude of the different terms follows the expected near-wall trend of the exact terms;
- implementation of the complete model for wall-bounded flows (channel flows) with and without frame rotation, with mostly satisfactory results. This marks the first time a complete ASBM has been applied to wall-bounded flows, with or without frame rotation.

# Chapter 2

# RANS and Turbulence Structure

This chapter provides some essential background that is needed in later chapters. Following a brief review of the equations governing the fluid motion, and of the Reynolds Averaged Navier Stokes (RANS) equations, both in a rotating frame, the closure problem is introduced. It is then argued that in addition to the Reynolds stresses, turbulence structure information is needed to provide a more complete description of a turbulent state, and thus can be used for creating improved turbulence models.

This provides the motivation for introducing a set of turbulence structure tensors and their properties as delineated in Kassinos and Reynolds (1994) and Kassinos, Reynolds, and Rogers (2001). The structure tensors introduced in this chapter are then modeled in Chapter 3 through algebraic approximations. The same structure tensors reappear in Chapter 4, where they are used for closure of the evolution equations for the turbulence kinetic energy and the large scale turbulent enstrophy.

## 2.1 Equations of motion

The equations governing the motion of an incompressible viscous fluid in a Cartesian rotating frame of reference are given by conservation of mass and momentum as in Greenspan (1968),

$$\frac{\partial u_i}{\partial x_i} = 0, \tag{2.1}$$

$$\frac{\partial u_i}{\partial t} + u_j \frac{\partial u_i}{\partial x_j} + 2\epsilon_{ijk}\Omega_j^f u_k = -\frac{\partial P^*}{\partial x_i} + \nu \frac{\partial^2 u_i}{\partial x_k \partial x_k}, \tag{2.2}$$

where $u_i$ is the velocity measured in the coordinate system rotating with constant angular velocity $\Omega_j^f$, and $x_j$, $t$, $P^*$, $\rho$, and $\nu$ represent respectively the position vector, time, reduced pressure, density, and kinematic viscosity. The reduced pressure is given by

$$P^* = \frac{p}{\rho} + \mathcal{U} - \frac{1}{2}(\epsilon_{ljk}\Omega_j^f x_k)(\epsilon_{lpq}\Omega_p^f x_q), \tag{2.3}$$

where $p$ is the thermodynamic pressure, $\mathcal{U}$ is such that a conservative body force per unit mass (*e.g.* gravity) is given by $\partial\mathcal{U}/\partial x_i$, and the last term represents the centripetal acceleration.

### 2.1.1 Reynolds-Averaged Navier-Stokes (RANS) equations

Traditional Reynolds decomposition is used in this chapter. The instantaneous flow field is decomposed into an ensemble average contribution and a fluctuating contribution

$$u_i = \bar{u}_i + u_i', \qquad p = \bar{p} + p', \tag{2.4}$$

where the overbar represents the averaged part and the prime represents the fluctuating part. Substituting into the equations of motion and averaging produces the incompressible RANS equations,

$$\frac{\partial \bar{u}_i}{\partial x_i} = 0, \tag{2.5}$$

$$\frac{\partial \bar{u}_i}{\partial t} + \bar{u}_j \frac{\partial \bar{u}_i}{\partial x_j} + 2\epsilon_{ijk}\Omega_j^f \bar{u}_k = -\frac{\partial \tilde{P}^*}{\partial x_i} + \nu \frac{\partial^2 \bar{u}_i}{\partial x_k \partial x_k} + \frac{\partial}{\partial x_j}\left(-\overline{u_i' u_j'}\right). \tag{2.6}$$

### 2.1.2 Closure

The last term in Equation (2.6) involves the Reynolds stress tensor, $R_{ij} = \overline{u_i' u_j'}$, and is representative of the transport brought about by the large scales of the turbulence. It is an unknown in the equations and the need for its specification is the penalty incurred by averaging the Navier-Stokes equations: the effect of all the detailed information discarded upon averaging must be accounted for in the RANS equations through $R_{ij}$.

In traditional one-point modeling, closure is obtained using only the mean flow, the Reynolds stresses, and a turbulence scalar, *i.e.*, any turbulence correlation $\mathcal{G}_{ij}$ (such as $R_{ij}$) is modeled at most as a function of the velocity gradient, frame rotation rate, the Reynolds stresses themselves, and a turbulent scale like $\varepsilon$, the dissipation rate of the turbulent kinetic energy.

$$\mathcal{G}_{ij} = \mathcal{G}_{ij}\left(\frac{\partial \bar{u}_i}{\partial x_j}, \Omega_k^f, R_{ij}, \varepsilon\right). \tag{2.7}$$

The information carried within the independent objects in Equation (2.7) does not provide any suggestion about the turbulence at different locations (nonlocal information). In fact, only the Reynolds stresses describe the anisotropy of the turbulence itself. However, the

Reynolds stresses describe only the componentality of the turbulence. If $u_1' = 0$, then $R_{11} = 0$, indicating 2C (two component) turbulence, which can be 1D (one dimensional), 2D or 3D. This information about the dimensionality of the turbulence is not contained within the Reynolds stresses and may be important for modeling. A glaring example is the property of material frame indifference of 2D turbulence to frame rotation aligned with the direction of independence, out of the 2D plane (Speziale 1981). In this case the turbulence is such that an observer rotating with the mean motion will be unaware of the rotation (material indifference). Clearly a turbulence model needs to be aware of the dimensional character of the turbulence to exhibit the same property. Everyday turbulence is not going to reach the 2D limit under normal deformations. Nevertheless, as structures are elongated in any particular direction by the mean deformation, a decreased effect of the frame rotation upon structures aligned with it should be expected.

Reynolds (1991), Kassinos and Reynolds (1994), and Kassinos *et al.* (2001) repeatedly point the shortcomings of representing a turbulent flow solely through the Reynolds stresses. To incorporate turbulence structure, they introduce new one-point objects in terms of gradients of the turbulent stream-function vector, as defined in the next section.

## 2.2 The Turbulent Stream-Function Vector and the Turbulence Structure Tensors

The turbulent stream-function vector, $\psi_k'$, is introduced to explore and elaborate concepts of turbulence structure. It is defined by

$$u_i' = \epsilon_{ijk}\frac{\partial \psi_k'}{\partial x_j}, \qquad \frac{\partial \psi_k'}{\partial x_k} = 0, \qquad \frac{\partial^2 \psi_i'}{\partial x_k \partial x_k} = -\omega_i'. \tag{2.8}$$

The turbulence structure tensors are then defined as

$$D_{ij} = \overline{\frac{\partial \psi_k'}{\partial x_i}\frac{\partial \psi_k'}{\partial x_j}}, \qquad F_{ij} = \overline{\frac{\partial \psi_i'}{\partial x_k}\frac{\partial \psi_j'}{\partial x_k}}, \qquad C_{ij} = \overline{\frac{\partial \psi_i'}{\partial x_k}\frac{\partial \psi_k'}{\partial x_j}}, \tag{2.9}$$

where $D_{ij}$, $F_{ij}$, and $C_{ij}$ are respectively the structure dimensionality, structure circulicity, and inhomogeneity tensors. These carry information about the large-scale, energy-bearing, structure of the turbulence not conveyed by the Reynolds stress tensor.

Note that the free indices in the dimensionality tensor are connected to the spatial derivatives. It is associated with the spatial isotropy of the turbulence structures. If $D_{11} = 0$,

then the turbulence is instantaneously 2D, every $\psi_i'$ is independent of the $x_1$ direction, and the turbulence consists of very long structures aligned with the $x_1$ direction.

The free indices in the circulicity tensor are connected to the stream function vectors. Equation (2.8) shows that the stream function vector is in turn related to the fluctuating vorticity. The circulicity tensor is then representative of the large scale structure of the vorticity/circulation field. If $F_{11} = 0$, then there is no large scale circulation about the $x_1$ direction. Alternatively, if $F_{11} \to 1$, most of the large scale circulation is concentrated around the $x_1$ axis.

The inhomogeneity tensor characterizes the degree of inhomogeneity of the turbulent field. It vanishes in homogeneous flows, which is evident by rewriting it as

$$C_{ij} = \overline{\frac{\partial \psi_i'}{\partial x_k}\frac{\partial \psi_k'}{\partial x_j}} = \frac{\partial}{\partial x_k}\left(\overline{\psi_i'\frac{\partial \psi_k'}{\partial x_j}}\right). \tag{2.10}$$

Kassinos, Reynolds, and Rogers (2001) note that it is significant in the near-wall region of wall-bounded flows. However, away from the wall, say $y^+ > 30$, Kassinos *et al.* note that the magnitude of $C_{ij}$ becomes small compared to the magnitude of the other structure tensors.

The structure tensors are related to each other and to the Reynolds stress tensor. This fundamental constitutive relation is obtained by substituting the identity (Jeffreys 1931)

$$\epsilon_{rst}\epsilon_{opq} = \delta_{ro}\delta_{sp}\delta_{tq} + \delta_{rp}\delta_{sq}\delta_{to} + \delta_{rq}\delta_{so}\delta_{tp} - \delta_{ro}\delta_{sq}\delta_{tp} - \delta_{rp}\delta_{so}\delta_{tq} - \delta_{rq}\delta_{sp}\delta_{to} \tag{2.11}$$

into the Reynolds stress definition

$$R_{ij} = \overline{u_i'u_j'} = \epsilon_{ist}\epsilon_{opq}\overline{\frac{\partial \psi_t'}{\partial x_s}\frac{\partial \psi_q'}{\partial x_p}} = R_{kk}r_{ij}, \tag{2.12}$$

resulting in the exact relationship,

$$R_{ij} + D_{ij} + F_{ij} - (C_{ij} + C_{ji}) = q^2\delta_{ij}, \tag{2.13}$$

where $q^2 = R_{kk}$ is twice the turbulent kinetic energy.

In the algebraic structure-based models developed so far (including the current effort), the structure tensors are modeled in a (locally) homogeneous framework, where the inhomogeneity tensor vanishes. The structure tensors are then built such that they obey the fundamental constitutive relation, Equation (2.13), without the $C_{ij}$ contribution. However in near-wall regions the assumption of vanishing $C_{ij}$ is poor. To reconcile a non-vanishing

inhomogeneity tensor with the desired simplicity of the homogeneous constitutive relation, the inhomogeneity tensor can be absorbed into modified dimensionality and circulicity tensors,

$$D_{ij}^{cc} = D_{ij} - \frac{1}{2}(C_{ij} + C_{ji}), \tag{2.14}$$

$$F_{ij}^{cc} = F_{ij} - \frac{1}{2}(C_{ij} + C_{ji}). \tag{2.15}$$

Both $D_{ij}^{cc}$ and $F_{ij}^{cc}$ are symmetric and they equal their parent quantities for locally homogeneous turbulence. Their traces equal twice the turbulent kinetic energy,

$$D_{kk}^{cc} = F_{kk}^{cc} = R_{kk} = q^2. \tag{2.16}$$

The drawback of this apparent simplicity is that the diagonal components of the modified structure tensors may become negative. In the current models, and in the model constructed in Chapter 3, the diagonal components are built such that they are never negative.

Substituting Equations (2.14) and (2.15) into Equation (2.13), gives a homogeneous-like constitutive relation,

$$R_{ij} + D_{ij}^{cc} + F_{ij}^{cc} = q^2 \delta_{ij}. \tag{2.17}$$

Substituting the energy-normalized structure tensors,

$$r_{ij} = \frac{R_{ij}}{q^2}, \qquad d_{ij}^{cc} = \frac{D_{ij}^{cc}}{q^2}, \qquad f_{ij}^{cc} = \frac{F_{ij}^{cc}}{q^2}, \tag{2.18}$$

into Equation (2.17), and dividing by $q^2$ gives the normalized form most commonly used,

$$r_{ij} + d_{ij}^{cc} + f_{ij}^{cc} = \delta_{ij}. \tag{2.19}$$

Note that only two of the structure tensors are independent. Given the Reynolds stresses and the structure dimensionality tensor, the structure circulicity follows from Equation (2.19). Kassinos and Reynolds (1994) point out that traditional Reynolds stress models, carrying only the Reynolds stress as model variable, effectively lump together structure dimensionality and circulicity information. Therefore they cannot isolate the correct dimensionality state of the turbulence.

In the next chapter an algebraic model for the "cc" tensors is developed, as no attempt is made at modeling the inhomogeneity tensor. Modeling information for $C_{ij}$ is too little and too restricted to construct a general model for it. It turns out incorporating the

inhomogeneity tensor into the other structure tensors should not be critical. The uncertainty in the modeled structure tensors, $D_{ij}$, and $F_{ij}$, is likely large near the wall, so even if exact information for $C_{ij}$ were available, it would not improve the degree of accuracy of the other tensors. More appropriately, ignoring any explicit model for $C_{ij}$ does not increase the error in the near wall area, as the overall error in modeling the structure tensors should not change significantly.

# Chapter 3

# Algebraic Structure-Based Model

The complete Algebraic Structure-Based Model (ASBM) consists of model evolution equations for the turbulent kinetic energy and for the large scale enstrophy of the turbulence, along with algebraic model equations that evaluate the normalized structure of the turbulence (including the Reynolds stresses), given the mean velocity gradients, a turbulent time scale, and a wall blocking parameter.

This chapter describes the algebraic model. The objective is to provide an algebraic procedure to evaluate the normalized turbulence structure (dimensionality, circulicity and Reynolds stresses), given the local state of the mean deformation normalized by a suitable turbulence time scale. The model is inspired by previous work by Kassinos and Reynolds (1994) and Reynolds and Kassinos (1995) on structure based turbulence modeling, and by recent work on algebraic structure based turbulence modeling by Reynolds, Kassinos, Langer, and Haire (2000) and Haire (2003).

The essence of the model is the representation of a general three-dimensional (3D), three-component (3C) turbulent field by the superposition of an ensemble of 2D-3C fields. Each of these fundamental 2D-3C fields can be thought of as an idealized turbulent eddy whose axis, or orientation, corresponds to the direction of independence of the 2D field. Each of these eddies supports motion around its axis as well as along it (3C). Averaging over a large ensemble of eddies gives relations for the structure tensors in terms of statistics of the eddy field.

The turbulence structure and the Reynolds stresses returned by the algebraic model depend on the choice of a specific reference frame, which may or may not be rotating. The model is ideally applied to the frame where the turbulence structure is at equilibrium, or closest to it.

## 3.1 Overview

Sections 3.2 and 3.3 describe basic ideas associated with the description of turbulence by a field of conceptual turbulent eddies, and the properties that are assigned to each eddy

in order to provide a quantitative "measure" of the turbulence.

Section 3.4 introduces ensemble averaging over a field of eddies. This provides statistical measures representative of the turbulence in terms of properties of the eddy ensemble. Section 3.5 then finds constitutive relations for the Reynolds stress and dimensionality tensors in terms of these eddy statistics. At this point conceiving a model for the turbulence structure means conceiving a model for the eddy statistics brought up in Section 3.4.

Vector and tensor representations of the eddy ensemble are modeled in terms of the mean deformation in Sections 3.6 through 3.8. Finally in Section 3.9 the scalar eddy structure parameters are modeled in terms of the local mean deformation. The model for the scalars is found by comparing states from the model Reynolds stresses and structure dimensionality tensors with target states, given different mean deformations.

Section 3.10 then sensitizes this model representation to the presence of impermeable walls, through the use of a blocking approach based on projection operators, aiming to retrieve the proper asymptotic behavior for the model Reynolds stresses.

Section 3.11 offers a brief summary of the model equations, and Section 3.12 explores the behavior of the homogeneous (unblocked) model to various normalized deformation rates.

## 3.2 Eddy Concepts

In this model, individual eddies are the building blocks in the description of a turbulent field. In order to proceed with the construction of the model, tools/measures for the characterization of these individual eddies will be introduced. Ensemble averages are then taken over a field of eddies, giving quantities representative of the eddy field along with constitutive equations relating the normalized Reynolds stresses and the turbulence structure in terms of the averaged eddy ensemble.

Three different families of eddies, characterized by their associated motion, are considered; vortical eddies, jetal eddies, and helical eddies. To further characterize the eddy motion, the possibility of eddy flattening is also introduced.

Vortical eddies represent 2D-2C fields where the motion of blobs of fluid that compose the eddy is around the axis of the eddy, with zero velocity along the axis of the eddy. This is typical of irrotational mean deformations. In fact the vortical mode is all that is needed to model turbulence in this case.

Jetal eddies correspond to 2D-1C fields where the motion is exclusively along the axis

of the eddy, with zero velocity around the axis. Rapid shear tends to generate this kind of motion, with a limiting state corresponding to counter-flowing jet streams (see Kassinos and Reynolds 1994).

Helical eddies can be thought of as the superposition of vortical eddies and jetal eddies. The tightness of the helix will depend on the relative contributions from the two modes. Generic turbulent fields are populated by helical eddies.

Flattening is used to describe the degree of asymmetry in the turbulent kinetic energy distribution around an eddy. A round eddy has no preferential direction. A fully flattened eddy may look like a sheet, with all motion and kinetic energy concentrated in a plane perpendicular to the direction of flattening.

## 3.3 Eddy Properties

To help in the construction of the different moments of the turbulence, each eddy is envisioned as a conglomerate of blobs of fluid. This approach follows from the Particle Representation Method (PRM) of Kassinos and Reynolds (1994). All blobs share a common eddy-axis direction vector, $\vec{a}$. Each has its own velocity vector, $\vec{V}$ (with a component aligned with $\vec{a}$, and the others perpendicular to it), and a gradient direction, $\vec{n}$, perpendicular to both $\vec{a}$ and $\vec{V}$ (which are not necessarily orthogonal). The PRM introduces also the stream function vector, $\vec{s}$, perpendicular to $\vec{V}$ and $\vec{n}$ (forming a mutually orthogonal vector triad). A flattening of the eddy is also allowed; from a round/axisymmetric distribution of its kinetic energy around the eddy axis to a fully-flattened distribution, when the kinetic energy is distributed in such a form that the eddy becomes a sheet.

Summarizing, the following properties provide a qualitative description of an individual eddy in the turbulence field:

- eddy-axis direction, $\vec{a}$;
- velocity, $\vec{V}$;
- gradient direction, $\vec{n}$;
- stream function, $\vec{s}$;
- jetal and vortical motions, $\vec{V} = (V_{jet})\vec{a} + (V_{vort})\vec{n} \times \vec{a}$;
- flattening direction, $\vec{b}$, and

- flattening intensity.

An advantage of the eddy-axis approach is its relative ease in producing realizable states for the Reynolds stresses and the turbulence structure, while maintaining the constitutive relation $r_{ij} + d_{ij} + f_{ij} = \delta_{ij}$, a consequence of the fact that $\vec{V}$, $\vec{n}$, and $\vec{s}$ form a vector triad.

## 3.4 Eddy Ensembles

Individual conceptual eddies constitute the building blocks of the model. A turbulence field is constructed by superposing a large ensemble of eddies. Taking an average over the whole ensemble produces quantities representative of the field. Angle brackets denote an ensemble-averaged quantity.

### 3.4.1 Eddy-Axis Tensor

The eddy-axis tensor is the energy-weighted average direction-cosine tensor of the eddy axes,

$$a_{ij} = \frac{1}{q^2}\langle V^2 a_i a_j \rangle, \tag{3.1}$$

where $q^2 = \langle V^2 \rangle$ is twice the turbulent kinetic energy. The eddy-axis tensor is determined by the mean deformation. Eddies, as material lines, tend to align with the direction of positive mean strain rate. They are rotated kinematically by mean or frame rotation.

### 3.4.2 Eddy-Flattening Tensor

The eddy flattening tensor is an ensemble average of the direction cosines of the flattening vector,

$$b_{ij} = \frac{1}{q^2}\langle V^2 b_i b_j \rangle. \tag{3.2}$$

### 3.4.3 Eddy Structure Parameters

#### Eddy Jetting Parameter, $\phi$

It is representative of the amount of energy in the jetal mode, and $(1 - \phi)$ represents the amount of energy in the vortical mode. Under irrotational deformations, eddies remain purely vortical, $\phi = 0$, and in this case the eddy-axis tensor coincides with the circulicity tensor. Rotation produces jetal eddies (Kassinos and Reynolds 1994), and in the limit of infinite rapid distortion $\phi \rightarrow 1$ for shear in a fixed frame;

**Eddy Helix Vector, $\gamma$**

The helix vector arises from the correlation between the jetal and vortical modes of motion. Hence $\gamma_k = 0$ for purely vortical or purely jetal turbulence. Typically $\gamma_k$ is aligned with the total vorticity vector (Kassinos and Reynolds 1994). The helix vector is the key factor in setting the shear stress level in turbulent fields.

**Eddy Flattening Parameter, $\chi$**

If the motion is not axisymmetric around the eddy axis, the eddy is called flattened. Under rapid irrotational deformation in a fixed frame eddies remain axisymmetric. Rotation tends to flatten the eddies in planes perpendicular to the rotation direction.

## 3.5 Reynolds Stress, Turbulence Dimensionality, and Turbulence Circulicity Constitutive Relations

The quantities above describe the average properties of a field of hypothetical eddies. Ultimately they facilitate introducing more physics, structure physics, into turbulence modeling. The merit of these quantities comes at the moment of evaluation of the turbulence structure and the Reynolds stresses. This evaluation is done by writing the Reynolds stresses and the turbulence structure in eddy-axis coordinates, through constitutive relations involving also the structure parameters. This work departs with earlier structure-based approaches in the treatment of eddy-flattening. As a result the constitutive relations depart from the ones reported previously (Reynolds *et al.* 2000, Haire 2003).

Conditional averaging is introduced to facilitate the derivation of the constitutive relations. Conditioned moments are formed by averaging over eddies that share common eddy-axis and eddy-flattening orientations. For an expanded derivation consult Appendix A. Firstly an expression for the dimensionality tensor is proposed. This is then used in the constitutive equation for the Reynolds stresses. The most general form for the conditioned dimensionality tensor, given an eddy-axis direction, $\vec{a}$, and a flattening direction, $\vec{b}$, is

$$\begin{aligned}\langle V^2 n_i n_j | \vec{a}, \vec{b} \rangle / \tilde{V}^2 = {} & C_1 \delta_{ij} + C_2 a_i a_j + C_3 b_i b_j + C_4 (a_i b_j + a_j b_i) \\ & + C_5 (\epsilon_{ipq} a_p b_q b_j + \epsilon_{jpq} a_p b_q b_i) + C_6 (\epsilon_{ipq} a_p b_q a_j + \epsilon_{jpq} a_p b_q a_i),\end{aligned} \tag{3.3}$$

where $\tilde{V}^2 = \langle V^2 | \vec{a}, \vec{b} \rangle$. Applying the orthogonality constraint, $a_j n_j = 0$, the normalization

constraint, $\langle V^2 n_i n_i | \vec{a}, \vec{b} \rangle / \tilde{V}^2 = 1$, and setting $C_3 = \tilde{\chi}$ and $C_5 = 0$, results in the conditioned dimensionality tensor

$$\begin{aligned} \langle V^2 n_i n_j | \vec{a}, \vec{b} \rangle / \tilde{V}^2 = {} & \tfrac{1}{2}\{1 - \tilde{\chi}[1 - (a_n b_n)^2]\}\delta_{ij} - \tfrac{1}{2}\{1 - \tilde{\chi}[1 + (a_n b_n)^2]\} a_i a_j \\ & + \tilde{\chi} b_i b_j - (a_n b_n)\tilde{\chi}(a_i b_j + a_j b_i). \end{aligned} \tag{3.4}$$

Writing the velocity vector in an eddy coordinate system, with a component normal to the eddy and a component aligned with the eddy axis direction results in

$$V_i = V(v_m a_m) a_i + V(\epsilon_{rst} v_r n_s a_t)\epsilon_{ipq} a_p n_q. \tag{3.5}$$

Taking the second moment of the velocity gives an expression for the conditioned stresses in terms of the eddy-axis vector and the conditioned dimensionality tensor,

$$\begin{aligned} R_{ij}^{|\vec{a},\vec{b}} = \langle V_i V_j | \vec{a}, \vec{b} \rangle = {} & \langle (v_m a_m)^2 V^2 a_i a_j | \vec{a}, \vec{b} \rangle \\ & + \langle (v_m a_m)(\epsilon_{rst} v_r n_s a_t) V^2 (\epsilon_{ipq} a_p a_j n_q + \epsilon_{jpq} a_p a_i n_q) | \vec{a}, \vec{b} \rangle \\ & + \langle (\epsilon_{rst} v_r n_s a_t)^2 V^2 \epsilon_{ipq}\epsilon_{jkl} a_p n_q a_k n_l | \vec{a}, \vec{b} \rangle. \end{aligned} \tag{3.6}$$

Using Identity (2.11), and defining

$$\tilde{\phi} \equiv (v_m a_m)^2, \tag{3.7}$$

$$\tilde{\gamma}_s n_s \equiv (\epsilon_{rst} v_r a_t)(v_m a_m) n_s, \tag{3.8}$$

gives

$$\begin{aligned} R_{ij}^{|\vec{a},\vec{b}} = {} & \langle V^2 \tilde{\phi} a_i a_j \rangle + \langle V^2 (1 - \tilde{\phi})[\tfrac{1}{2}(\delta_{ij} - a_i a_j) + \tilde{\chi}\{\tfrac{1}{2}[1 - (a_n b_n)^2]\delta_{ij} \\ & - \tfrac{1}{2}[1 + (a_n b_n)^2] a_i a_j - b_i b_j + (a_n b_n)(a_i b_j + a_j b_i)\}] \rangle \\ & + \langle V^2 \tilde{\gamma}_s (\epsilon_{ipq} a_p a_j + \epsilon_{jpq} a_p a_i)[\tfrac{1}{2}\{1 - \tilde{\chi}[1 - (a_n b_n)^2]\}\delta_{qs} + \tilde{\chi} b_q b_s - \tilde{\chi}(a_n b_n)(a_s b_q)] \rangle. \end{aligned} \tag{3.9}$$

Following Kassinos and Reynolds (1994) define

$$q^2 r_{ij} \equiv \langle V_i V_j \rangle, \qquad q^2 d_{ij}^{cc} \equiv \langle V^2 n_i n_j \rangle, \qquad q^2 a_{ij} \equiv \langle V^2 a_i a_j \rangle, \qquad q^2 b_{ij} \equiv \langle V^2 b_i b_j \rangle, \tag{3.10}$$

$$q^2 \phi \equiv \langle V^2 \tilde{\phi} \rangle, \qquad q^2 \gamma_k \equiv \langle V^2 \tilde{\gamma}_k \rangle, \qquad q^2 \chi \equiv \langle V^2 \tilde{\chi} \rangle, \tag{3.11}$$

respectively the energy-weighted normalized Reynolds stress tensor, eddy-axis tensor, eddy-flattening tensor, and the energy-weighted structure jetal parameter, structure helix vector, and structure flattening parameter.

The final step in the modeling process involves taking the ensemble average over all eddies (eddy-axis orientations and flattening directions, $\vec{a}$ and $\vec{b}$). The ensemble-averaged normalized structure- and Reynolds-stress tensors become

$$\begin{aligned} d_{ij}^{cc} &= \tfrac{1}{2}[1-\chi(1-a_{nm}b_{mn})]\delta_{ij} \\ &\quad -\tfrac{1}{2}[1-\chi(1+a_{nm}b_{mn})]a_{ij}+\chi b_{ij}-\chi(a_{in}b_{nj}+a_{jn}b_{ni}), \end{aligned} \tag{3.12}$$

$$\begin{aligned} r_{ij} &= (1-\phi)\tfrac{1}{2}(\delta_{ij}-a_{ij})+\phi a_{ij} \\ &\quad +(1-\phi)\chi\,[\tfrac{1}{2}(1-a_{nm}b_{mn})\delta_{ij}-\tfrac{1}{2}(1+a_{nm}b_{mn})a_{ij}-b_{ij}+a_{in}b_{nj}+a_{jn}b_{ni}] \\ &\quad +(-\gamma\Omega_k^T/\Omega^T)(\epsilon_{ipr}a_{pj}+\epsilon_{jpr}a_{pi})\{\tfrac{1}{2}[1-\chi(1-a_{nm}b_{mn})]\delta_{kr}+\chi b_{kr}-\chi a_{kn}b_{nr}\}. \end{aligned} \tag{3.13}$$

The normalized (modified) circulicity tensor $f_{ij}^{cc}$ is not an independent quantity. It can be obtained through the basic constitutive relation (2.19) as

$$f_{ij}^{cc} = \delta_{ij} - r_{ij} - d_{ij}^{cc}. \tag{3.14}$$

## 3.6 Eddy-Axis Tensor Model

Following Reynolds *et al.* (2000), the eddy-axis tensor, $a_{ij}$, is computed on the analysis frame, where the turbulence might be at equilibrium or very close to it. This is typically a rotating frame. The eddy axis is computed with no reference to the frame rotation, as it is only kinematically rotated by it (Kassinos and Reynolds 1994, Haire 2003). The evaluation is divided in two parts. Initially a strained eddy axis, $a_{ij}^s$, is evaluated based on the irrotational part of the mean deformation. Next a rotation operation is applied, sensitizing the eddy-axis tensor to mean rotation. This procedure produces eddy-axis tensor states that mimic the limiting states produced under RDT for different combinations of mean strain with on-plane mean rotation, while guaranteeing realizability of the eddy-axis tensor. For details see Appendix B.

The strained $a_{ij}^s$ is given by

$$a_{ij}^s = \frac{1}{3}\delta_{ij} + \frac{(S_{ik}^* a_{kj}^s + S_{jk}^* a_{ki}^s - \frac{2}{3}S_{mn}^* a_{nm}^s \delta_{ij})\tau}{a_0 + 2\sqrt{\tau^2 S_{kp}^* S_{kq}^* a_{pq}^s}}, \tag{3.15}$$

where $S_{ij}^* = S_{ij} - S_{kk}\delta_{ij}/3$ is the traceless strain-rate tensor, and $a_0 = 1.6$ is a "slow" constant. $a_0$ is determined simultaneously with other model constants to ensure the model satisfies a canonical boundary-layer state (see Equation 3.68). Equation 3.15 was initially

proposed by Reynolds *et al.* (2000) (Haire 2003 proposed a derivation based on equilibrium considerations). It gives realizable states tor the eddy-axis tensor under irrotational deformations. The coefficient of 2 in the denominator allows it to produce the correct limiting eddy-axis tensor for arbitrary rapid irrotational deformations.

The final expression for the homogeneous eddy-axis tensor, $a_{ij}$ (for near-wall regions see Equation 3.72), is obtained by applying a rotation transformation to the strained eddy-axis tensor, $a^s_{ij}$,

$$a_{ij} = H_{ik}H_{jl}a^s_{kl}. \tag{3.16}$$

The rotation tensor is constructed as

$$H_{ij} = \delta_{ij} + h_1\frac{\Omega_{ij}}{\sqrt{\Omega^2_{pp}}} + h_2\frac{\Omega_{ik}\Omega_{kj}}{\Omega^2_{pp}}, \tag{3.17}$$

where $\Omega^2_{pp} = \Omega_{pq}\Omega_{pq}$. $H_{ij}$ is required to satisfy the orthonormal conditions,

$$H_{ik}H_{jk} = \delta_{ij}, \qquad H_{ki}H_{kj} = \delta_{ij}. \tag{3.18}$$

The orthonormality condition requires

$$h_1 = \sqrt{2h_2 - h_2^2/2}. \tag{3.19}$$

$h_2$ is determined with reference to RDT for combined plane strain and rotation, where

$$S^*_{ij} = \frac{1}{2}\begin{pmatrix} 0 & \Gamma & 0 \\ \Gamma & 0 & 0 \\ 0 & 0 & 0 \end{pmatrix}, \qquad \Omega_{ij} = \frac{1}{2}\begin{pmatrix} 0 & \Omega & 0 \\ -\Omega & 0 & 0 \\ 0 & 0 & 0 \end{pmatrix}. \tag{3.20}$$

By considering the kinematic distortion of line elements by this mean flow, Reynolds *et al.* (2000) find that the eddy-axis tensor evolves over time to a fixed point where

$$a_{11} = \frac{\Gamma + \Omega}{2\Gamma}, \qquad a_{22} = \frac{\Gamma - \Omega}{2\Gamma}, \qquad a_{12} = \frac{\sqrt{\Gamma^2 - \Omega^2}}{2\Gamma}, \qquad \text{for } \Gamma - \Omega \geq 0. \tag{3.21}$$

This determines $h_2$ for this flow. Results are extended to generic flows with

$$h_2 = \begin{cases} 2 - 2\sqrt{\frac{1}{2}(1 + \sqrt{1 - r})} & \text{if } r \leq 1 \\ 2 - 2\sqrt{\frac{1}{2}(1 - \sqrt{1 - 1/r})} & \text{if } r \geq 1, \end{cases} \tag{3.22}$$

where

$$r = \frac{a_{pq}\Omega_{qr}S^*_{rp}}{S^*_{kn}S^*_{nm}a_{mk}}. \tag{3.23}$$

## 3.7 Flattening Tensor Model

The flattening tensor $b_{ij}$ is modeled in terms of the mean rotation rate vector and the frame rotation rate vector,

$$b_{ij} = \frac{(\Omega_i + C_b\Omega_i^f)(\Omega_j + C_b\Omega_j^f)}{(\Omega_k + C_b\Omega_k^f)(\Omega_k + C_b\Omega_k^f)}, \tag{3.24}$$

where $\Omega_i$ and $\Omega_i^f$ are respectively the mean vorticity and the frame vorticity vectors. To capture the correct sign of the secondary shear stresses for the case of shear with streamwise frame rotation (see section 3.12.4), $C_b = -1.0$. This choice for $C_b$ implies $b_{ij}$ is also dependent on the particular choice for the analysis frame. This again reflects the fact that algebraic models are built for application in frames where the turbulence is closest to an equilibrium condition.

## 3.8 Helix Vector Model

The helix vector $\gamma_k$ is taken as aligned with the total rotation vector,

$$\gamma_k = \gamma \frac{\Omega_k^T}{\sqrt{\Omega_k^T \Omega_k^T}}. \tag{3.25}$$

From 2D RDT it is found that the shear stress correlates well with the normal stresses (see discussion around Equation 3.45), suggesting $\gamma$ can be modeled as

$$\gamma = \beta \sqrt{\frac{2\phi(1-\phi)}{1+\chi}}. \tag{3.26}$$

Equation (3.26) introduces $\beta$, which is indicative of the degree of correlation between fluctuating velocities in different directions.

## 3.9 Structure Scalars

Modeling $\phi$, $\beta$ (see Equation 3.26), and $\chi$ is a crucial part in the construction of the model. The equations for these scalars are found by comparing target turbulent states (well-defined Reynolds-stress and structure-dimensionality tensor configurations), with the result obtained with the constitutive equations of Section 3.5, given a local mean deformation. A

set of parameter values is chosen to mimic the isotropic turbulent state (the eddy structure is expected to consist of axisymmetric ($\chi = 0$), vortical ($\phi = 0$) eddies). Tentative functional forms for the same parameters are chosen with reference to RDT, by comparing RDT stresses and structure tensors with model results (Section 3.5 with eddy-axis tensor and eddy-flattening tensor computed for the given deformation). Interpolation functions (along with model constants) are then chosen to bridge these limiting states (isotropy and RDT). They are selected specially to match a canonical state of sheared turbulence, observed in the log region of a boundary layer.

### 3.9.1 Parameterization

The structure scalars are defined in terms of the mean parameters $\eta_m$, representative of the ratio of mean rotation to mean strain, $\eta_f$, representative of the ratio of frame rotation to mean strain, and $a^2$, a measure of anisotropy. The parameters are defined by

$$\eta_m \equiv \sqrt{\frac{\hat{\Omega}_m^2}{\hat{S}^2}}, \tag{3.27}$$

$$\eta_f \equiv \eta_m - \text{sign}(X)\sqrt{\frac{\hat{\Omega}_T^2}{\hat{S}^2}}, \tag{3.28}$$

$$a^2 \equiv a_{pq}a_{pq}, \tag{3.29}$$

where $\hat{\Omega}_m^2\tau^2$ is a measure of the strength of the mean rotation, $\hat{\Omega}_T^2\tau^2$ is a measure of the strength of the total rotation, and $\hat{S}^2\tau^2$ is a measure of the strength of the mean strain. These are defined by

$$\hat{\Omega}_m^2 \equiv -a_{ij}\Omega_{ik}\Omega_{kj}, \qquad \hat{\Omega}_T^2 \equiv -a_{ij}\Omega_{ik}^T\Omega_{kj}^T, \qquad \hat{S}^2 \equiv a_{ij}S_{ik}S_{kj}, \qquad X \equiv a_{ij}\Omega_{ik}^T S_{kj}, \tag{3.30}$$

and $\tau$, which represents a suitable time scale of the turbulence.

### 3.9.2 Exact Homogeneous 2D RDT Solutions

Throughout the model development there is a strong effort to make it consistent with RDT solutions, aiming to improve model dependability and realizability for a wide range of mean deformations, as well as to obtain guidance in the functional shape chosen for the structure parameters. These RDT forms are later blended with 3C-3D isotropic solutions, in such a way that key intermediate, equilibrium states are matched.

Reynolds and coworkers found analytical solutions for limiting states of the turbulence structure at infinite values of the total shear (or strain) applied, in RDT of three-component (3C), two-dimensional (2D) turbulence for homogeneous flows in the presence of frame rotation:

- Kassinos and Reynolds (to be submitted) investigated 2D turbulence (independent of $x_1$) in homogeneous shear with varying degrees of frame rotation, $\Omega_3^f = \Omega^f$, aligned with the mean flow vorticity, $\Omega_3 = -dU/dy = -\Gamma$,

- Reynolds, Kassinos, and Langer (unpublished) investigated 2D turbulence (independent of $x_1$) in homogeneous hyperbolic flows (plane strain combined with on-plane mean rotation, *e.g.* $S_{12}$ and $\Omega_{12}$, $S_{12}/\Omega_{12} < 1$), again with varying degrees of frame vorticity orthogonal to the mean deformation (aligned with the mean vorticity when that is present).

These solutions identify a trapezoidal region on a $(\eta_f, \eta_m)$ plane for which turbulence grows. The shear flows correspond to $\eta_m = 1$ and any $\eta_f$, while the hyperbolic flows correspond to the region $0 \leq \eta_m < 0$ and any $\eta_f$. The ASBM attempts to capture the RDT value of the structure scalars in this region, in particular the value of $\beta$, which is fundamental in determining the Reynolds shear stress and thus the production of turbulent kinetic energy. $\beta$ should decrease to zero outside of this turbulence growth trapezoidal region.

### Choice of Analysis Frame

To facilitate direct comparison between the limiting RDT results and the ASBM, the RDT results are reported in a coordinate system aligned with the principal coordinates of the eddy-axis tensor, where $a^2 = 1$ (for these RDT limits). Of the flows analyzed here, in the "shear in a rotating frame" and the "plane strain in a rotating frame" cases, this coordinate system coincides with that in which the deformation is originally written (see Equations 3.32 and 3.34). Note that the mean deformation is given in a frame rotating at a rate such that the mean deformation itself, and the limiting RDT forms for the Reynolds stresses and turbulence structure, are constant in this frame.

For the "combined mean strain and mean rotation in a fixed frame" case (Equation 3.39), the results (3.40a–f) are quoted again in principal coordinates of the eddy-axis tensor. Note however that these are not the same coordinates chosen to represent the mean deformation.

As the mean rotation grows compared to the mean strain, the principal coordinates of the eddy-axis tensor turn, as can be seen in Equation (3.21).

### Shear in a Rotating Frame

Kassinos and Reynolds investigated incompressible homogeneous 2D (independent of $x_1$) turbulence subjected to mean shear, $\eta_m = 1$, in a frame rotating about the $x_3$ axis, where

$$G_{ij} = \Gamma \delta_{i1}\delta_{j2}, \qquad \Omega^f_{ij} = \tfrac{1}{2}\Omega^f_z \epsilon_{zji}, \qquad \Omega^f_z = \Omega^f \delta_{z3}, \tag{3.31}$$

are respectively the mean velocity gradient tensor, the frame rotation-rate tensor, and the frame vorticity vector. The frame rotation parameter is $\eta_f = \Omega^f/\Gamma = -\Omega^f_{12}/S_{12}$. In matrix form,

$$S^*_{ij} = \frac{1}{2}\begin{pmatrix} 0 & \Gamma & 0 \\ \Gamma & 0 & 0 \\ 0 & 0 & 0 \end{pmatrix}, \quad \Omega_{ij} = \frac{1}{2}\begin{pmatrix} 0 & \Gamma & 0 \\ -\Gamma & 0 & 0 \\ 0 & 0 & 0 \end{pmatrix}, \quad \Omega^f_{ij} = \frac{1}{2}\begin{pmatrix} 0 & -\Omega^f & 0 \\ \Omega^f & 0 & 0 \\ 0 & 0 & 0 \end{pmatrix}. \tag{3.32}$$

The RDT equations in this case are

$$\frac{\partial u_i'}{\partial x_i} = 0,$$
$$\frac{\partial u_i'}{\partial t} + \Gamma x_2 \frac{\partial u_i'}{\partial x_1} = -\Gamma u_2' \delta_{i1} - \frac{1}{\rho}\frac{\partial p'}{\partial x_i} - 2\Omega^f_{iz} u_z'.$$

Considering turbulence independent of the $x_1$-direction results in

$$\frac{\partial u_1'}{\partial t} = -\Gamma u_2 - 2\Omega^f_{12} u_2', \qquad \frac{\partial u_2'}{\partial t} = -\frac{1}{\rho}\frac{\partial p'}{\partial x_2} - 2\Omega^f_{21} u_1', \qquad \frac{\partial u_3'}{\partial t} = -\frac{1}{\rho}\frac{\partial p'}{\partial x_3},$$
$$\frac{\partial u_1'}{\partial x_1} + \frac{\partial u_2'}{\partial x_2} = 0.$$

Fourier methods are used to find the solution for the Reynolds stresses and dimensionalities. Table 3.1 summarizes the limiting structure and Reynolds stress tensor components for infinite total shear, $\Gamma t$, for the most general initial conditions considered by Kassinos and Reynolds.

Note that in the range $0 < \eta_f < 1$,

$$\frac{|r_{12}|}{\sqrt{r_{11}r_{22}}} = 1. \tag{3.33}$$

| | $\eta_f < 0, \eta_f > 1$ | $0 < \eta_f < 1$ | $\eta_f = 0$ | $\eta_f = 1$ |
|---|---|---|---|---|
| $d_{11}$ | 0 | 0 | 0 | 0 |
| $d_{22}$ | 1/2 | 0 | 1/4 | 1/4 |
| $d_{33}$ | 1/2 | 1 | 3/4 | 3/4 |
| $d_{12}$ | 0 | 0 | 0 | 0 |
| $r_{11}$ | $\frac{\eta_f - 1}{2\eta_f - 1}$ | $1 - \eta_f$ | 1 | 0 |
| $r_{22}$ | $\frac{\eta_f}{2(2\eta_f - 1)}$ | $\eta_f$ | 0 | 3/4 |
| $r_{33}$ | $\frac{\eta_f}{2(2\eta_f - 1)}$ | 0 | 0 | 1/4 |
| $r_{12}$ | 0 | $-\sqrt{\eta_f(1-\eta_f)}$ | 0 | 0 |

Table 3.1: Exact turbulence structure results for shear in a rotating frame. $\eta_f \equiv \Omega_f/\Gamma$

### Plane Strain in a Rotating Frame

In the solution found by Reynolds *et al.* for hyperbolic flows ($\eta_m < 1$), the Reynolds stress and structure dimensionality tensors are given by integrals of hypergeometric functions; there is no simple algebraic form as in the shear case analyzed above. To simplify the model developed later, a polynomial approximation for the exact solution along the line $\eta_m = 0$ is determined. Then the parameters in the region $0 < \eta_m < 1$ are found by interpolating between the results along the lines $\eta_m = 0$ and $\eta_m = 1$.

Here the analysis is restricted for incompressible homogeneous 2D (independent of $x_1$) turbulence subjected to mean plane strain in a frame rotating about the $x_3$ axis. In matrix form, the mean strain rate, mean rotation rate, and mean frame rotation rate tensors are

$$S^*_{ij} = \begin{pmatrix} \Gamma & 0 & 0 \\ 0 & -\Gamma & 0 \\ 0 & 0 & 0 \end{pmatrix}, \quad \Omega_{ij} = \begin{pmatrix} 0 & 0 & 0 \\ 0 & 0 & 0 \\ 0 & 0 & 0 \end{pmatrix}, \quad \Omega^f_{ij} = \frac{1}{2} \begin{pmatrix} 0 & -\Omega^f & 0 \\ \Omega^f & 0 & 0 \\ 0 & 0 & 0 \end{pmatrix}, \tag{3.34}$$

where again,

$$\Omega^f_{ij} = \tfrac{1}{2}\Omega^f_z \epsilon_{zji}, \qquad \Omega^f_z = \Omega^f \delta_{z3}. \tag{3.35}$$

Considering turbulence independent of the $x_1$-direction, the RDT equations for this case are

$$\frac{\partial u_1'}{\partial t} - \Gamma x_2 \frac{\partial u_1'}{\partial x_2} = -\Gamma u_1' - 2\Omega_{12}^f u_2',$$
$$\frac{\partial u_2'}{\partial t} - \Gamma x_2 \frac{\partial u_2'}{\partial x_2} = \Gamma u_2' - \frac{1}{\rho}\frac{\partial p'}{\partial x_2} - 2\Omega_{21}^f u_1',$$
$$\frac{\partial u_3'}{\partial t} - \Gamma x_2 \frac{\partial u_3'}{\partial x_2} = -\frac{1}{\rho}\frac{\partial p'}{\partial x_3},$$
$$\frac{\partial u_1'}{\partial x_1} + \frac{\partial u_2'}{\partial x_2} = 0.$$

Fourier methods are again used to find the solution for the Reynolds stresses and dimensionalities. The solution for different tensor components involves integrals of hypergeometric functions. Tabulated values of the solution ($\eta_m = 0$) are given on Table 3.2. The frame rotation parameter is now $\eta_f = \Omega^f/\Gamma = \Omega_{12}^f/S_{11}$, the ratio of frame vorticity to the mean strain rate.

A good fit to the discrete values from Table 3.2 is given by

$$d_{33} = \frac{1}{2} - \frac{1}{2}\left[0.342\frac{(2\eta_f)^2}{3/4} + (1-0.342)\left(\frac{(2\eta_f)^2}{3/4}\right)^6\right], \tag{3.36}$$

$$r_{11} = 0.145\left[\frac{(2\eta_f)^2}{3/4} - \left(\frac{(2\eta_f)^2}{3/4}\right)^9\right], \tag{3.37}$$

for $0 \le (2\eta_f)^2 \le 3/4$, where $\eta_f = \Omega_{12}^f/\Gamma$. If $(2\eta_f)^2 > 3/4$, then $r_{33} = d_{22} = 1$.

Note that then for plane strain in a rotating frame, each line on Table 3.2 gives

$$\frac{|r_{12}|}{\sqrt{r_{11}r_{22}}} \approx 0.95. \tag{3.38}$$

### Combined Mean Strain and Mean Rotation in a Fixed Frame

To help determine the interpolation function between $\eta_m = 0$ and $\eta_m = 1$, the solution for the 2D turbulence problem of mean strain combined with mean rotation, with no frame rotation, is determined. In a coordinate system $x_i$, the mean deformation has the following matrix form,

$$S_{ij}^* = \frac{1}{2}\begin{pmatrix} 0 & \Gamma & 0 \\ \Gamma & 0 & 0 \\ 0 & 0 & 0 \end{pmatrix}, \quad \Omega_{ij} = \frac{1}{2}\begin{pmatrix} 0 & \Omega & 0 \\ -\Omega & 0 & 0 \\ 0 & 0 & 0 \end{pmatrix}, \quad \Omega_{ij}^f = \begin{pmatrix} 0 & 0 & 0 \\ 0 & 0 & 0 \\ 0 & 0 & 0 \end{pmatrix}. \tag{3.39}$$

| $2\lvert\eta_f\rvert$ | $r_{11}$ | $r_{22}$ | $r_{33}$ | $r_{12}$ | $d_{22}$ | $d_{33}$ |
|---|---|---|---|---|---|---|
| 0 | 0.00 | 0.50 | 0.50 | 0.00 | 0.50 | 0.50 |
| 0.01 | 0.000020457 | 0.49997045 | 0.500009087 | 0.0030684 | 0.50001743 | 0.49998258 |
| 0.1 | 0.0020465 | 0.497034 | 0.5009196 | 0.030595 | 0.501755 | 0.498245 |
| 0.2 | 0.0081940 | 0.48799 | 0.503816 | 0.060627 | 0.507185 | 0.492815 |
| 0.3 | 0.018453 | 0.47239 | 0.509156 | 0.089429 | 0.51683 | 0.48317 |
| 0.4 | 0.032777 | 0.44929 | 0.51793 | 0.11607 | 0.53179 | 0.46821 |
| 0.5 | 0.050892 | 0.41692 | 0.53219 | 0.13904 | 0.55422 | 0.44578 |
| 0.6 | 0.071728 | 0.37173 | 0.55654 | 0.15541 | 0.58857 | 0.41143 |
| 0.7 | 0.091148 | 0.30529 | 0.60356 | 0.15810 | 0.64600 | 0.35400 |
| 0.75 | 0.095793 | 0.25723 | 0.64698 | 0.14834 | 0.69279 | 0.30722 |
| 0.79 | 0.091532 | 0.20464 | 0.70383 | 0.12897 | 0.74872 | 0.25128 |
| 0.8 | 0.088294 | 0.18829 | 0.72341 | 0.12140 | 0.76701 | 0.23299 |
| 0.85 | 0.040454 | 0.067237 | 0.89230 | 0.048868 | 0.913094 | 0.086906 |
| 0.86 | 0.017884 | 0.028178 | 0.953938 | 0.021009 | 0.963211 | 0.036789 |
| 0.865 | 0.0033232 | 0.0050950 | 0.9915818 | 0.0038486 | 0.9933132 | 0.0066868 |
| 0.866 | 0.000083844 | 0.00012784 | 0.99978831 | 0.0000968 | 0.99983204 | 0.00016796 |
| $\sqrt{3/4}$ | 0.00 | 0.00 | 1.00 | 0.00 | 1.00 | 0.00 |

Table 3.2: Integration results for plane strain in a rotating frame. $\eta_f \equiv \Omega_f/\Gamma$

The RDT equations in this frame are

$$\frac{\partial u_i'}{\partial x_i} = 0,$$

$$\frac{\partial u_i'}{\partial t} + (\Gamma+\Omega)x_2\frac{\partial u_i'}{\partial x_1} + (\Gamma-\Omega)x_1\frac{\partial u_i'}{\partial x_2} = -(\Gamma+\Omega)u_2'\delta_{i1} - (\Gamma-\Omega)u_1'\delta_{i2} - \frac{1}{\rho}\frac{\partial p'}{\partial x_i} - 2\Omega_{iz}^f u_z'.$$

The velocities and coordinates are first transformed into velocities and coordinates in a Cartesian frame aligned with the axis of independence of the 2D turbulence, where $a_{11} = 1$. To solve the equations, the coordinate system is further transformed into one deforming with the mean flow (Rogallo transformation). In this system the convective terms, with their explicit dependence on the coordinate axes, vanish. Fourier methods can then be used to find the solution. In this case the integration for the structure dimensionality and the Reynolds stress tensors can be carried out analytically in the infinite deformation limit,

$\Gamma t \to \infty$, to obtain (in a coordinate system aligned with the principal direction of the eddy-axis tensor)

$$r_{22} = r_{33} \to \frac{1}{2}\left[1 + \frac{8}{3}(1 - \ln 2)\zeta^2\right]^{-1}, \tag{3.40a}$$

$$r_{11} \to \frac{8}{3}(1 - \ln 2)\zeta^2\left[1 + \frac{8}{3}(1 - \ln 2)\zeta^2\right]^{-1}, \tag{3.40b}$$

$$r_{12} \to -2(1 - \ln 2)\zeta\left[1 + \frac{8}{3}(1 - \ln 2)\zeta^2\right]^{-1}, \tag{3.40c}$$

$$d_{22} \to r_{33} - \frac{1}{3}(\pi^2 - 12\ln 4 + 3\ln^2 4)\zeta^2\left[1 + \frac{8}{3}(1 - \ln 2)\zeta^2\right]^{-1}, \tag{3.40d}$$

$$d_{33} \to r_{22} + \frac{1}{3}(8 + \pi^2 - 16\ln 4 + 3\ln^2 4)\zeta^2\left[1 + \frac{8}{3}(1 - \ln 2)\zeta^2\right]^{-1}, \tag{3.40e}$$

$$\zeta^2 = \frac{\eta_m^2}{1 - \eta_m^2}, \tag{3.40f}$$

where $\eta_m = \Omega/\Gamma$. Again, to facilitate comparison with the algebraic model, the structure and Reynolds stress tensors are written in principal coordinates of the eddy-axis tensor (found with resort to Equation 3.21), instead of the original coordinates in which the mean deformation was written (Equation 3.39).

Note that in combined mean strain and mean rotation (no frame rotation),

$$\frac{|r_{12}|}{\sqrt{r_{11}r_{22}}} \approx 0.96. \tag{3.41}$$

### 3.9.3 ASBM Solutions

To determine the structure parameters based on the information gathered from the exact RDT solutions, the form of the algebraic Reynolds stress and dimensionality tensors needs to be determined for the same flows. In all cases the direction of the mean and/or frame rotation rate vectors is chosen to be aligned with the $x_3$ direction. Also, in all cases the eddy-axis tensor approaches the one component (1C) point, $a^2 = 1$ in the limit of infinite total strain, when the exact solutions apply. Then in principal coordinates of the eddy-axis tensor,

$$a_{11} = 1, \qquad b_{33} = 1. \tag{3.42}$$

Taking $\Omega_3^T/\sqrt{\Omega_k^T\Omega_k^T} = -1$, results in the following ASBM predictions:

$$d_{11} = 0, \quad d_{12} = 0, \quad d_{22} = \tfrac{1}{2}(1-\chi), \quad d_{33} = \tfrac{1}{2}(1+\chi), \tag{3.43}$$

$$r_{11} = \phi, \quad r_{12} = -\tfrac{1}{2}\gamma(1+\chi), \quad r_{22} = \tfrac{1}{2}(1-\phi)(1+\chi), \quad r_{33} = \tfrac{1}{2}(1-\phi)(1-\chi). \tag{3.44}$$

The model for $\gamma$, Equation (3.26), can be better understood now. It is chosen based on the observation that in the limit of infinite total strain, in RDT, when $r_{12}$ does not vanish, it correlates well with $\sqrt{r_{11}r_{22}}$ (see Equations 3.33, 3.38, and 3.41). $\beta$ is then introduced as a parameter in

$$r_{12} = \beta\sqrt{r_{11}r_{22}}. \tag{3.45}$$

Using the ASBM representation (Equations 3.44) in both sides yields the form chosen for $\gamma$,

$$\tfrac{1}{2}\gamma(1+\chi) = \beta\sqrt{\phi\tfrac{1}{2}(1-\phi)(1+\chi)},$$

$$\gamma = \beta\sqrt{2\phi(1-\phi)/(1+\chi)}. \tag{3.26}$$

Therefore, instead of modeling $\gamma$ directly, the expression above is used in the hope that modeling $\beta$ is much simpler (in fact, in the $a^2 = 1$ plane $\beta = 1$ or $\beta = 0$, depending on whether the turbulent kinetic energy is expected to increase or not).

### 3.9.4 Structure Scalar Models

The structure parameters are defined in a three-dimensional space, in terms of $\eta_m$, $\eta_f$, and $a^2$, which were introduced in Equations 3.27, 3.28, and 3.29. Comparing the 2D RDT exact solutions for the Reynolds stresses and the turbulence structure from Section 3.9.2, with the corresponding ASBM solutions from Section 3.9.3, gives models for the structure parameters in the limit of infinite distortion.

The structure parameters are first defined in a generic $a^2$ plane, along the $\eta_f$ and $\eta_m$ directions, trying to match the 2D RDT solutions when applicable. The structure parameters are then specifically sensitized to the degree of anisotropy of the turbulence, measured along the $a^2$ direction. In this final step an adjustment is made to ensure the structure parameters meet minimal function continuity requirements (found by requiring continuous gradients of the turbulent shear stress in shear flows, *e.g.* a channel flow).

In the generic $a^2$ plane, the structure parameters are defined along the mean-shear line, $\eta_m = 1$, and along the plane-strain line, $\eta_m = 0$, for a generic $a^2$ plane. The structure

parameters are then interpolated or extrapolated in the same $a^2$ plane, depending on the flow location in this $a^2$ plane, specified in terms of $\eta_f$ and $\eta_m$.

In the following, the subscripts "0" and "1" applied to $\phi$, $\beta$, and $\chi$, refer to values along the lines $\eta_m = 0$ and $\eta_m = 1$, respectively. The superscript "*" is used to denote values on the $a^2$ plane where $\eta_m = 0$ and $\eta_m = 1$ were evaluated. The final symbol for the structure parameters is devoid of indices.

**Generic $a^2$ Plane, $\eta_m = 1$ (Mean Flow Corresponds to Shear).**

Comparing the RDT solution, Table 3.1, to the ASBM solution, Equations (3.43) and (3.44), leads to the forms below. Recall that the subscript "1" indicates values computed along the line $\eta_m = 1$.

If $\eta_f < 0$,

$$\phi_1 = \frac{\eta_f - 1}{3\eta_f - 1}, \quad \beta_1 = \frac{1}{1 - b_0 \dfrac{\eta_f}{(1-a^2)}\left(1 + \sqrt{(a^2 - \frac{1}{3})}\right)}, \quad \chi = \frac{1}{2}\beta_1. \tag{3.46}$$

If $0 < \eta_f < 1$,

$$\phi_1 = (1 - \eta_f), \quad \beta_1 = 1, \quad \chi_1 = \frac{1}{2} + \frac{1}{2}\left(1 - \frac{(1-\eta_f)^2}{1 + b_1\eta_f/(1-a^2)}\right). \tag{3.47}$$

If $\eta_f > 1$,

$$\phi_1 = \frac{\eta_f - 1}{3\eta_f - 1}, \quad \beta_1 = \frac{1}{1 + b_2 \dfrac{(\eta_f - 1)}{(1-a^2)}\eta_f\sqrt{(a^2 - \frac{1}{3})}}, \quad \chi_1 = 1 - \frac{(1-\beta_1)(\eta_f - 1)}{(1-a^2) + (\eta_f - 1)}, \tag{3.48}$$

where

$$b_0 = 1.0 \qquad b_1 = 100 \qquad b_2 = 0.8 \tag{3.49}$$

were optimized for channel flow with spanwise frame rotation (aligned with mean flow rotation). Notes:

- $\phi_1(\eta_f \to \pm\infty) \to 1/3$ instead of $1/2$ (suggested by Table 3.1) so that $r_{12} \to 0$ when $\eta_f \to \pm\infty$, regardless of $a_{ij}$. In RDT, $a_{11} \to 1$ and $r_{12} \to 0$ regardless of $\phi$. However, in more general flows it is possible to have $\eta_f \to \pm\infty$ with finite deformations (for example near the zero velocity gradient position in a rotating channel flow). In this case, coupling $\phi \to 1/3$ with $\beta, \chi \to 0$ implies $r_{12} \to 0$ regardless of $a_{ij}$;

- factors of $(1-a^2)$ enforce $\beta \to 0$ when appropriate (RDT limit);
- factors of $(\eta_f\sqrt{a^2-1/3} \propto \Omega^f\tau)$ are used to decrease $\beta_1$, especially at small $\eta_f < 0$ or $\eta_f > 1$, for larger frame rotation rates (consider $\Gamma\tau \propto \sqrt{a^2-1/3}$ and $\eta_f \propto \Omega^f\tau/\Gamma\tau$). A smaller $\beta$ is needed to get the large asymmetries observed in spanwise rotating channel flows. Originally a large constant was used instead of this form, but while that gave a good asymmetry for the high rotation numbers, it also displayed a large asymmetry at small rotation numbers. Hence a function that vanishes at small rotations was chosen.
- for simplicity $\chi_1$ is defined in terms of $\beta_1$ (except where indicated otherwise).

**Generic $a^2$ Plane, $\eta_m = 0$ (Mean Flow Corresponds to Plane Strain).**

Comparing the RDT polynomial approximations, Equations (3.36) and (3.37), to the ASBM solution, Equations (3.43) and (3.44), leads to the following (recall that the subscript "0" is used to indicate values computed along the line $\eta_m = 0$):

If $\eta_f \leq \sqrt{3}/4$,

$$\phi_0 = 0.145\left[\frac{(2\eta_f)^2}{3/4} - \left(\frac{(2\eta_f)^2}{3/4}\right)^9\right], \tag{3.50}$$

$$\beta_0 = 1, \tag{3.51}$$

$$\chi_0 = -\left[0.342\frac{(2\eta_f)^2}{3/4} + (1-0.342)\left(\frac{(2\eta_f)^2}{3/4}\right)^6\right], \tag{3.52}$$

else, if $\eta_f > \sqrt{3}/4$,

$$\beta_0 = \left[1 + b_3\frac{(\eta_f - \sqrt{3}/4)}{(1-a^2)}\eta_f\sqrt{(a^2-\tfrac{1}{3})}\right]^{-1}, \tag{3.53}$$

$$\chi_0 = -\beta_0, \tag{3.54}$$

$$\phi_0 = (1-\beta_0)/3, \tag{3.55}$$

where $b_3 = 1.0$. Equations (3.53–3.55) are arbitrary functional forms. The objective is to retrieve $\phi_0 = 1/3$ and $\chi_0 = \beta_0 = 0$ for large $\eta_f$ and/or $a^2 \to 1$. The 2D-RDT plane strain solution actually applies for all $\eta_f$, predicting $\phi = 0$ and $\chi = -1$ for $\eta_f > \sqrt{3}/4$. So both the functional shapes and the threshold of $\eta_f$ after which they are applied are arbitrary.

### Generic $a^2$ Plane, Interpolation Between $\eta_m = 0$ and $\eta_m = 1$

As mentioned earlier, there is a trapezoidal region in the $(\eta_m, \eta_f, a^2 = 1)$ plane where the turbulence kinetic energy grows for two-dimensional turbulence. There is an exact solution for the Reynolds stresses and for the structure dimensionalities (and in turn for the structure parameters) for each point in this parallelogram, which however is not in a simple algebraic form. It involves integrals of hypergeometric functions. To circumvent specifying values at each point, values are specified along the edges of the parallelogram, and then interpolated inside. The interpolation actually is done for every point between the lines $\eta_m = 0$ and $\eta_m = 1$, it just relates to an exact solution inside the quadrangle; outside of it the exact solution predicts decay of turbulence, so all that is required is something that drives the turbulence to zero, notably $\beta \to 0$.

The interpolation function is selected based on the simpler case of combined mean strain and mean rotation in a fixed frame, $\eta_f = 0$, for which an exact closed-form RDT-solution exists for the turbulence structure. The variation of the exact solution between $\eta_m = 0$ and $\eta_m = 1$, for other values of $\eta_f$ is not expected to differ substantially. Other interpolation schemes could be tried in the future if deemed necessary.

Comparing the 2D RDT solution for combined mean strain and mean rotation in a fixed frame, Equations (3.40a–f), to the ASBM solution, Equations (3.43) and (3.44), gives the variation for the structure parameters along $0 \leq \eta_m \leq 1$, when $\eta_f = 0$,

$$\phi = \frac{\frac{8}{3}(1 - \ln 2)\eta_m^2/(1 - \eta_m^2)}{1 + \frac{8}{3}(1 - \ln 2)\eta_m^2/(1 - \eta_m^2)} \approx \eta_m^{2.25}, \tag{3.56}$$

$$\chi = \frac{1 + \frac{2}{3}(8 + \pi^2 - 16\ln 4 + 3\ln^2 4)\eta_m^2/(1 - \eta_m^2)}{1 + \frac{8}{3}(1 - \ln 2)\eta_m^2/(1 - \eta_m^2)} \approx 0.185\eta_m^{2.25}. \tag{3.57}$$

Notice the discontinuity between the value of $\chi$ for shear on a stationary frame, $\chi = 1/2$, and its limiting value for combined strain and rotation, $\chi \approx 0.185$. On this work the former value is used in the shear limit. The approximate profiles are used nevertheless as guides to the interpolation formulas.

To simplify the interpolation, the trapezoid where there is turbulence growth is transformed into a rectangle with the transformation

$$\eta_* \equiv -\eta_m + [4/\sqrt{3} + (2 - 4/\sqrt{3})\eta_m]\eta_f. \tag{3.58}$$

The structure parameters are then interpolated along lines of constant $\eta_*$ (in the region

$\eta_m \leq 1$) according to

$$\phi^* = \phi_0(\eta_*) + [\phi_1(\eta_*) - \phi_0(\eta_*)]\eta_m^2, \tag{3.59}$$

$$\beta^* = \beta_0(\eta_*) + [\beta_1(\eta_*) - \beta_0(\eta_*)]\eta_m^2, \tag{3.60}$$

$$\chi^* = \chi_0(\eta_*) + [\chi_1(\eta_*) - \chi_0(\eta_*)]\eta_m^4. \tag{3.61}$$

Note that the combined mean strain and rotation solution is abandoned in favor of a profile that reaches $\chi = 1/2$ smoothly at the shear point.

### Generic $a^2$ Plane, Extrapolation for $\eta_m > 1$

There is no exact steady solution for the region $\eta_m > 1$. In this region the turbulence structure probably reaches a limiting state where it oscillates periodically (see Blaisdell and Shariff 1996). On the other hand the algebraic model responds to the amount of deformation applied. If the normalized deformation rate is steady, the response of the model is also steady, so it cannot predict a limit cycle. Nevertheless rotation is expected to have a decorrelating effect on the turbulence, so the structure parameters are modeled to reflect this. In particular, as the mean rotation grows for a fixed strain ($\eta_m \to \infty$), $\beta$ and $\chi$ are driven to zero, while $\phi$ is driven to 1/3 (for consistency with the case of infinite $\eta_f$ in the case $\eta_m = 1$ investigated previously). Hence the structure parameters are extrapolated from the $\eta_m > 1$ line according to

$$\phi^* = 1/3 + \frac{(\phi_1(\eta_f) - 1/3)}{1 + (\eta_m - 1)/(1 - a^2)}, \tag{3.62}$$

$$\beta^* = \frac{\beta_1(\eta_f)}{1 + (\eta_m - 1)/(1 - a^2)}, \tag{3.63}$$

$$\chi^* = \frac{\chi_1(\eta_f)}{1 + (\eta_m - 1)/(1 - a^2)}. \tag{3.64}$$

These are also arbitrary functions.

### $a^2$ Direction (Anisotropy Characterization), and Function Continuity

So far the structure parameters have been set on a given $a^2$ plane. For $\phi_1$ this is the $a^2 = 1$ plane, except for a possible dependence of $\eta_m$ and $\eta_f$ on the state of the eddy-axis tensor. The other scalars, $\beta_1$ and $\chi_1$, have been sensitized to $a^2$ in some form, depending on the position of the flow in the $(\eta_m, \eta_f)$ plane. At this point there are two final conditions to be met:

(i) in isotropic (undeformed) turbulence with $a^2 = 1/3$, the structure is expected to consist of axisymmetric, ($\chi = 0$), vortical, ($\phi = 0$), eddies;

(ii) the structure parameters $\phi$, $\gamma$, and $\chi$, need to be C1 continuous functions of $\eta_f$, for all $\eta_f$. When $\eta_f \to \eta_m$, $\beta$ needs to be only C0 continuous with respect to $\eta_f$, while $\phi$ needs to be $O((\eta_f - \eta_m)^3)$ as $\eta_f \to \eta_m$. These requirements arrive because of the requirement that the Reynolds stresses be C1 continuous, such that their spatial gradient in the momentum equation be C0 continuous.

These conditions are explored in more detail at the end of this section, looking at the particular case of shear in a rotating frame.

The final model for the structure parameters, satisfying these conditions, is (for near-wall regions see Equations 3.80 and 3.81)

$$\phi = \phi^* \left( \frac{(\eta_m - \eta_f)^2}{(\eta_m - \eta_f)^2 + (1 - a^2)^2} \right) \left( \frac{|\eta_m - \eta_f| \sqrt{\frac{3}{2}(a^2 - \frac{1}{3})}}{|\eta_m - \eta_f| \sqrt{\frac{3}{2}(a^2 - \frac{1}{3})} + p_0 (1 - a^2)} \right), \tag{3.65}$$

$$\beta = \beta^*, \tag{3.66}$$

$$\chi = \chi^* \left[ \frac{3}{2} \left( a^2 - \frac{1}{3} \right) \right]^{p_1}, \tag{3.67}$$

where

$$p_0 = 1.3 \qquad p_1 = 1.0 \tag{3.68}$$

were optimized along with $a_0$ (Equation 3.15) in order to satisfy the key condition on a boundary layer in zero pressure gradient observed experimentally,

$$\frac{R_{12}}{q^2} = -0.15, \quad \text{simultaneously with} \quad \frac{P}{\varepsilon} = -4 r_{12} \frac{S_{12} k}{\varepsilon} = 1, \tag{3.69}$$

where $x_1$ and $x_2$ are respectively the streamwise and wall-normal directions. Further guidance for the model constants was provided by the normal stresses ($r_{11} = 0.53$, $r_{22} = 0.19$, and $r_{33} = 0.28$ are representative values in the log region of the DNS of Kim (1992), for a channel flow at $Re_\tau = 385$).

Notes:

- the factor $[3/2(a^2 - 1/3)]$ is an interpolant between the isotropic state, when it is zero, and the 1C condition for $a_{ij}$ ($a^2 = 1$), when it is one;
- the factors of $(1 - a^2)$ in $\phi$ are such that the RDT form is recovered for $a^2 = 1$, while the factors of $(\eta_m - \eta_f)$ give the proper degree of continuity required of $\phi$ such that item (ii) above is satisfied.

To elaborate in the functional form used in Equations 3.65 and 3.67 consider the case of shear in a spanwise-rotating frame. The mean deformation is given by Equation (3.32), the flattening tensor is $b_{ij} = \delta_{i3}\delta_{j3}$ and the eddy-axis tensor becomes

$$a_{ij} = \begin{pmatrix} a_{11} & a_{12} & 0 \\ a_{12} & a_{22} & 0 \\ 0 & 0 & a_{33} \end{pmatrix}. \tag{3.70}$$

The normalized Reynolds stress tensor then is (recall $r_{33} = 1 - r_{11} - r_{22}$)

$$\begin{aligned} r_{11} &= (1-\phi)\tfrac{1}{2}(1-a_{11}) + \phi a_{11} + (1-\phi)\chi\left[\tfrac{1}{2}(1-a_{33}) - \tfrac{1}{2}(1+a_{33})a_{11}\right] \\ &\quad + (-\gamma\Omega_3^T/\Omega^T)a_{21}[1+\chi(1-a_{33})], \end{aligned} \tag{3.71a}$$

$$\begin{aligned} r_{22} &= (1-\phi)\tfrac{1}{2}(1-a_{22}) + \phi a_{22} + (1-\phi)\chi\left[\tfrac{1}{2}(1-a_{33}) - \tfrac{1}{2}(1+a_{33})a_{22}\right] \\ &\quad + (\gamma\Omega_3^T/\Omega^T)a_{12}[1+\chi(1-a_{33})], \end{aligned} \tag{3.71b}$$

$$\begin{aligned} r_{12} &= -(1-\phi)\tfrac{1}{2}a_{12} + \phi a_{12} + (1-\phi)\chi\left[-\tfrac{1}{2}(1+a_{33})a_{12}\right] \\ &\quad + (\gamma\Omega_3^T/\Omega^T)(a_{11}-a_{22})\tfrac{1}{2}[1+\chi(1-a_{33})]. \end{aligned} \tag{3.71c}$$

A first observation is that in a fixed frame of reference with positive $\Gamma = G_{12}$, the ASBM (Equations 3.15 and 3.16) predicts $a_{22} = a_{33} < a_{11}$ and $a_{12} > 0$. Additionally, when $\Gamma\tau \to 0$, the ASBM predicts $a_{11} - a_{22} = O((\Gamma\tau)^2)$ and $a_{12} = O(\Gamma\tau)$. Inspection of the constitutive relation, Equation (3.71c) reveals that if $\phi > 1/3$ as $\Gamma\tau \to 0$, then $r_{12} > 0$, *i.e.* a negative eddy viscosity in an equivalent Boussinesq approximation, which should not happen in this flow (homogeneous shear in a fixed frame of reference). Enforcing $\phi \to 0$ when $\Gamma\tau \to 0$ prevents it from happening.

The continuity requirements of the structure parameters were analyzed in detail for the case of shear flow in a rotating frame, corresponding to all the wall-bounded flows investigated in the present work. Particular attention is given to the shear stress $r_{12}$. For a given frame rotation rate, condition (ii) above requires continuity of $\partial r_{12}/\partial\eta_f(\eta_f)$. Inspection of equation (3.71c) shows that this in turn requires $\phi(\eta_f)$, $\chi(\eta_f)$, and $\gamma(\eta_f)$ to be C1 continuous. C1 continuity of $\gamma$ requires in turn $\beta(\eta_f)$ to be C1 continuous (if $\phi \neq 0$) and $\sqrt{\phi}$ to be C1 continuous. Along the shear line ($\eta_m$=1) Equations (3.46), (3.47), and (3.48) were made piecewise continuous. The boundary at $\eta_f = 0$ is not an issue, because no two adjacent points in a channel flow cross this boundary. In fact, $\eta_f \to \pm 0$ as either wall of a channel is approached. The boundary at $\eta_f = 1$ definitely is crossed somewhere in the flow.

Because $\phi = 0$ at this point, $\beta$ need only be C0 continuous. It can be shown by expanding $\phi$ in a Taylor series that the C1 continuity requirement on $\sqrt{\phi}$ demands $\phi = O((\eta_f - 1)^3)$ as $\eta_f \to 1$. Equation (3.65) was constructed to achieve just that.

## 3.10 Wall Blockage

As a no-slip wall is approached, the tangential components of the velocity are driven to zero through the action of viscous forces. Additionally, the velocity vector is reoriented into planes parallel to the wall through an inviscid mechanism (wall blocking) which acts over distances far larger than the viscous length scale. The end result is that the velocity component normal to the wall is driven to zero faster than the tangential components.

Here wall blocking is modeled through the use of a modified projection operator, applied to the tensor (and/or vector) to be blocked, as in Reynolds *et al.* (2000). The strength of the projection depends on the proximity to the nearest wall, as measured by a scalar.

In the structure-based model it is postulated that at the wall all eddies shall lie in the plane of the wall. Wall-blocking is then introduced to reorient the eddies into planes parallel to the wall. The structure parameters are also sensitized to wall blocking, such that the velocity components induced by the eddies are consistent with the asymptotic behavior or the turbulence velocities near walls.

If all eddies are parallel to the wall, the jetal mode of motion represents motion strictly parallel to the wall. The vortical mode however typically involves a velocity perpendicular to the wall. To eliminate this contribution, two different approaches can be proposed. The first regards flattening of the vortical motion around the eddies. If vortical motion were to happen on a fully flattened eddy (resembling a sheet on the plane of the wall), then no normal velocity would be generated. Alternatively, one can postulate the absence of vortical motion at the wall, allowing only jetal motion. This also prevents the existence of a normal velocity at the wall.

It would seem that a less intrusive form of blocking would enforce flattening of the vortical part of the motion only. However, this would require some form of conditional sampling and flattening, which increases the complexity of modeling. Simpler alternatives are (i) fully flattening all eddies on the plane of the wall or (ii) enforcing fully jetal eddies.

Full flattening is not attractive, because of its secondary effect of causing $d_{22} \to 1$ (taking $x_2$ to be the direction normal to the wall). The fully jetal alternative is more palatable,

as least in the presence of shear. Shear flows in the presence of walls display mostly jetal motion anyway, so enforcing $\phi = 1$ does not change the character of the eddy representation substantially. However, applying the model in shear-free wall-bounded flows may require a reevaluation of this approach.

### Blockage: Modeling Approach

Following Reynolds *et al.* (2000), the homogeneous eddy-axis tensor, $a^h_{ij}$, is computed based on the homogeneous algebraic procedure, Equations (3.15) and (3.16) (note that the superscript "h" has been added in the current section). It is then partially projected onto planes parallel to the wall,

$$a_{ij} = H_{ik}H_{jl}a^h_{kl}, \tag{3.72}$$

where the superscript $h$ indicates an homogeneous, unblocked, quantity. Similarly to the regular projection operator (see Strang 1993), the partial-projection operator is defined as

$$H_{ik} = \frac{1}{D_a}(\delta_{ik} - B_{ik}), \qquad D_a^2 = 1 - (2 - B_{kk})a^h_{mn}B_{nm}, \tag{3.73}$$

where $D_a^2$ is such that the trace of $a_{ij}$ remains unity. The blockage tensor $B_{ij}$ gives the strength and the direction of the projection. If the wall-normal direction is $x_2$, then $B_{22}$ is the sole nonzero component, and varies between 0 (no blocking) far enough from the wall, to 1 (full blocking) at the wall. If $B_{22} = 1 - O(y)$ as $y \to 0$ (approaching the wall), then the "2"-component of the blocked tensor is dampened as $O(y)$. Thus $a_{12} = O(y)$ and $a_{22} = O(y^2)$, while the trace $a_{ii} = 1$ is preserved.

Inspired by Durbin and coworkers (Durbin and Pettersson Reif 2002; Parneix *et al.* 1998), $B_{ij}$ is computed by a method involving an elliptic relaxation equation,

$$L^2\frac{\partial^2\Phi}{\partial x_k \partial x_k} = \Phi, \qquad L\frac{u_\tau}{\nu} = 23, \tag{3.74}$$

$$\Phi = 1 \quad \text{at solid boundaries,} \tag{3.75}$$

$$\Phi_{,n} \equiv \frac{\partial\Phi}{\partial x_n} = 0 \quad \text{at open boundaries,} \tag{3.76}$$

where $x_n$ is the direction normal to the boundary. $B_{ij}$ is computed by

$$B_{ij} = \frac{\Phi_{,i}\Phi_{,j}}{\Phi_{,k}\Phi_{,k}}\Phi \quad \text{if} \quad \Phi_{,k}\Phi_{,k} > 0. \tag{3.77}$$

If all gradients of $\Phi$ vanish, $B_{ij}$ is computed from an average over surrounding points. Expanding on a Taylor series,

$$B_{ij} = \frac{\Phi_{,ip}\Phi_{,jp}}{\Phi_{,kq}\Phi_{,kq}}\Phi \quad \text{if} \quad \Phi_{,k}\Phi_{,k} = 0. \tag{3.78}$$

The length scale in the elliptic relaxation equation, (3.74), is modeled as a constant: a first order model. In a parallel channel flow, this implies that $B_{22}$ becomes a hyperbolic cosine function of the distance to the wall. However in complex flows $u_\tau$ (used for normalizing $L$ in Equation 3.74) may be ill defined. For instance, near the separation and reattachment points of a complex flow $u_\tau$ vanishes. Additionally, in a complex flow region (*e.g.* near a corner) it may not be clear what should be used for $u_\tau$. Therefore, in general flows a more elaborate model for $L$, in terms of local turbulent ($k^{3/2}/\varepsilon$) and Kolmogorov ($(\nu^3/\varepsilon)^{1/4}$) length scales, should be adopted.

The specific value for $L$ was chosen to reproduce the intercept $C$ in the logarithmic law of the wall for the mean velocity,

$$U/u_\tau = (1/\kappa)\log(yu_\tau/\nu) + C$$

where $U$ is the local mean velocity, $u_\tau^2$ is the wall shear stress divided by the density, and $y$ is the distance to the wall. The blocking modification reduces the Reynolds shear stress near the wall, with the amount of reduction depending on the value of $L$. $L$ then has a strong influence over the intercept $C$ in the log law. Away from the wall, the wall blocking modification dies out, so it does not affect the slope of the log law.

In Reynolds *et al.* (2000) the projection operation was also performed on the homogeneous Reynolds stresses. Here this approach is abandoned, and instead the structure and the Reynolds stresses are computed based on blocked $a_{ij}$, $\phi$, and $\gamma_k$. This generates realizable tensors even in presence of wall blocking.

Turning back to the channel flow, with $B_{22} = 1 - O(y)$, $a_{12} = O(y)$, and $a_{22} = O(y^2)$, the blocked normalized Reynolds-stress components (Equations 3.71b,c) become

$$r_{22} = (1-\phi)\tfrac{1}{2} + (1-\phi)\chi\,[\tfrac{1}{2}(1-a_{33})] + (\gamma\Omega_3^T/\Omega^T)a_{12}[1+\chi(1-a_{33})] + O(y^2), \tag{3.79a}$$

$$r_{12} = (\gamma\Omega_3^T/\Omega^T)a_{11}\tfrac{1}{2}[1+\chi(1-a_{33})] + O(y). \tag{3.79b}$$

The proper asymptotic behavior of the Reynolds stresses, $r_{12} \propto O(y)$ and $r_{22} \propto O(y^2)$, is recovered if the jetal parameter behaves as $\phi = 1 - O(y^2)$, and the helix parameter $\gamma$ behaves

as $\gamma = O(y)$. To achieve that, they are blocked using

$$\phi = 1 + (\phi^h - 1)(1 - B_{kk})^2, \tag{3.80}$$

$$\gamma = \gamma^h (1 - B_{kk}), \tag{3.81}$$

where $\phi^h$ and $\gamma^h$ are respectively the homogeneous jetal parameter and the homogeneous helix parameter. The trace, $B_{kk}$, is used instead of the component in the wall-normal direction, $B_{nn}$ (no summation) where $x_n$ is the wall-normal direction. They are both $1 - O(y)$ near the wall, but $B_{kk} = \Phi$ is simpler because it does not require the specification of a wall-normal direction everywhere in the flow. Away from the wall, when $B_{kk} \to 0$, both parameters approach their homogeneous values.

A consequence of this approach is that as the structure tensors are derived from the eddy-axis tensor, realizability is automatically satisfied for $r_{ij}$, $d_{ij}$ and $f_{ij}$. Furthermore the fundamental constitutive equation relating the three tensors remains satisfied, as the representation of the vector triad ($\vec{v}$, $\vec{s}$, $\vec{n}$) in eddy-axis coordinates remains unaltered.

## 3.11 Model Summary

Given a mean strain-rate tensor, mean rotation-rate tensor and frame-rotation-rate tensor, $S_{ij}$, $\Omega_{ij}$, and $\Omega^f_{ij}$ respectively, with the total rotation-rate tensor $\Omega^T_{ij} = \Omega_{ij} + \Omega^f_{ij}$, and a time scale of the turbulence, $\tau$, compute:

### 3.11.1 Homogeneous Structure

**Strained $a^s_{ij}$.**

$$a^s_{ij} = \frac{1}{3}\delta_{ij} + \frac{(S^*_{ik}a^s_{kj} + S^*_{jk}a^s_{ki} - \frac{2}{3}S^*_{mn}a^s_{nm}\delta_{ij})\tau}{a_0 + 2\sqrt{\tau^2 S^*_{kp}S^*_{kq}a^s_{pq}}}, \tag{3.15}$$

where $S^*_{ij} = S_{ij} - S_{kk}\delta_{ij}/3$ is the traceless strain-rate tensor.

**Rotation Operation, Producing the Homogeneous $a_{ij}$.**

$$a_{ij} = H_{ik}H_{jl}a^s_{kl}, \tag{3.16}$$

where

$$H_{ij} = \delta_{ij} + h_1 \frac{\Omega_{ij}}{\sqrt{\Omega_{pp}^2}} + h_2 \frac{\Omega_{ik}\Omega_{kj}}{\Omega_{pp}^2}, \tag{3.17}$$

where $\Omega_{pp}^2 = \Omega_{pq}\Omega_{pq}$, and

$$h_1 = \sqrt{2h_2 - h_2^2/2}, \tag{3.19}$$

$$h_2 = \begin{cases} 2 - 2\sqrt{\frac{1}{2}(1+\sqrt{1-r})} & \text{if } r \le 1 \\ 2 - 2\sqrt{\frac{1}{2}(1-\sqrt{1-1/r})} & \text{if } r \ge 1, \end{cases} \tag{3.22}$$

$$r = \frac{a_{pq}\Omega_{qr}S_{rp}^*}{S_{kn}^* S_{nm}^* a_{mk}}. \tag{3.23}$$

**Flattening Tensor Model**

$$b_{ij} = \frac{(\Omega_i + C_b\Omega_i^f)(\Omega_j + C_b\Omega_j^f)}{(\Omega_k + C_b\Omega_k^f)(\Omega_k + C_b\Omega_k^f)}, \tag{3.24}$$

where $\Omega_i$ and $\Omega_i^f$ are respectively the mean vorticity and the frame vorticity vectors.

**Helix Vector Model**

$$\gamma_k = \gamma \frac{\Omega_k^T}{\sqrt{\Omega_k^T \Omega_k^T}}, \qquad \gamma = \beta\sqrt{\frac{2\phi(1-\phi)}{1+\chi}}. \tag{3.25–3.26}$$

**Structure Scalars: Parameterization**

$$\eta_m \equiv \sqrt{\frac{\hat{\Omega}_m^2}{\hat{S}^2}}, \qquad \eta_f \equiv \eta_m - \text{sign}(X)\sqrt{\frac{\hat{\Omega}_T^2}{\hat{S}^2}}, \qquad a^2 \equiv a_{pq}a_{pq}, \tag{3.27–3.29}$$

$$\hat{\Omega}_m^2 \equiv -a_{ij}\Omega_{ik}\Omega_{kj}, \qquad \hat{\Omega}_T^2 \equiv -a_{ij}\Omega_{ik}^T\Omega_{kj}^T, \qquad \hat{S}^2 \equiv a_{ij}S_{ik}S_{kj}, \qquad X \equiv a_{ij}\Omega_{ik}^T S_{kj}. \tag{3.30}$$

**Structure Scalars; $a^2$ Plane, $\eta_m = 1$**

If $\eta_f < 0$,

$$\phi_1 = \frac{\eta_f - 1}{3\eta_f - 1}, \quad \beta_1 = \frac{1}{1 - b_0 \dfrac{\eta_f}{(1-a^2)}\left(1 + \sqrt{(a^2 - \frac{1}{3})}\right)}, \quad \chi = \frac{1}{2}\beta_1, \tag{3.46}$$

else, if $0 < \eta_f < 1$,

$$\phi_1 = (1 - \eta_f), \quad \beta_1 = 1, \quad \chi_1 = \frac{1}{2} + \frac{1}{2}\left(1 - \frac{(1-\eta_f)^2}{1 + b_1\eta_f/(1-a^2)}\right), \tag{3.47}$$

else, if $\eta_f > 1$,

$$\phi_1 = \frac{\eta_f - 1}{3\eta_f - 1}, \quad \beta_1 = \frac{1}{1 + b_2 \dfrac{(\eta_f - 1)}{(1-a^2)}\eta_f\sqrt{(a^2 - \frac{1}{3})}}, \quad \chi_1 = 1 - \frac{(1-\beta_1)(\eta_f - 1)}{(1-a^2) + (\eta_f - 1)}. \tag{3.48}$$

**Structure Scalars; $a^2$ Plane, $\eta_m = 0$**

If $\eta_f \leq \sqrt{3}/4$,

$$\phi_0 = 0.145\left[\frac{(2\eta_f)^2}{3/4} - \left(\frac{(2\eta_f)^2}{3/4}\right)^9\right], \tag{3.50}$$

$$\beta_0 = 1, \tag{3.51}$$

$$\chi_0 = -\left[0.342\frac{(2\eta_f)^2}{3/4} + (1 - 0.342)\left(\frac{(2\eta_f)^2}{3/4}\right)^6\right], \tag{3.52}$$

else, if $\eta_f > \sqrt{3}/4$,

$$\beta_0 = \left[1 + b_3\frac{(\eta_f - \sqrt{3}/4)}{(1-a^2)}\eta_f\sqrt{(a^2 - \tfrac{1}{3})}\right]^{-1}, \tag{3.53}$$

$$\chi_0 = -\beta_0, \tag{3.54}$$

$$\phi_0 = (1 - \beta_0)/3. \tag{3.55}$$

**Structure Scalars; $a^2$ Plane, Interpolation Along the $(\eta_m, \eta_f)$ Directions**

If $\eta_m \leq 1$,

$$\eta_* \equiv -\eta_m + [4/\sqrt{3} + (2 - 4/\sqrt{3})\eta_m]\eta_f, \tag{3.58}$$

$$\phi^* = \phi_0(\eta_*) + [\phi_1(\eta_*) - \phi_0(\eta_*)]\eta_m^2, \tag{3.59}$$

$$\beta^* = \beta_0(\eta_*) + [\beta_1(\eta_*) - \beta_0(\eta_*)]\eta_m^2, \tag{3.60}$$

$$\chi^* = \chi_0(\eta_*) + [\chi_1(\eta_*) - \chi_0(\eta_*)]\eta_m^4, \tag{3.61}$$

else, if $\eta_m > 1$

$$\phi^* = 1/3 + \frac{(\phi_1(\eta_f) - 1/3)}{1 + (\eta_m - 1)/(1 - a^2)}, \tag{3.62}$$

$$\beta^* = \frac{\beta_1(\eta_f)}{1 + (\eta_m - 1)/(1 - a^2)}, \tag{3.63}$$

$$\chi^* = \frac{\chi_1(\eta_f)}{1 + (\eta_m - 1)/(1 - a^2)}. \tag{3.64}$$

**Structure Scalars, Final Homogeneous Expression**

$$\phi = \phi^* \left( \frac{(\eta_m - \eta_f)^2}{(\eta_m - \eta_f)^2 + (1 - a^2)^2} \right) \left( \frac{|\eta_m - \eta_f| \sqrt{\frac{3}{2}(a^2 - \frac{1}{3})}}{|\eta_m - \eta_f| \sqrt{\frac{3}{2}(a^2 - \frac{1}{3})} + p_0(1 - a^2)} \right), \tag{3.65}$$

$$\beta = \beta^*, \tag{3.66}$$

$$\chi = \chi^* \left[ \frac{3}{2} \left( a^2 - \frac{1}{3} \right) \right]^{p_1}. \tag{3.67}$$

### 3.11.2 Wall Blockage

In what follows a subscript $h$ indicates a homogeneous quantity, as computed above. The homogeneous quantities are modified for near wall effects as

$$a_{ij} = H_{ik} H_{jl} a_{kl}^h, \tag{3.72}$$

$$H_{ik} = \frac{1}{D_a}(\delta_{ik} - B_{ik}), \qquad D_a^2 = 1 - (2 - B_{kk}) a_{mn}^h B_{nm}, \tag{3.73}$$

$$\phi = 1 + (\phi^h - 1)\,(1 - B_{kk})^2\,, \tag{3.80}$$

$$\gamma = \gamma^h\,(1 - B_{kk})\,, \tag{3.81}$$

where

$$B_{ij} = \begin{cases} \dfrac{\Phi_{,i}\Phi_{,j}}{\Phi_{,k}\Phi_{,k}}\Phi & \text{if} \quad \Phi_{,k}\Phi_{,k} > 0 \\ \dfrac{\Phi_{,ip}\Phi_{,jp}}{\Phi_{,kq}\Phi_{,kq}}\Phi & \text{if} \quad \Phi_{,k}\Phi_{,k} = 0, \end{cases} \tag{3.77–3.78}$$

and

$$L^2\frac{\partial^2\Phi}{\partial x_k \partial x_k} = \Phi, \quad L\frac{u_\tau}{\nu} = 23, \tag{3.74}$$

$$\Phi = 1 \quad \text{at solid boundaries,} \tag{3.75}$$

$$\Phi_{,n} \equiv \frac{\partial\Phi}{\partial x_n} = 0 \quad \text{at open boundaries,} \tag{3.76}$$

where $x_n$ is the direction normal to the boundary.

Finally the structure parameters are modified as

$$\phi = 1 + (\phi^h - 1)\,(1 - B_{kk})^2\,, \tag{3.80}$$

$$\gamma = \gamma^h\,(1 - B_{kk})\,, \tag{3.81}$$

Note that $\chi$ is not modified near the wall.

### Normalized Structure Tensors: Reynolds Stress, Dimensionality, and Circulicity

$$\begin{aligned} d_{ij}^{cc} &= \tfrac{1}{2}[1 - \chi(1 - a_{nm}b_{mn})]\delta_{ij} \\ &\quad - \tfrac{1}{2}[1 - \chi(1 + a_{nm}b_{mn})]a_{ij} + \chi b_{ij} - \chi(a_{in}b_{nj} + a_{jn}b_{ni}), \end{aligned} \tag{3.12}$$

$$\begin{aligned} r_{ij} &= (1-\phi)\tfrac{1}{2}(\delta_{ij} - a_{ij}) + \phi a_{ij} \\ &\quad + (1-\phi)\chi\,[\tfrac{1}{2}(1 - a_{nm}b_{mn})\delta_{ij} - \tfrac{1}{2}(1 + a_{nm}b_{mn})a_{ij} - b_{ij} + a_{in}b_{nj} + a_{jn}b_{ni}] \\ &\quad + (-\gamma\Omega_k^T/\Omega^T)(\epsilon_{ipr}a_{pj} + \epsilon_{jpr}a_{pi})\{\tfrac{1}{2}[1 - \chi(1 - a_{nm}b_{mn})]\delta_{kr} + \chi b_{kr} - \chi a_{kn}b_{nr}\}, \end{aligned} \tag{3.13}$$

$$f_{ij}^{cc} = \delta_{ij} - r_{ij} - d_{ij}. \tag{3.14}$$

### Model Constants

The set of model constants used with the model are

$$a_0 = 1.6, \quad C_b = -1.0, \quad b_0 = 1.0, \quad b_1 = 100, \quad b_2 = 0.8, \quad b_3 = 1.0, \quad p_0 = 1.3, \quad p_1 = 1.0. \tag{3.82}$$

## 3.12 Response of the Homogeneous ASBM to Various Normalized Deformation Rates

The behavior of the algebraic model equations that determine the turbulence structure and Reynolds stresses is investigated for various normalized deformation rates, corresponding to different mean flows and different ratios of the turbulent time scale to the mean flow time scale. In particular the model response to frame rotation is sought. It cannot be overemphasized that the results from this section do *not* correspond to a time integration of the turbulence equations. The algebraic equations for the turbulence structure (section 3.11.1) return a turbulent state to a given mean normalized deformation rate, irrespective of any time history. Results here display the response of the algebraic equations (the algebraic model for the structure) to different combinations of mean normalized deformation rates.

### 3.12.1 Irrotational Flows

Flows with no mean and frame rotation (*e.g.* plane strain or axisymmetric contraction/expansion) correspond to the $(0,0)$ point in the $(\eta_m, \eta_f)$ plane, and the algebraic expressions for the structure scalars return $\phi = \chi = 0$ (implying $\gamma_k = 0$) irrespective of the normalized strain rate (which is measured here by $a^2$). The constitutive relations (3.12–3.14) then return

$$d_{ij} = r_{ij} = \tfrac{1}{2}(\delta_{ij} - a_{ij}), \qquad f_{ij} = a_{ij}, \tag{3.83}$$

as predicted in Kassinos and Reynolds (1994).

### 3.12.2 Axisymmetric Flows in a Rotating Frame

The mean deformation is given by

$$S^*_{ij} = \begin{pmatrix} \Gamma & 0 & 0 \\ 0 & -\Gamma/2 & 0 \\ 0 & 0 & -\Gamma/2 \end{pmatrix}, \quad \Omega_{ij} = \begin{pmatrix} 0 & 0 & 0 \\ 0 & 0 & 0 \\ 0 & 0 & 0 \end{pmatrix}, \quad \Omega^f_{ij} = \begin{pmatrix} 0 & 0 & 0 \\ 0 & 0 & \Omega^f \\ 0 & -\Omega^f & 0 \end{pmatrix}, \tag{3.84}$$

with $\Gamma > 0$ for axisymmetric contraction, and $\Gamma < 0$ for axisymmetric expansion.

Figure 3.1 displays $b_{ij} = r_{ij} - \delta_{ij}/3$, the normalized anisotropy of the Reynolds stress tensor, versus normalized strain rate, with and without imposed frame rotation ($\Omega^f = 2|\Gamma|$). Figure 3.1(a) explores $b_{ij}$ for the axisymmetric contraction case. In the fixed frame the turbulence is completely vortical, and as the eddy-axis tensor aligns with the direction of positive strain, the axial component of the Reynolds stress decays rapidly, Figure 3.1(a). In presence of frame rotation the jetal mode is activated, and the axial component of the Reynolds normal stress does not decay as fast initially. Eventually, for very large $\Gamma\tau$, the eddy-axis tensor becomes aligned with the direction of rotation and the turbulence becomes materially indifferent to the rotation, and the Reynolds stress components become the same as without rotation.

Figure 3.1(b) shows $b_{ij}$ for the axisymmetric expansion case. Again the eddy-axis tensor aligns with the direction of positive strain, now orthogonal to the axis of symmetry. In the fixed frame case (no jetal mode), in the limit of very large normalized deformation rates, the Reynolds stresses become one-component. In presence of frame rotation, the jetal and helical modes are activated, and the anisotropy of the stresses does not grow so strong. In this case the eddy-axis tensor never becomes aligned with the direction of the frame rotation ($a_{22} = a_{33} \to 1/2$ as $\Gamma\tau \to \infty$), so the turbulence is affected by the rotation at all levels of $\Gamma\tau$.

### 3.12.3 Shear Flow in a Spanwise Rotating Frame

The mean deformation is given by

$$S^*_{ij} = \begin{pmatrix} 0 & \Gamma & 0 \\ \Gamma & 0 & 0 \\ 0 & 0 & 0 \end{pmatrix}, \quad \Omega_{ij} = \begin{pmatrix} 0 & \Gamma & 0 \\ -\Gamma & 0 & 0 \\ 0 & 0 & 0 \end{pmatrix}, \quad \Omega^f_{ij} = \begin{pmatrix} 0 & -\Omega^f & 0 \\ \Omega^f & 0 & 0 \\ 0 & 0 & 0 \end{pmatrix}. \tag{3.85}$$

Figure 3.2 shows the normalized Reynolds stress versus mean normalized strain rate, for several ratios of frame rotation to mean rotation. The amount of frame rotation in the different figures is quantified by $\eta_f = -\Omega^f_{12}/\Omega^f_{12}$, the ratio of the (counter)-rotation of the frame to the rotation rate of the mean flow (shear). In all cases the eddy-axis tensor reacts in precisely the same way to the different normalized strain rates because the eddy-axis tensor is computed in the rotating frame; as it is affected only kinematically by frame rotation, it is insensitive to the amount of frame rotation. However the stress states are very different

for the different $\eta_f$ because the stresses are dynamically affected by the frame rotation. In the ASBM this effect comes through the structure parameters. The structure parameters were built with guidance from an asymptotic solution to RDT of the same problem (shear with spanwise frame rotation). Hence the model shows the same kind of behavior brought in by this fitting.

Note that for zero frame rotation the $r_{11}$ component is largest, but as $\eta_f$ increases the other normal components become more important. Note the dramatic effect on the shear stress $r_{12}$. As the frame counter-rotation grows, $r_{12}$ initially grows larger, corresponding to increased turbulence activity, but eventually becomes weaker as the frame counter-rotation overcomes the mean rotation. The ratio of turbulence production to turbulence dissipation, $P/\varepsilon = -4r_{12}\Gamma\tau$ where $\tau = k/\varepsilon$, is directly proportional to $r_{12}$, and once the ratio becomes smaller than unity turbulence decay is observed.

In the previous model, (Reynolds *et al.* 2000), $r_{12}$ would change sign for the larger values of $\eta_f$ shown. In the current version a conscious effort was made to postpone this to larger $\eta_f$ and normalized strain rates. When $r_{12}$ becomes positive, the turbulence production rate becomes negative! More discomforting though is the fact that this amounts to a negative effective eddy viscosity (in standard two-equation models $\nu_T \propto -r_{12}/(\Gamma\tau)$), which can have a destabilizing effect on numerical schemes. In particular the previous ASBM would predict positive $r_{12}$ for *any* normalized strain rate if $\eta_f$ was large enough. Near the zero velocity gradient region, in spanwise rotating channel flows, $\eta_f \to \infty$, and the model solution would predict odd oscillations of the shear stress near this region (as $\eta_f$ decreases $r_{12}$ would change sign again, clearly at odds with the DNS). Great efforts were taken in the optimization of the structure coefficients, especially $\beta$, so that this situation could be avoided.

### 3.12.4 Shear Flow in a Streamwise Rotating Frame

The mean deformation is given by

$$S^*_{ij} = \begin{pmatrix} 0 & \Gamma & 0 \\ \Gamma & 0 & 0 \\ 0 & 0 & 0 \end{pmatrix}, \quad \Omega_{ij} = \begin{pmatrix} 0 & \Gamma & 0 \\ -\Gamma & 0 & 0 \\ 0 & 0 & 0 \end{pmatrix}, \quad \Omega^f_{ij} = \begin{pmatrix} 0 & 0 & 0 \\ 0 & 0 & -\Omega^f \\ 0 & \Omega^f & 0 \end{pmatrix}. \tag{3.86}$$

For the mean flow given, the eddy-axis tensor and the eddy-flattening tensor are of the

form

$$a_{ij} = \begin{pmatrix} a_{11} & a_{12} & 0 \\ a_{12} & a_{22} & 0 \\ 0 & 0 & a_{33} \end{pmatrix}, \qquad b_{ij} = \begin{pmatrix} b_{11} & 0 & b_{13} \\ 0 & 0 & 0 \\ b_{13} & 0 & b_{33} \end{pmatrix}. \tag{3.87}$$

For the particular case of shear, the algebraic eddy-axis model predicts $a_{22} = a_{33}$. Then using the constitutive Equations (3.13) and (3.12), selected Reynolds-stress components can be explicitly written as

$$\begin{aligned} r_{13} &= -(1-\phi)\chi\, a_{22}\, b_{13} + (\gamma\Omega_3^T/\Omega^T)\, a_{12}\, \chi\, b_{13}\, (1-a_{33}) \\ &\quad + (\gamma\Omega_1^T/\Omega^T)\, a_{12}\, [\tfrac{1}{2}(1-\chi) + \tfrac{1}{2}\, \chi\, (2b_{11} - a_{11}\, b_{11} + a_{33}\, b_{33})], \end{aligned} \tag{3.88}$$

$$r_{23} = (1-\phi)\chi\, a_{12}\, b_{13}, \tag{3.89}$$

$$d_{13} = \chi\, a_{22}\, b_{13}, \qquad d_{23} = -\chi\, a_{12}\, b_{13}. \tag{3.90}$$

The sign of $b_{13}$ depends on the sign of $C_b$. Equation (3.24) becomes

$$b_{13} = \frac{C_b \Omega_1^f \Omega_3}{(C_b\Omega_1^f)^2 + (\Omega_3)^2}. \tag{3.91}$$

The case of shear with streamwise rotation is very challenging and exposes some difficulties with algebraic models in general, and the ASBM in particular. The Reynolds-stress tensor becomes fully populated as the presence of streamwise rotation activates the secondary shear stresses $r_{13}$ and $r_{23}$. It is not clear what should be the sign of these secondary stresses. Equations (3.89) and (3.90) show that the signs of $r_{23}$, $d_{13}$, and $d_{23}$ are directly dependent on $b_{13}$ which in turn depends on $C_b$. When the frame rotation is aligned with the mean rotation, the sign and magnitude of $C_b$ are immaterial.

Shear with streamwise rotation does not benefit from the guidance of the asymptotic behavior of exact solutions (two-dimensional turbulence aligned with the $x_1$ direction as used in section 3.9.2 is indifferent to rotation around the $x_1$-axis). Nevertheless some guidance can be obtained by comparing the relative influence of streamwise frame rotation on the flow by means of the Particle Representation Model (PRM) of Kassinos and Reynolds (1994). Specifically, the PRM was used to help determine the proper sign of the secondary stresses given a particular frame rotation direction. The PRM allows the time integration of turbulence statistics in the Rapid Distortion Limit (RDT) of homogeneous turbulence.

Figure 3.3(a) compares PRM solutions for the Reynolds stress tensor in the no frame rotation case to solutions for $\Omega^f_{23}/\Omega_{23} = -0.5$. Figure 3.3(b) gives the same comparison for the dimensionality tensor. It is observed that:

- the effect on the normal stresses and the shear stress $r_{12}$ is noticeable but small. Same for the dimensionality tensor components;
- $d_{13} > 0$, $d_{23} < 0$, $r_{23} > 0$, and $r_{13} > 0$ for small deformations.

Figures 3.4(a) and (3.4(b)) compare the response of the ASBM for the Reynolds stresses and dimensionality tensor respectively, for different normalized rates of shear in a fixed frame and in streamwise-rotating frame with $\Omega^f_{23}/\Omega_{23} = -0.5$.

A direct comparison between the PRM and the ASBM results is not possible, as they are very different things. The PRM represents integration in time, while the ASBM stresses represent solely the output of the algebraic equations to a given normalized shear rate $\Gamma\tau$. Nevertheless relative behavior between the rotating frame case to the fixed frame case can be investigated. The ASBM results were obtained with $C_b = -1.0$. This gives flattening $b_{13} < 0$ and hence secondary Reynolds stresses and dimensionality components with sign consistent with the PRM. Larger magnitudes of $C_b$ do not affect the solution substantially. Smaller magnitudes decrease the primary shear stress further. As compared to the PRM solution,

- the principal Reynolds shear stress, $r_{12}$, shows excessive sensitivity. This carries over to the solution of streamwise rotating channel flows, which will display too much turbulence suppression;
- the secondary stresses are much smaller then what is attained with the RDT solution (PRM). This will also be observed later in the streamwise rotating channel flow.

A surprising result seen in the dimensionality curves (PRM) is that $d_{22} > d_{33}$ for the larger times. The exact solution for 2D RDT predicts $d_{33} = 3/4$ and $d_{22} = 1/4$. This discrepancy is not yet understood.

Part of the deficiency of the ASBM should be attributed to a carryover effect from the spanwise rotation case. The structure parameters were optimized for matching the observed suppression of turbulence in presence of *spanwise* frame rotation. The ASBM however responds to rotation through scalars, which as such cannot distinguish the direction of the

frame rotation. Thus any rotation is seen as stabilizing rotation, resulting in the suppression of the shear stress in the ASBM. Nevertheless the ASBM can be less susceptible to the streamwise frame rotation: as the eddy-axis tensor aligns with the streamwise direction (due to shear), it becomes less sensitive to rotation about this particular direction (material frame indifference). Standard models do not have material frame indifference built-in, so they become more susceptible to errors because of the optimization for the spanwise rotation case.

## 3.13 Summary

In this chapter a turbulent field is represented through an ensemble of hypothetical eddies, with assigned properties that provide a measure of the turbulence. The Reynolds stresses and the structure tensors are decomposed onto this eddy field, resulting in constitutive relations for the Reynolds stress and structure tensors in terms of statistics of the eddy field — the eddy-axis tensor, the eddy-flattening tensor, the helix vector, and scalars representative of the eddy structure. The definition of these scalars is the heart of the chapter. They are chosen to match the isotropic turbulence state, and selected RDT limiting states. Intermediate states are computed through blending functions chosen with care to match a canonical shear state, among other criteria.

The model can be outlined as:

$$r_{ij} = r_{ij}(a_{ij}, b_{ij}, \phi, \gamma, \chi), \qquad d_{ij} = d_{ij}(a_{ij}, b_{ij}, \phi, \gamma, \chi),$$

where (homogeneous part — unsensitized to possible presence of walls)

$$a^h_{ij} = a^h_{ij}(S_{ij}\tau, \Omega_{ij}\tau), \qquad b_{ij} = b_{ij}(\Omega_{ij}\tau, \Omega^f_{ij}\tau), \qquad \phi^h, \gamma^h, \chi = f(S_{ij}\tau, \Omega_{ij}\tau, \Omega^f_{ij}, a^h_{ij}).$$

The influence of a wall is imparted to the eddy statistics through

$$a_{ij} = f^a(a^h_{ij}, B_{ij}), \qquad \phi = g(\phi^h, B_{kk}), \qquad \gamma = h(\gamma^h, B_{kk}),$$

where $B_{ij}$ is a local measure of the influence of a wall.

The homogeneous model has been explored for diverse normalized mean-deformation-rates (axisymmetric deformations, and shear in presence of spanwise and streamwise frame-rotation). The model provided realizable and physically acceptable states for the deformations tested. However, in the streamwise frame rotation mode, the model displayed excessive

sensitivity to the frame rotation. This is most likely a consequence of the emphasis in using the spanwise frame rotation case in defining the eddy structure parameters, to the detriment of the streamwise case. In turn this is blamed on the fact that the structure parameters are sensitive to rotation through scalars, which obviously cannot impart a direction of rotation in its final representation.

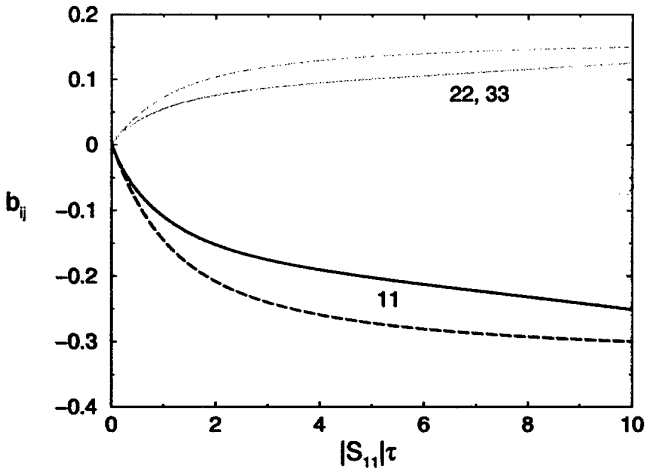


(a)

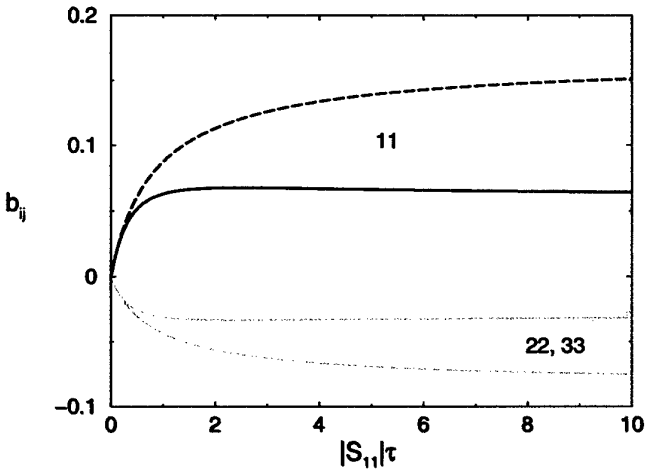


(b)

Figure 3.1: ASBM stress states for (a) axisymmetric contraction, and (b) axisymmetric expansion: with no swirl (dashed lines); and with swirl $\Omega_{23}^f = 2|S_{11}|$ (solid lines).

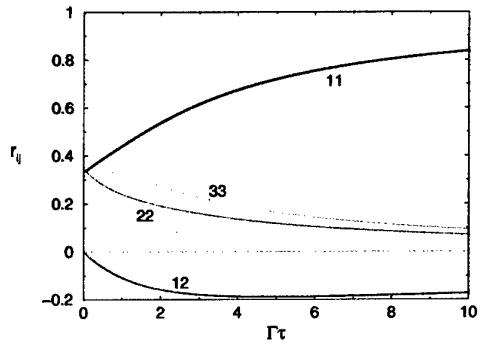


(a) $\eta_f = 0$

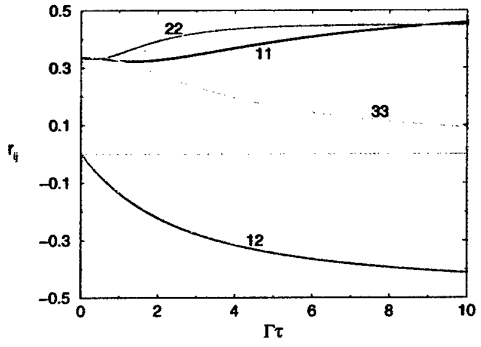


(b) $\eta_f = 0.5$

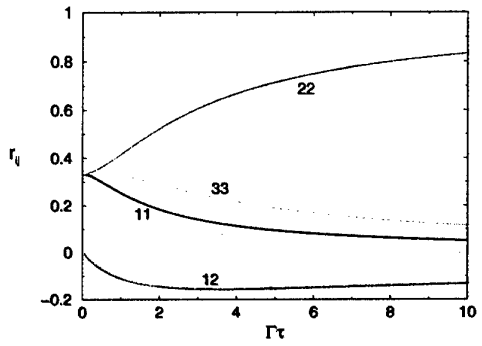


(c) $\eta_f = 1$

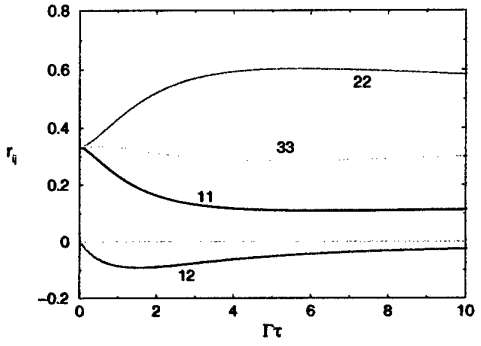


(d) $\eta_f = 1.5$

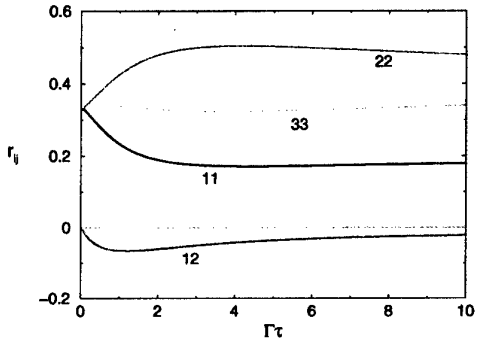


(e) $\eta_f = 2$

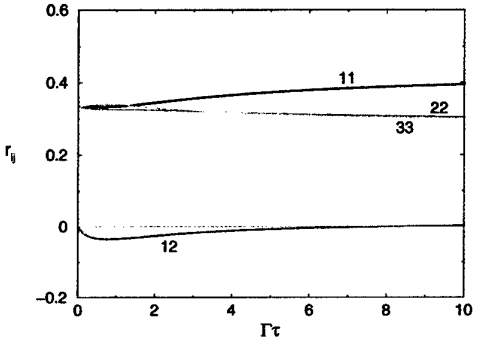


(f) $\eta_f = -2$

Figure 3.2: ASBM stress states for homogeneous shear in a frame rotating about the spanwise axis: (a) non-rotating frame; (b)-(e) counter-rotating frame; (f) co-rotating frame .

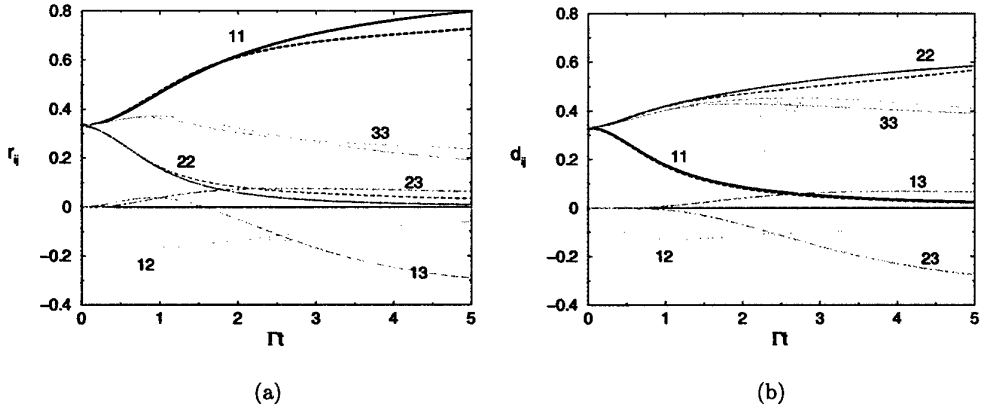


Figure 3.3: Comparison of time integration of turbulence statistics in RDT (PRM of Kassinos and Reynolds 1994) of homogeneous shear in a fixed frame (solid lines) and in a streamwise-rotating frame with $\Omega_{23}^f = -\Omega_{12}/2$. Dotted lines, dashed line: "13" component. Dot-dashed line: "13" component. (a) Reynolds stresses $r_{ij}$; (b) dimensionalities $d_{ij}$.

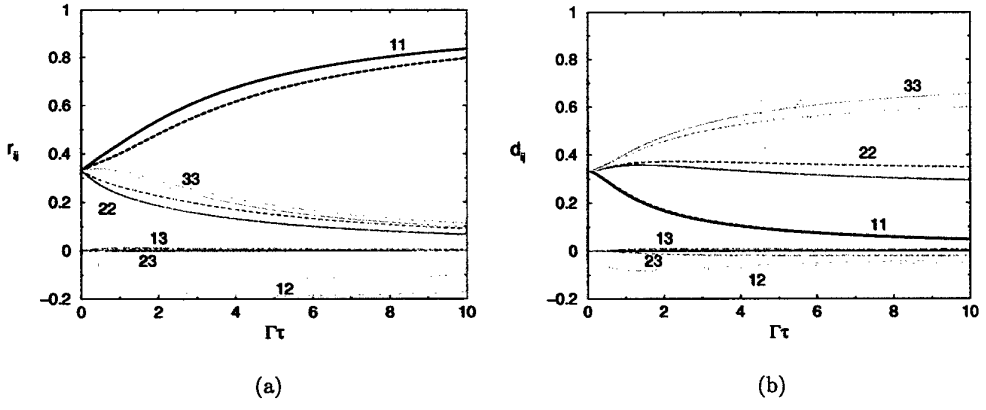


Figure 3.4: Comparison of ASBM response to different normalized shear-rates in a fixed frame (solid lines) and in a streamwise-rotating frame with $\Omega_{23}^f = -\Omega_{12}/2$. Dotted lines, dashed line: "13" component. Dot-dashed line: "13" component: (a) Reynolds stresses $r_{ij}$; (b) dimensionalities $d_{ij}$.

# Chapter 4

# Scale Equations

In this chapter two scale equations are proposed to complement the algebraic structure-based turbulence model introduced in Chapter 3. The scale equations proposed here are the extension, for inhomogeneous wall-bounded flows, of the model equations suggested by Reynolds, Langer, and Kassinos (2002) (RLK02) for homogeneous flows.

The extension of the model equations is such that:

- it returns the homogeneous forms of RLK02 when applicable;
- the source terms in the evolution equations for the scales have proper asymptotic behavior when approaching a solid wall;
- the model scale equations are consistent with the existence of a logarithmic region in a wall-bounded flow;
- the model scale equations should not show any spurious behavior near the edge of a shear layer (near a turbulent/non-turbulent interface).

RLK02 follow Obukhov (1941) and Singh and Lumley (1971) and hypothesize an averaging process, denoted by brackets, that can extract the large-scale coherent motions. For example this could be a POD modal decomposition that captures the energy-containing turbulence and the associated large-scale vorticity. Combined with the time (or ensemble) average (denoted by overbar), gives the triple decomposition (see Reynolds and Hussain 1972) for the velocity field,

$$u_i = \bar{u}_i + \tilde{u}_i + u_i'', \tag{4.1}$$

$$\langle u_i \rangle = \bar{u}_i + \tilde{u}_i, \qquad \overline{\langle u_i \rangle} = \bar{u}_i, \qquad \overline{\langle \tilde{u}_i \rangle} = 0, \tag{4.2}$$

and for the vorticity field,

$$\omega_i = \bar{\omega}_i + \tilde{\omega}_i + \omega_i'', \tag{4.3}$$

$$\langle \omega_i \rangle = \bar{\omega}_i + \tilde{\omega}_i, \qquad \overline{\langle \omega_i \rangle} = \bar{\omega}_i, \qquad \overline{\langle \tilde{\omega}_i \rangle} = 0. \tag{4.4}$$

A single prime was used in Chapter 2 to indicate fluctuating quantities in the Reynolds decomposition. Double primes are used here to distinguish the current small-scale fluctuations from the former. Then an overbar over a variable denotes an average value, a tilde over a variable denotes a large-scale coherent fluctuation, and a double prime denotes the remaining incoherent fluctuation. It is assumed that the averaging operations commute with differentiation, and that the different modes are not correlated, that is,

$$\overline{\tilde{u}_i u_j''} = 0, \qquad \overline{\bar{u}_i \tilde{u}_j} = \bar{u}_i \overline{\tilde{u}_j} = 0, \qquad \langle \tilde{u}_i u_j'' \rangle = \tilde{u}_i \langle u_j'' \rangle = 0. \tag{4.5}$$

This is a consequence of the remaining incoherent scales representing uncorrelated motion. Thus, even if the large-scale motions and the incoherent motions have same frequency or wavelength, they do not have any phase correlation, so that the average product vanishes.

## 4.1 Overview

In preparation for choosing appropriate near-wall scaling factors for different terms of the evolution equations for the turbulence scalars, a summary of the expected asymptotic behavior for the flow variables is given in Section 4.2. Sections 4.3 and 4.4 introduce time and length scales, respectively used in the normalization of the mean deformation in Chapter 3, and in scaling source/sink terms in the scale equations.

Sections 4.5 and 4.6 introduce the evolution equations for the turbulent kinetic energy and for the large scale turbulent enstrophy respectively, and looks at specific model choices for the different terms in the equations. Section 4.7 briefly points proper boundary conditions for the coupled system of scale equations.

Section 4.8 then looks at the log region of a boundary layer, and at the interface between turbulent and non-turbulent flows. This determines conditions to be satisfied by the model constants, such that the model conforms to accepted behavior in these regions.

There are no results explored in this chapter, as it depends on the specification of a given turbulent state, which is done in this work using the algebraic equations from Chapter 3. Full model results (scale equations coupled with algebraic structure equations) follow in Chapter 5.

## 4.2 Near-Wall Asymptotic Behavior

Taking $x_i = \{x, y, z\}$, $\tilde{u}_i = \{\tilde{u}, \tilde{v}, \tilde{w}\}$, and $\bar{u}_i = \{U(y), V \equiv 0, W \equiv 0\}$, the near-wall expansions for turbulent fluctuations and statistics, with the $y$-direction as the wall-normal direction, are

$$\tilde{u} = b_1 y + c_1 y^2 + O(y^3), \tag{4.6a}$$

$$\tilde{v} = c_2 y^2 + O(y^3), \tag{4.6b}$$

$$\tilde{w} = b_3 y + c_3 y^2 + O(y^3), \tag{4.6c}$$

$$\tilde{p} = p_0 + p_1 y + p_2 y^2 + O(y^3), \tag{4.6d}$$

$$U = B_1 y + C_1 y^2 + O(y^3), \tag{4.6e}$$

where all the different coefficients are functions of $x$ and $z$. Though the expressions have been written only for the large-scale fluctuations, they apply equally to the small-scale fluctuations, with different coefficients.

It follows that the near-wall expansion for the fluctuating vorticities are

$$\tilde{\omega}_x = \tilde{w}_{,y} - \tilde{v}_{,z} = b_3 + 2c_3 y + O(y^2), \tag{4.7a}$$

$$\tilde{\omega}_y = \tilde{u}_{,z} - \tilde{w}_{,x} = (b_{1,z} - b_{3,x}) y + O(y^2), \tag{4.7b}$$

$$\tilde{\omega}_z = \tilde{v}_{,x} - \tilde{u}_{,y} = -b_1 - 2c_1 y + O(y^2). \tag{4.7c}$$

## 4.3 Time Scale

The algebraic equations developed in Chapter 3 respond to the mean deformation normalized with a turbulence time scale, $\tau$ (strictly $\tau$ is needed only for normalizing the mean strain rate in Equation 3.15 — it cancels out in other places where a mean-velocity gradient or a frame rotation-rate appears). $\tau$ is defined as

$$\tau^2 = \left(\frac{k}{\varepsilon}\right)^2 + \left(C_\tau \sqrt{\frac{\nu}{\varepsilon}}\right)^2, \tag{4.8}$$

where $C_\tau = 2.0$. Away from walls, in high Reynolds number regions, this gives the familiar definition $\tau = k/\varepsilon$. Near the wall (or in low Reynolds number regions) the time scale has a lower bound in terms of its viscous counterpart.

The coefficient $C_\tau$ was chosen so that the prediction of the algebraic model (Section 3.11) for the energy-normalized Reynolds stresses would closely resemble the wall values given in the DNS database for channel flow (Moser, Kim, and Mansour 1999).

## 4.4 Length Scale

A length scale is used for the extension of the $k$ and the $\tilde{\omega}^2$ evolution equations, with the specific requirement that it shall not vanish at a wall. For homogeneous flows, a dimensionally consistent form is

$$l_h^2 = \frac{k}{\tilde{\omega}^2}, \tag{4.9}$$

where $l_h$ is the homogeneous length scale. Its wall value is zero. It can be made nonzero through the addition of a Kolmogorov length scale, or it can be made nonzero through the addition of an inviscid correction. Both are valid approaches.

The selected form uses an inviscid correction,

$$l^2 = \frac{l_h^2}{1 + C_{l1}} \left[ 1 + \frac{C_{l1}}{(1 - B_{kk})^2} \right] \left[ 1 + C_{l2} \frac{\partial l_h}{\partial x_k} \frac{\partial l_h}{\partial x_k} \right]. \tag{4.10}$$

$B_{ii}$ was introduced in Chapter 3 and is representative of the proximity of a wall. It is $O(y^2)$, so that the form adopted renders $l^2$ finite, $O(y^0)$, as a wall is approached.

The term in the second square brackets effectively brings a nonlocal contribution to the length scale. The idea is that a given spatial location may be affected by larger eddies "centered" in other spatial positions. In the logarithmic region of a boundary layer, for instance, the length scale grows with distance from the wall. It is then possible to imagine that the turbulence is locally affected by eddies larger than the local eddies. This nonlocal correction is important for matching the mean velocity profile in the logarithmic region of a boundary layer.

## 4.5 Turbulent Kinetic Energy Equation

Substituting the triple decomposition (Equation 4.1) into the Navier-Stokes equations, Equation (2.2), and applying successively the large-scale coherent averaging (brackets), and

the time/ensemble averaging gives an equation for mean velocity $\bar{u}_i$,

$$\frac{\partial \bar{u}_i}{\partial x_i} = 0, \tag{4.11}$$

$$\frac{\partial \bar{u}_i}{\partial t} + \bar{u}_j \frac{\partial \bar{u}_i}{\partial x_j} + 2\epsilon_{ijk}\Omega_j^f \bar{u}_k = -\frac{\partial \bar{P}^*}{\partial x_i} + \nu \frac{\partial^2 \bar{u}_i}{\partial x_k \partial x_k} - \frac{\partial R_{ij}}{\partial x_j}, \tag{4.12}$$

where $R_{ij} = \overline{\bar{u}_i \bar{u}_j} + \overline{u_i'' u_j''}$ is the total Reynolds stress tensor, the third term on the left is the Coriolis acceleration term, and $\bar{P}^*$ encompasses the centripetal acceleration term,

$$P^* = \frac{\bar{p}}{\rho} + \bar{\mathcal{U}} - \frac{1}{2}(\epsilon_{ljk}\Omega_j^f x_k)(\epsilon_{lpq}\Omega_p^f x_q), \tag{4.13}$$

and $\bar{\mathcal{U}}$ is an average conservative body force.

Subtracting the equation for $\bar{u}_i$ from the equation obtained after the first averaging process, $(\bar{u}_i + \tilde{u}_i)$, gives the equation for $\tilde{u}_i$. Multiplying by $\tilde{u}_i$ gives the equation for the large-scale kinetic energy as reported in RLK02,

$$\underbrace{\frac{\partial \overline{\tilde{u}_i \tilde{u}_i}/2}{\partial t} + \bar{u}_j \frac{\partial \overline{\tilde{u}_i \tilde{u}_i}/2}{\partial x_j}}_{\substack{\text{DKDT} \\ \text{mean Lagrangian increase}}} = \underbrace{(-\overline{\tilde{u}_i \tilde{u}_j})\frac{\partial \bar{u}_i}{\partial x_j}}_{\substack{\text{TKML} \\ \text{transfer from mean}}} - \underbrace{\overline{(-\langle u_j'' u_i'' \rangle)\frac{\partial \tilde{u}_i}{\partial x_j}}}_{\substack{\text{TKLS} \\ \text{transfer to small scales}}} - \underbrace{\nu \overline{\frac{\partial \tilde{u}_i}{\partial x_j}\frac{\partial \tilde{u}_i}{\partial x_j}}}_{\substack{\text{DKL} \\ \text{dissipation by} \\ \text{large scales}}}$$

$$- \underbrace{\frac{\partial}{\partial x_j}\left( \underbrace{\frac{1}{\rho}\overline{\tilde{p}\tilde{u}_j}}_{\text{FKP}_j} + \underbrace{\overline{\tilde{u}_j \tilde{u}_i \tilde{u}_i}/2}_{\text{FKL}_j} + \underbrace{\overline{\tilde{u}_i \langle u_i'' u_j'' \rangle}}_{\text{FKS}_j} + \underbrace{\left[ -\nu \frac{\partial \overline{\tilde{u}_i \tilde{u}_i}/2}{\partial x_j} \right]}_{\text{FK}\nu_j} \right)}_{\text{spatial flux}}. \tag{4.14}$$

Similarly the small-scale kinetic energy equation is (RLK02),

$$\underbrace{\frac{\partial \overline{u_i'' u_i''}/2}{\partial t} + \bar{u}_j \frac{\partial \overline{u_i'' u_i''}/2}{\partial x_j}}_{\substack{\text{Dk''DT} \\ \text{mean Lagrangian increase}}} = \underbrace{(-\overline{u_i'' u_j''})\frac{\partial \bar{u}_i}{\partial x_j}}_{\substack{\text{Tk''ML} \\ \text{transfer from mean}}} + \underbrace{\overline{(-\langle u_j'' u_i'' \rangle)\frac{\partial \tilde{u}_i}{\partial x_j}}}_{\substack{\text{TKLS} \\ \text{transfer from large scales}}} - \underbrace{\nu \overline{\frac{\partial u_i''}{\partial x_j}\frac{\partial u_i''}{\partial x_j}}}_{\substack{\text{Dk''L} \\ \text{dissipation by} \\ \text{small scales}}}$$

$$- \underbrace{\frac{\partial}{\partial x_j}\left( \underbrace{\frac{1}{\rho}\overline{p'' u_j''}}_{\text{Fk''P}_j} + \underbrace{\overline{\tilde{u}_j u_i'' u_i''}/2}_{\text{Fk''L}_j} + \underbrace{\overline{u_i'' u_i'' u_j''}}_{\text{Fk''S}_j} + \underbrace{\left[ -\nu \frac{\partial \overline{u_i'' u_i''}/2}{\partial x_j} \right]}_{\text{Fk''}\nu_j} \right)}_{\text{spatial flux}}. \tag{4.15}$$

RLK02 chose the *total* kinetic energy as the first turbulence scale. Adding the large-scale coherent kinetic energy to the small-scale kinetic energy, Equations (4.14) and (4.15)

respectively, gives

$$\frac{\partial k}{\partial t}+\bar{u}_j\frac{\partial k}{\partial x_j}=-R_{ij}\frac{\partial \bar{u}_i}{\partial x_j}-\overline{(-\langle u_j''u_i''\rangle)\frac{\partial \tilde{u}_i}{\partial x_j}}-\nu\overline{\frac{\partial \tilde{u}_i}{\partial x_j}\frac{\partial \tilde{u}_i}{\partial x_j}}+\left[\overline{(-\langle u_j''u_i''\rangle)\frac{\partial \tilde{u}_i}{\partial x_j}}-\nu\overline{\frac{\partial u_i''}{\partial x_j}\frac{\partial u_i''}{\partial x_j}}\right] \tag{4.16}$$

$$-\frac{\partial}{\partial x_j}\left(\frac{1}{\rho}\overline{p'u_j'}+\overline{u_j'u_i'u_i'}/2-\nu\frac{\partial k}{\partial x_j}\right),$$

where $k=\overline{u_i'u_i'}/2$, $u'=\tilde{u}+u''$, and $p'=\tilde{p}+p''$.

The next step can be more controversial. Clearly the term responsible for transfer from the large scales to the small scales, TKLS, strictly cancels out and the dissipation is represented by the sum of the dissipation by large scales, DKL, and by small scales, Dk″L. The latter represents the bulk part of the dissipation in high Reynolds number flows. In RLK02 the *total* dissipation is modeled as the sum of DKL and TKLS, with the implied assumption that TKLS and Dk″L balance each other. This choice follows the concept that what should be modeled is the transfer of energy down the cascade, rather than the dissipation at the small scales directly. It has a powerful physical appeal; it is attractive to model a large-scale process instead of providing an ad-hoc expression for small-scale phenomena. Here the approach of RLK02 is followed, the term within brackets in Equation (4.16) is dropped, and the final equation for the turbulent kinetic energy becomes

$$\frac{\partial k}{\partial t}+\bar{u}_j\frac{\partial k}{\partial x_j}=-R_{ij}\frac{\partial \bar{u}_i}{\partial x_j}-\varepsilon-\frac{\partial}{\partial x_j}\left(\frac{1}{\rho}\overline{p'u_j'}+\overline{u_j'u_i'u_i'}/2-\nu\frac{\partial k}{\partial x_j}\right), \tag{4.17}$$

where $\varepsilon$, the dissipation rate of turbulent kinetic energy, is

$$\varepsilon=\underbrace{\overline{(-\langle u_j''u_i''\rangle)\frac{\partial \tilde{u}_i}{\partial x_j}}}_{\substack{\text{TKLS}\\ \text{transfer to small scales}}}+\underbrace{\nu\overline{\frac{\partial \tilde{u}_i}{\partial x_j}\frac{\partial \tilde{u}_i}{\partial x_j}}}_{\substack{\text{DKL}\\ \text{dissipation by}\\ \text{large scales}}}. \tag{4.18}$$

### 4.5.1 Term-by-Term Modeling

The first term on the right-hand-side of Equation (4.17) represents energy transfer from the mean flow to the large scales of the turbulence (best known as production of turbulence kinetic energy) and does not require modeling. The remaining terms are modeled such as to resemble the near-wall asymptotic behavior of the exact terms and to revert to the homogeneous RLK02 form. Table 4.1 summarizes the modifications done to the model

proposed by RLK02, as well as the near-wall asymptotic behavior of the exact terms. In the sequence the changes are briefly commented. The symbol $\overline{\text{fd}}$ is introduced to shorten the notation,

$$\overline{\text{fd}} \equiv f_{ij}^{cc} d_{ji}^{cc}. \tag{4.19}$$

| Term | exact term | $y \to 0$ | Current model | RLK02 |
|---|---|---|---|---|
| TKLS | $\overline{(-\langle u_j'' u_i'' \rangle) \frac{\partial \tilde{u}_i}{\partial x_j}}$ | $O(y^3)$ | $F_\varepsilon k \frac{k^{1/2}}{l}$ | $F_\varepsilon k \tilde{\omega}$ |
| | | | $F_\varepsilon = C_\varepsilon (3\overline{\text{fd}})^{1/6}$ | $F_\varepsilon = C_\varepsilon (3\overline{\text{fd}})$ |
| DKL | $\nu \overline{\frac{\partial \tilde{u}_i}{\partial x_j} \frac{\partial \tilde{u}_i}{\partial x_j}}$ | $O(1)$ | $\nu \tilde{\omega}^2$ | $\nu \tilde{\omega}^2$ |
| triple product | $-\frac{\partial}{\partial x_j} \left( \overline{u_j' u_i' u_i'}/2 \right)$ | $O(y^3)$ | $\frac{\partial}{\partial x_j} \left( \frac{\alpha_k}{\sigma_k} r_{jk} \frac{\sqrt{k}\, l}{F_\varepsilon} \frac{\partial \overline{\tilde{u}_i \tilde{u}_i}/2}{\partial x_k} \right)$ | – |
| + pressure transport | $-\frac{\partial}{\partial x_j} \left( \overline{p' u_j'} \right)$ | $O(y^2)$ | | |

Table 4.1: Summary of terms in the large-scale turbulent kinetic energy equation, their asymptotic behavior as a wall at $y = 0$ is approached, the current model form, and the original model form in RLK02.

### 4.5.2 TKLS: Transfer to Small Scales

$$\text{TKLS} \equiv \overline{(-\langle u_j'' u_i'' \rangle) \frac{\partial \tilde{u}_i}{\partial x_j}} = F_\varepsilon k \frac{k^{1/2}}{l}, \qquad F_\varepsilon = C_\varepsilon (3\overline{\text{fd}})^{1/6}. \tag{4.20}$$

The current model has the proper asymptotic behavior as the wall is approached, as $\sqrt{k} = O(y)$ and $l = O(1)$ as $y \to 0$. More importantly, the nonlocal modification to $l^2$ (the $C_{l2}$ term in Equation 4.10) effectively changes $C_\varepsilon$ in different parts of the flow. This modification is necessary to match velocity profiles from DNS of channel flow. The drawback of this modification is that $F_\varepsilon$ had to be modified from RLK02, to incorporate the 1/6-th

power in $C_\varepsilon(3\overline{\text{fd}})^{1/6}$. $F_\varepsilon$ is used to shut down the cascade of energy from large scales to small scales in rotating turbulence.

The introduction of $C_{l2}$ also implies that $\sigma_{\tilde{\omega}^2}/\sigma_k < 1.5$ for proper behavior near the edge of a turbulent/non-turbulent interface (see Section 4.8.1), as opposed to $\sigma_{\tilde{\omega}^2}/\sigma_k < 2$ when $C_{l2} = 0$. As shown in Section 4.8.2, matching the log-law when $F_\varepsilon = C_\varepsilon(3\overline{\text{fd}})$ requires $\sigma_{\tilde{\omega}^2}/\sigma_k = 1.9$ when $C_{l2} \neq 0$. If $F_\varepsilon = C_\varepsilon(3\overline{\text{fd}})^{1/6}$ then $\sigma_{\tilde{\omega}^2}/\sigma_k = 1.45$ when $C_{l2} \neq 0$.

In RLK02 the specific value of $C_\varepsilon$ was found to be immaterial for high Reynolds number flows, as it could be absorbed by the other model constants. In wall-bounded flows, the value of $C_\varepsilon$ becomes an important parameter as one bridges the near-wall layer. Results shown in the present work were obtained with a constant value for all flows,

$$C_\varepsilon = 0.3. \tag{4.21}$$

### 4.5.3 DKL: Dissipation by Large Scales

Expanding $\nu\tilde{\omega}^2 = \nu\overline{\tilde{\omega}_i\tilde{\omega}_i}$ in terms of velocity gradients, and using the continuity equation for the fluctuations, gives the identity,

$$\text{DKL} \equiv \nu\overline{\frac{\partial\tilde{u}_i}{\partial x_j}\frac{\partial\tilde{u}_i}{\partial x_j}} = \nu\tilde{\omega}^2 + \nu\frac{\partial^2\overline{\tilde{u}_i\tilde{u}_j}}{\partial x_i\partial x_j}. \tag{4.22}$$

Note that DKL is strictly the *homogeneous* dissipation. It differs from the "true" dissipation by gradients of the Reynolds stresses. The true dissipation is positive definite and represents the work performed by a stress against a deformation.

The second term in the right, the second derivative term, is actually very small compared to the sum of $\nu\tilde{\omega}^2$ and TKLS and it will be dropped for simplicity. DKL is then modeled as

$$\text{DKL} = \nu\tilde{\omega}^2. \tag{4.23}$$

### 4.5.4 FK: Spatial Flux

The transport term consists of a turbulent contribution and a viscous contribution. The viscous flux, $FK\nu_j$, does not require modeling. When integration down to the wall is considered this is a dominant term, $O(1)$ as $y \to 0$. Otherwise it is negligible in high Reynolds number regions. The flux of velocity fluctuations and the flux of pressure fluctuations have different near wall asymptotic behaviors. The latter is $O(y^2)$ as $y \to 0$, while the former is

$O(y^4)$. The whole turbulence-induced flux is traditionally modeled as a gradient-diffusion process. Cazalbou and Bradshaw (1993) conducted *a priori* analysis of turbulent transport in wall-bounded flows and confirmed good results for the representation of turbulent transport in terms of gradient diffusion models. In DNS of channel flow at several Reynolds numbers (Moser *et al.* 1999) the pressure flux is significantly smaller than the velocity flux away from the wall, and has opposite sign. Figure 4.1 shows this for the $Re_\tau = 590$ case. The pressure-velocity correlation was available from the DNS database and the total flux was integrated from its gradient given in the turbulent kinetic energy equation balance given in the database (the triple product follows by subtraction). The sum of both turbulence fluxes resembles the velocity flux, and it can be successfully modeled away from the wall (for the DNS channel flow database) as

$$\frac{1}{\rho}\overline{p'u_2'} + \overline{u_2'u_i'u_i'}/2 \approx -0.25 R_{22}\frac{k}{\varepsilon}\frac{dk}{dy}. \tag{4.24}$$

Figure 4.2 shows the total kinetic energy flux (using wall normalization) versus distance to the wall for the DNS of channel flow at the three Reynolds numbers, compared to the model above.

The final form used in this work aims to reproduce the right hand side of Equation (4.24), while reproducing the near-wall asymptotic behavior of the triple-product term,

$$\frac{1}{\rho}\overline{p'u_j'} + \overline{u_j'u_i'u_i'}/2 = -\frac{\alpha_k}{\sigma_k} r_{jk}\frac{\sqrt{k}\,l}{F_\varepsilon}\frac{\partial k}{\partial x_k}. \tag{4.25}$$

Away from the wall TKLS dominates the dissipation rate $\varepsilon$, so that $k^{1/2}l \approx k^2/\varepsilon$ and Equation (4.25), applied to the channel flow, falls back to Equation (4.24). Thus $\alpha_k/\sigma_k$ should be close to $2 \times 0.25$. Note that the ratio of $\alpha_k$ to $\sigma_k$ is the important quantity, so that $\sigma_k$ can be chosen as 1, without loss of generality. The model is $O(y^4)$ near the wall which agrees with the asymptotic behavior of the triple product. The pressure-transport term is $O(y^3)$, so the overall model transport near the wall grows slower than the real transport. This is however a second order effect. It is important to get viscous transport much larger than turbulent transport near the wall.

## 4.6 Large-Scale Turbulent Enstrophy

The starting point to build the large-scale turbulent enstrophy equation is the instantaneous vorticity equation, obtained by taking the curl of the continuity equation and the

Navier-Stokes equation, Equations (2.1) and (2.2) respectively,

$$\frac{\partial w_p}{\partial x_p} = 0, \tag{4.26}$$

$$\frac{\partial \omega_p}{\partial t} + u_j \frac{\partial \omega_p}{\partial x_j} = \omega_j s_{jp} - \omega_p s_{pp} + 2\Omega_j^f \frac{\partial u_p}{\partial x_j} + \nu \frac{\partial^2 \omega_p}{\partial x_k \partial x_k}. \tag{4.27}$$

The large-scale turbulent enstrophy equation is obtained following the same procedure followed to get the large-scale turbulent kinetic energy equation. In short, after substituting the triple decomposition for the vorticity, Equation (4.3), the application successive averaging operations permits the isolation of equations for the mean vorticity, $\bar{\omega}_i$, and for the large-scale vorticity, $\tilde{\omega}_i$. Taking the product of the latter equation with $\tilde{\omega}_i$, and averaging produces the desired result. The final exact equation for the large-scale turbulent enstrophy is reproduced from RLK02,

$$\underbrace{\frac{\partial \overline{\tilde{\omega}_i \tilde{\omega}_i}/2}{\partial t} + \bar{u}_j \frac{\partial \overline{\tilde{\omega}_i \tilde{\omega}_i}/2}{\partial x_j}}_{\substack{\text{DWDT} \\ \text{mean Lagrangian increase}}} = \underbrace{(-\overline{\tilde{u}_j \tilde{\omega}_i}) \frac{\partial \bar{\omega}_i}{\partial x_j}}_{\substack{\text{TWML} \\ \text{transfer from mean}}} - \underbrace{(-\overline{\langle u_j'' \omega_i'' \rangle}) \frac{\partial \tilde{\omega}_i}{\partial x_j}}_{\substack{\text{TWLS} \\ \text{transfer to small scales}}} + \underbrace{\overline{\tilde{\omega}_i \tilde{\omega}_j} \frac{\partial \bar{u}_i}{\partial x_j}}_{\substack{\text{PLLM} \\ \text{production by} \\ \text{mean stretching}}} \tag{4.28}$$

$$+ \underbrace{\overline{\tilde{\omega}_i \tilde{\omega}_j \frac{\partial \tilde{u}_i}{\partial x_j}}}_{\substack{\text{PLLL} \\ \text{production by} \\ \text{self stretching}}} + \underbrace{\bar{\omega}_j \overline{\tilde{\omega}_i \frac{\partial \tilde{u}_i}{\partial x_j}} + \overline{\tilde{\omega}_i \left\langle \omega_j'' \frac{\partial u_i''}{\partial x_j} \right\rangle}}_{\substack{\text{PLML, PLSS} \\ \text{production by} \\ \text{cross-scale stretching}}} - \underbrace{\nu \overline{\frac{\partial \tilde{\omega}_i}{\partial x_j} \frac{\partial \tilde{\omega}_i}{\partial x_j}}}_{\substack{\text{DWL} \\ \text{dissipation by} \\ \text{large scales}}}$$

$$- \underbrace{\frac{\partial}{\partial x_j} \left( \underbrace{\overline{\tilde{u}_j \tilde{\omega}_i \tilde{\omega}_i}/2}_{\text{FWL}_j} + \underbrace{\overline{\tilde{\omega}_i \langle \omega_i'' u_j'' \rangle}}_{\text{FWS}_j} + \underbrace{\left[ -\nu \frac{\partial \overline{\tilde{\omega}_i \tilde{\omega}_i}/2}{\partial x_j} \right]}_{\text{FW}\nu_j} \right)}_{\text{spatial flux}}.$$

### 4.6.1 Term-by-Term Modeling

The "mean Lagrangian increase" and the viscous diffusive flux terms do not entail any modeling. The other terms are modeled such as to resemble the near-wall asymptotic behavior of the exact terms, and to have them revert to the homogeneous form proposed by RLK02. Note that TWML and PLML vanish for homogeneous turbulence. Table 4.2 summarizes the modifications imposed on the model proposed by RLK02, as well as the near-wall asymptotic behavior of the exact terms. In the sequence the changes are briefly

commented. The symbol $\overline{\text{rdf}}$ is introduced to shorten the notation,

$$\overline{\text{rdf}} \equiv r_{ij} d^{cc}_{jk} f^{cc}_{ki}. \tag{4.29}$$

| Term | exact term | $y \to 0$ | Current model | RLK02 |
|---|---|---|---|---|
| TWML | $(-\overline{\tilde{u}_j\tilde{\omega}_i})\frac{\partial\bar{\omega}_i}{\partial x_j}$ | $O(y^2)$ | 0 | 0 |
| TWLS | $\overline{(-\langle u_j''\omega_i''\rangle)\frac{\partial\tilde{\omega}_i}{\partial x_j}}$ | $O(y)$ | $C_{\tilde{\omega}^2 T}\tilde{\omega}^2\frac{\sqrt{k}}{l}$ | $C_{\tilde{\omega}^2 T}\tilde{\omega}^3$ |
| PLLM | $\overline{\tilde{\omega}_i\tilde{\omega}_j}\frac{\partial\bar{u}_i}{\partial x_j}$ | $O(y)$ | $\tilde{\omega}^2 f^{cc}_{ij}\frac{\partial\bar{u}_i}{\partial x_j}$ | $\tilde{\omega}^2 f_{ij}\frac{\partial\bar{u}_i}{\partial x_j}$ |
| PLLL +PLSS | $\overline{\tilde{\omega}_i\tilde{\omega}_j\frac{\partial\tilde{u}_i}{\partial x_j}} + \overline{\tilde{\omega}_i\left\langle\omega_j''\frac{\partial u_i''}{\partial x_j}\right\rangle}$ | $O(y)$ | $C_{\tilde{\omega}^2 P}(9\overline{\text{rdf}})\tilde{\omega}^2\frac{\sqrt{k}}{l}$ | $C_{\tilde{\omega}^2 P}(9\overline{\text{rdf}})\tilde{\omega}^3$ |
| PLML | $\bar{\omega}_j\overline{\tilde{\omega}_i\frac{\partial\tilde{u}_i}{\partial x_j}}$ | $O(y)$ | 0 | 0 |
| DWL | $\nu\overline{\frac{\partial\tilde{\omega}_i}{\partial x_j}\frac{\partial\tilde{\omega}_i}{\partial x_j}}$ | $O(1)$ | $C_{\tilde{\omega}^2\nu}\nu\frac{\tilde{\omega}^2}{l^2}$ | $C_{\tilde{\omega}^2\nu}\nu\frac{\tilde{\omega}^4}{k}$ |
| $\text{FWL}_{j,j}$ $+\text{FWS}_{j,j}$ | $-\frac{\partial}{\partial x_j}\left(\overline{\tilde{u}_j\tilde{\omega}_i\tilde{\omega}_i}/2 + \overline{\tilde{\omega}_i\langle\omega_i''u_j''\rangle}\right)$ | $O(y)$ | $\frac{\partial}{\partial x_j}\left(\frac{\alpha_k}{\sigma_{\tilde{\omega}^2}}r_{jk}\frac{\sqrt{k}\,l}{F_\varepsilon}\frac{\partial\tilde{\omega}^2/2}{\partial x_k}\right)$ | – |

Table 4.2: Summary of terms in the large-scale turbulent enstrophy equation, their asymptotic behavior as a wall at $y = 0$ is approached, the current model form, and the original model form in RLK02.

### 4.6.2 TWML: Transfer from Mean Flow

This term vanishes in homogeneous turbulence, as the velocity gradients can be at most a function of time so that the spatial derivative of the mean vorticity must necessarily vanish. Substituting the near-wall expansions, Equations (4.6a–e) and (4.7a–c) into TWML's definition, it is found to be $O(y^2)$ near the wall, as indicated in Table 4.2. The large-scale velocity-vorticity correlation can be separated into a symmetric part and an antisymmetric part. The latter part has an exact representation in terms of gradients of Reynolds stresses. Consider the identity

$$\epsilon_{ijk}\overline{\tilde{\omega}_i\tilde{u}_j} = (\overline{\tilde{u}_k\tilde{u}_p})_{,p} - (\overline{\tilde{u}_p\tilde{u}_p}/2)_{,k}. \tag{4.30}$$

Writing the correlation in terms of its symmetric/antisymmetric decomposition,

$$\overline{\tilde{\omega}_i\tilde{u}_j} = X_{ij} + \epsilon_{ijn}Y_n, \tag{4.31}$$

and substituting into Equation (4.30) gives

$$Y_k = \frac{1}{2}[(\overline{\tilde{u}_k\tilde{u}_p})_{,p} - (\overline{\tilde{u}_p\tilde{u}_p}/2)_{,k}]. \tag{4.32}$$

There is no exact representation for the symmetric part. Robinson, Harris, and Hassan (1995) proposed an *ad-hoc* gradient-diffusion model using an isotropic turbulent eddy viscosity. Generalizing that model to account for anisotropic Reynolds stresses ultimately produces,

$$X_{ij} = \frac{1}{2}\left(\overline{\tilde{\omega}_i\tilde{u}_j} + \overline{\tilde{\omega}_j\tilde{u}_i}\right), \tag{4.33}$$

$$= C_3\left(r_{il}\,k\,\tau\,\frac{\partial\Omega_j}{\partial x_l} + r_{jl}\,k\,\tau\,\frac{\partial\Omega_i}{\partial x_l}\right), \tag{4.34}$$

where $C_3$ is a model constant, $\tau$ is a time scale, $k$ is the turbulent kinetic energy, and $\Omega_j$ represents the mean flow vorticity vector.

Alternatively, Bernard (1990) conducted a Lagrangian analysis and found

$$\overline{\tilde{\omega}_j\tilde{u}_i} = -PR_{ik}\frac{\partial\Omega_j}{\partial x_k} + Q\overline{u_i\frac{\partial u_j}{\partial x_k}}\Omega_k, \tag{4.35}$$

where $P$ and $Q$ are Lagrangian integral time scales. It then results

$$X_{ij} = -P\left(r_{il}\,k\,\frac{\partial\Omega_j}{\partial x_l} + r_{jl}\,k\,\frac{\partial\Omega_i}{\partial x_l}\right) + \frac{Q}{2}\frac{\partial R_{ij}}{\partial x_l}\Omega_l. \tag{4.36}$$

Note that Bernard's form has an extra term with a different tensorial form, when compared to Robinson *et al.*. Attempts to model the terms containing $\overline{\tilde{\omega}_j\tilde{u}_i}$ were conducted here, but no definitive conclusion could be reached. These terms are important in the buffer layer of a wall-bounded flow. However there is already uncertainty on the form of the other terms in the $\tilde{\omega}^2$-equation in the same region, so these could be unintentionally overcoming the requirement for modeling the vorticity-velocity correlation terms. As no clear improvement could be discerned including these terms so far, terms involving $\overline{\tilde{\omega}_j\tilde{u}_i}$ were neglected in the present analysis.

### 4.6.3 [TWLS -(PLLL+PLSS)]: Transfer to Small Scales and Production by Self-Stretching and Cross-Stretching

Following RLK02, this combination is modeled such that in 2D-2C homogeneous turbulence TWLS does not vanish and (PLLL+PLSS) does vanish. The form chosen in RLK02 is not appropriate in near-wall regions, as it predicts the sum of these terms to be $O(1)$ as $y \to 0$, contrary to the exact term. It is important to fix this anomaly as the near-wall balance should be restricted *only* to the viscous diffusion term and the large-scale dissipation term. To reconcile the RLK02 form with the desired near-wall asymptotic behavior it is altered to

$$\overline{(-\langle u_j''\omega_i''\rangle)\frac{\partial\tilde{\omega}_i}{\partial x_j}} - \left(\overline{\tilde{\omega}_i\left\langle\tilde{\omega}_j\frac{\partial\tilde{u}_i}{\partial x_j}\right\rangle} + \overline{\tilde{\omega}_i\left\langle\omega_j''\frac{\partial u_i''}{\partial x_j}\right\rangle}\right) = \left[C_{\tilde{\omega}^2T} - (9\overline{\mathrm{rdf}})C_{\tilde{\omega}^2P}\right]\tilde{\omega}^2\frac{\sqrt{k}}{l}. \quad (4.37)$$

RLK02 found that when $F_\varepsilon = (3\overline{\mathrm{fd}})$, $C_{\tilde{\omega}^2T}/C_\varepsilon = 25/14$ and $C_{\tilde{\omega}^2P}/C_\varepsilon = 20/21$ matched decay rates of homogeneous turbulence in fixed and rotating frames of reference. The analysis of RLK02 was revisited to match the same decay rates with the updated $F_\varepsilon = (3\overline{\mathrm{fd}})^{1/6}$ (for a small wavenumber part of the spectrum proportional to the square of the wavenumber as in the selection of RLK02 chosen), resulting in

$$\frac{C_{\tilde{\omega}^2T}}{C_\varepsilon} = 2.56, \qquad \frac{C_{\tilde{\omega}^2P}}{C_\varepsilon} = 1.73. \quad (4.38)$$

### 4.6.4 PLLM: Production by Mean Stretching

The model remains the same used in RLK02. Its essence is the fact that the normalized correlation $\overline{\tilde{\omega}_i\tilde{\omega}_j}/\tilde{\omega}^2$ is intimately related to the normalized circulicity tensor, as can be

inferred from Chapter 2,

$$\overline{\tilde{\omega}_i\tilde{\omega}_j}\frac{\partial\bar{u}_i}{\partial x_j} = \tilde{\omega}^2 f_{ij}^{cc}\frac{\partial\bar{u}_i}{\partial x_j}. \tag{4.39}$$

### 4.6.5 PLML: Production by Cross-Stretching

This term is identically zero in homogeneous turbulence. This result follows from

$$\overline{\tilde{\omega}_i\frac{\partial\tilde{u}_i}{\partial x_j}} = \overline{\tilde{\omega}_i\left(\frac{\partial\tilde{u}_i}{\partial x_j} - \frac{\partial\tilde{u}_j}{\partial x_i}\right)} + \overline{\tilde{\omega}_i\frac{\partial\tilde{u}_j}{\partial x_i}}, \tag{4.40}$$

$$= \epsilon_{kji}\overline{\tilde{\omega}_k\tilde{\omega}_i} + \frac{\partial\overline{\tilde{\omega}_i\tilde{u}_j}}{\partial x_i} = \frac{\partial\overline{\tilde{\omega}_i\tilde{u}_j}}{\partial x_i}, \tag{4.41}$$

which vanishes in homogeneous situations. To get the last expression note that the large-scale vorticity is divergence-free. Closure for this term again requires a model for $\overline{\tilde{\omega}_i\tilde{u}_j}$. As in the TWML term, this will also be kept zero for the current model.

### 4.6.6 DWL: Dissipation by Large Scales

The choice used in RLK02 is not appropriate in near-wall regions. It is made finite at the wall by introducing the length scale in its definition,

$$\nu\overline{\frac{\partial\tilde{\omega}_i}{\partial x_j}\frac{\partial\tilde{\omega}_i}{\partial x_j}} = C_{\tilde{\omega}^2\nu}\,\nu\frac{\tilde{\omega}^2}{l^2}. \tag{4.42}$$

RLK02 find $C_{\tilde{\omega}^2\nu} = 5/6$ to match the turbulent kinetic energy decay rate at small turbulent Reynolds numbers (final period of decay).

## 4.7 Wall Boundary-Conditions

The boundary conditions used at a solid wall refer only to the turbulent kinetic energy, $k$. It is constrained to satisfy its near-wall asymptotic behavior. There is no boundary condition that needs to be satisfied by the large-scale turbulent enstrophy. It adjusts itself near the wall to ensure that the proper behavior of the turbulent kinetic energy is enforced.

The boundary conditions are then applied to the couple system $k$-$\tilde{\omega}^2$ as

$$k = 0, \qquad \frac{\partial k}{\partial x_n} = 0, \tag{4.43}$$

where $x_n$ is the direction normal to the wall.

## 4.8 Compatibility with Canonical Flow Regions

Enforcing simultaneous compatibility with a turbulent/non-turbulent interface and a logarithmic region determines the ratio of the numerical coefficient of the transport term for the scale equations. It also reinforces model behavior consistent with observed log-law behavior, as well as lack of spurious solutions near the edge of a turbulent/non-turbulent interface.

### 4.8.1 The Edge of a Turbulent Region: Turbulent/Non-Turbulent Interface

The edge of a turbulent region should not be important as far as increased mixing due to turbulence is concerned, as very little happens there. It is important as it may relate to the entrainment of non-turbulent flow into a turbulent flow region. In modeling it relates to the sensitivity of the solution inside a turbulent layer to the conditions outside. The objective here is to find potential constraints regarding model constants, in order to avoid spurious solutions.

A turbulent front is investigated in an effort to ensure the model is consistent with a well-behaved solution in this region. Cazalbou, Spalart, and Bradshaw (1994) and Cazalbou and Chassaing (2002) discuss the essential physics associated with the presence of a front. In short, a sharp interface between turbulent and non-turbulent fluid is expected so that turbulence statistics should vanish at a finite distance instead of extending into the shear-free region. Additionally they notice that budgets of modeled and real turbulence kinetic energy should reduce to a balance between turbulent diffusion and mean convective transport. The same applies to the modeled second scale equation. A simple model problem to investigate the front region is proposed; the unsteady nonlinear diffusion problem. In one space dimension, particularized to the current model,

$$\frac{\partial U}{\partial t} = -\frac{\partial R_{12}}{\partial y}, \tag{4.44}$$

$$\frac{\partial k}{\partial t} = \frac{\partial}{\partial y}\left(\frac{\nu_T}{\sigma_k}\frac{\partial k}{\partial y}\right), \tag{4.45}$$

$$\frac{\partial \tilde{\omega}^2/2}{\partial t} = \frac{\partial}{\partial y}\left(\frac{\nu_T}{\sigma_{\tilde{\omega}^2}}\frac{\partial \tilde{\omega}^2/2}{\partial y}\right), \tag{4.46}$$

where

$$\nu_T = 2C_\nu r_{22} \frac{\sqrt{k}\, l}{F_\varepsilon}. \tag{4.47}$$

Near the front the length scale and the dissipation of the turbulent kinetic energy, Equations (4.10) and (4.18), become

$$l^2 = \frac{k}{\tilde{\omega}^2}\left[1 + C_{l2}\frac{\partial(\sqrt{k}/\tilde{\omega})}{\partial y}\frac{\partial(\sqrt{k}/\tilde{\omega})}{\partial y}\right], \tag{4.48}$$

$$\varepsilon = F_\varepsilon k \frac{\sqrt{k}}{l}. \tag{4.49}$$

Cazalbou, Spalart, and Bradshaw (1994) find solutions in terms of the distance to the edge,

$$z = ct - y, \tag{4.50}$$

where $c$ is the propagation velocity of the front. Following Paullay *et al.* (1985), the solution near the edge is found in terms of a power expansion in terms of the distance to the edge,

$$U = A_u z^n, \qquad k = A_k z^p, \qquad \tilde{\omega} = A_w z^q, \tag{4.51}$$

where $n$, $p$, $q$, $A_u$, $A_k$, and $A_{\tilde{\omega}}$ should all be positive. The model problem and its solution assume that:

- the turbulence generated in the core of the shear layer spreads with a finite velocity into the non-turbulent fluid — thus displaying a sharp interface at a finite distance;
- the fronts of the mean velocity, turbulence kinetic energy, and the second scale always coincide;
- the budget of each scale equation reduces to a balance between the time rate of change and turbulent diffusion in the vicinity of the front.

Substituting Equations (4.51) into Equation (4.45) (turbulent kinetic energy) gives

$$A_k c p z^{p-1} = \frac{A_k^{5/2}\sqrt{C_{l2}}C_\nu p\sqrt{(p-2q)^2}(-2+\frac{5p}{2}-2q)r_{22}}{A_w^2 F_\varepsilon \sigma_k} z^{(-3+\frac{5p}{2}-2q)}. \tag{4.52}$$

Comparing powers of $z$,

$$q = \tfrac{3}{4}p - 1. \tag{4.53}$$

Comparing coefficients,

$$c = \frac{A_k^{3/2}\sqrt{C_{l2}}C_\nu\sqrt{(p-4)^2}r_{22}p}{2A_w^2F_\varepsilon\sigma_k}. \tag{4.54}$$

Substituting Equations (4.51) into Equation (4.46) (large-scale enstrophy), using Equations (4.53) and (4.54), and comparing coefficients gives $p$,

$$p = \frac{4\sigma_k}{3\sigma_k - 2\sigma_{\tilde{\omega}^2}}. \tag{4.55}$$

Thus

$$2q = \frac{4\sigma_{\tilde{\omega}^2}}{3\sigma_k - 2\sigma_{\tilde{\omega}^2}}. \tag{4.56}$$

For compliance with the current analysis Equations (4.55) and (4.56) require $\sigma_{\tilde{\omega}^2}/\sigma_k > 3/2$.

In order to analyze the $U$-momentum equation, the functional form of $R_{12}$ has to be specified. Assuming $(\partial U/\partial y)\tau$ approaches zero at the front, the current ASBM (Chapter 3) produces the limiting form of $R_{12}$ (following an analysis similar to Haire 2003),

$$R_{12} = -\frac{1}{3a_0}k\frac{\partial U}{\partial y}\frac{k}{\varepsilon}. \tag{4.57}$$

Near the front the dissipation rate, $\varepsilon$, and the time scale, $\tau = k/\varepsilon$, become

$$\varepsilon = \frac{4\sqrt{A_k}A_w^2F_\varepsilon z^{-1+2p}}{\sqrt{C_{l2}}\sqrt{(p-4)^2}}, \tag{4.58}$$

$$\tau = \frac{k}{\varepsilon} = \frac{\sqrt{A_k}\sqrt{C_{l2}}\sqrt{(p-4)^2}z^{1-p}}{4A_w^2F_\varepsilon}. \tag{4.59}$$

Substituting Equations (4.51) into Equation (4.44) (mean momentum), using Equations (4.53) and (4.54), and comparing coefficients gives $n$, the exponent of the velocity expansion,

$$n = \frac{6a_0C_\nu pr_{22}}{\sigma_k}. \tag{4.60}$$

$n$ will be positive for $p > 0$.

The condition to be satisfied in order for $(\partial U/\partial y)\tau \to 0$ can be found by expressing it in terms of the expansions above,

$$\frac{\partial U}{\partial y}\tau = -\frac{\sqrt{A_k}A_u\sqrt{C_{l2}}\sqrt{(p-4)^2}nz^{n-p}}{4A_w^2F_\varepsilon}. \tag{4.61}$$

It will approach zero if $(n-p) > 0$,

$$n - p = p\left(\frac{6a_0C_\nu r_{22} - \sigma_k}{\sigma_k}\right). \tag{4.62}$$

When $(\partial U/\partial y)\tau \to 0$, it follows that $r_{22} \to 1/3$, so the constraint becomes

$$2a_0C_\nu \geq \sigma_k. \tag{4.63}$$

### Compatibility Requirement Summary

Summarizing, the near-edge analysis yields the following constraints, which should be satisfied in order to achieve a well-behaved solution:

- $\sigma_{\tilde{\omega}^2}/\sigma_k < 3/2$ (Equations 4.55, 4.56, and 4.60);
- $2a_0C_\nu \geq \sigma_k$ (Equation 4.63).

The values used in the present work, $a_0 = 1.6$, $C_\nu = 0.25$, and $\sigma_k = 1$ violate the constraint above. As a compromise solution, $a_0$ could itself be made a function of the normalized strain rate. It would be made higher at zero applied strain rate, and then it would taper off towards the optimized value above. For example,

$$a_0 = 1.6 + a_0' \exp(-a_0'' S^2 \tau^2). \tag{4.64}$$

This work is concentrated on wall-bounded flows which do not have free-stream boundaries. It is then futile to optimize the amplitude ($a_0'$) and delay ($a_0''$) of the above modification here. Any optimization should be done with a flow where it matters. For instance, Haire (2003) found that the spreading rates of self-similar free shear flows varied inversely with $a_0$. The optimization is left as a recommendation for future work.

### 4.8.2 The Log Layer

The log layer is investigated in detail to ensure that the model is consistent with observed behavior of the mean flow and the turbulence quantities. In the log layer of a high-Reynolds-number flow, the scale equations become

$$\frac{dk}{dt} = 0 = (-R_{12})\frac{\partial U}{\partial y} - F_\varepsilon k\frac{\sqrt{k}}{l} + \frac{d}{dy}\left(\frac{\alpha_k}{\sigma_k} r_{22}\frac{\sqrt{k}\,l}{F_\varepsilon}\frac{dk}{dy}\right), \tag{4.65}$$

$$\frac{d\tilde{\omega}^2/2}{dt} = 0 = \tilde{\omega}^2 f_{12}^{cc}\frac{\partial U}{\partial y} - C_0\tilde{\omega}^2\frac{\sqrt{k}}{l} + \frac{d}{dy}\left(\frac{\alpha_k}{\sigma_{\tilde{\omega}^2}} r_{22}\frac{\sqrt{k}\,l}{F_\varepsilon}\frac{d\tilde{\omega}^2/2}{dy}\right), \tag{4.66}$$

$$l^2 = \frac{k}{\tilde{\omega}^2}\left[1 + C_{l2}\left(\frac{d\sqrt{k}/\tilde{\omega}}{dy}\right)^2\right], \tag{4.67}$$

where $C_0 = \left[C_{\tilde{\omega}^2 T} - (9 r_{ij} d_{jk}^{cc} f_{ji}^{cc}) C_{\tilde{\omega}^2 P}\right]$ and $\sigma_k = 1$ (Section 4.5.4).

In a high-Reynolds-number log layer

$$\frac{\partial U}{\partial y} = \frac{u_\tau}{\kappa y}, \qquad \frac{-R_{12}}{k} = \frac{u_\tau^2}{k} = 2(-r_{12}) = a_1, \qquad k = \text{constant}. \tag{4.68}$$

where $u_\tau^2$ is the wall shear-stress. $a_1 = 0.3$ is a well-accepted value (showing up as $C_\mu = 0.09$ in most eddy-viscosity models). The Von Kármán constant, $\kappa$, is somewhat more controversial. Traditionally $\kappa = 0.41$ has been used. However there are recent indications that high Reynolds numbers boundary layers may be better represented by smaller values, say $\kappa = 0.38$ (Österlund *et al.* 2000). The normalized turbulence structure is also constant in the log layer. Kim (1992) gives the normalized structure tensors in a channel flow at $Re_\tau = 385$. Even though it is a fairly low Reynolds number, and $k$ varies throughout the layer (as does $R_{12}$), the normalized structure is fairly constant with representative values

$$r_{ij} = \begin{bmatrix} 0.53 & -0.15 & 0 \\ -0.15 & 0.19 & 0 \\ 0 & 0 & 0.28 \end{bmatrix}, \; d_{ij}^{cc} = \begin{bmatrix} 0.19 & -0.07 & 0 \\ -0.07 & 0.35 & 0 \\ 0 & 0 & 0.46 \end{bmatrix}, \; f_{ij}^{cc} = \begin{bmatrix} 0.29 & 0.22 & 0 \\ 0.22 & 0.45 & 0 \\ 0 & 0 & 0.26 \end{bmatrix}, \quad (4.69)$$

and it follows that

$$9 r_{ij} d_{jk}^{cc} f_{ji}^{cc} = 0.65, \qquad 3 r_{ij} d_{ji}^{cc} = 0.90. \quad (4.70)$$

In a high Reynolds number log layer, the Reynolds shear stress is roughly constant, $(-R_{12}) = u_\tau^2$. By virtue of constant turbulent kinetic energy, the transport term in its equation vanishes, resulting in a balance between production and dissipation, $P = \varepsilon$. This implies the following log-law relationships,

$$\varepsilon = F_\varepsilon k \frac{\sqrt{k}}{l} = u_\tau^2 \frac{u_\tau}{\kappa y} = \frac{u_\tau^3}{\kappa y}, \quad (4.71)$$

$$l = \frac{F_\varepsilon k^{3/2}}{u_\tau^3} \kappa y = \frac{F_\varepsilon \kappa}{(-2r_{12})^{3/2}} y = l_0 y. \quad (4.72)$$

Substituting Equation (4.72) into Equation (4.67) and solving for $\tilde{\omega}$,

$$\tilde{\omega} = \frac{1}{y} \sqrt{\frac{k}{2l_0^2}} \left( 1 + \sqrt{1 + 4 C_{l2} l_0^2} \right) = \frac{\tilde{\omega}_0}{y}. \quad (4.73)$$

Now substituting Equations (4.72), (4.73), and (4.68) into Equation (4.66),

$$\frac{\tilde{\omega}_0^2}{y^2} f_{12}^{cc} \frac{u_\tau}{\kappa y} - C_0 \frac{\tilde{\omega}_0^2}{y^2} \frac{\sqrt{k}}{l_0 y} + \frac{\alpha_k}{\sigma_{\tilde{\omega}^2}} \frac{r_{22}\sqrt{k}}{F_\varepsilon} \frac{d}{dy} \left( -l_0 y \frac{\tilde{\omega}_0^2}{y^3} \right) = 0,$$

$$\frac{f_{12}^{cc}}{\kappa} - C_0 \frac{2|r_{12}|}{F_\varepsilon \kappa} + \frac{\alpha_k}{\sigma_{\tilde{\omega}^2}} \frac{r_{22}}{|2r_{12}|^2} 2\kappa = 0,$$

thus

$$\frac{1}{\sigma_{\tilde{\omega}^2}} = \frac{2}{\kappa^2 \alpha_k} \frac{(r_{12})^2}{r_{22}} \left( \frac{C_0}{F_\varepsilon} |2r_{12}| - f_{12}^{cc} \right). \quad (4.74)$$

Enforcing compatibility with the log law constrains the value of $\sigma_{\tilde{\omega}^2}$. Conversely, estimating $\sigma_{\tilde{\omega}^2}$ according to Equation (4.74) dictates the predicted value of $\kappa$ for the model. Note that both $C_\varepsilon$ and $C_{l2}$ are absent from the constraint, indicating that the slope of the log law in *high* Reynolds number flows is independent of them. However, both constants affect the solution in the near-wall region, thus affecting the constant (intercept) in the logarithmic law for the mean velocity.

**Compatibility Requirement**

Using $\kappa = 0.38$ and the structure given by Equations (4.69) and (4.70), with $\alpha_k = 0.25$ ($\sigma_k = 1$), then if $F_\varepsilon = C_\varepsilon(3\overline{\text{fd}})$ as in RLK02 (with corresponding $C_0$), results in $\sigma_{\tilde{\omega}^2} = 1.93$. This violates the edge analysis requirement $\sigma_{\tilde{\omega}^2}/\sigma_k < 3/2$. For compliance with both the log law and the front analysis, $F_\varepsilon$ was modified in the current work (and corresponding $C_0$). Choosing it to be $F_\varepsilon = C_\varepsilon(3\overline{\text{fd}})^{1/6}$, results in

$$\sigma_{\tilde{\omega}^2} = 1.45. \tag{4.75}$$

bringing $\sigma_{\tilde{\omega}^2}$ into compliance with both the log law and the turbulence front constraints.

## 4.9 Summary of the Scale Equations

To set up model scale equations with a firm background, standard Reynolds decomposition (mean and fluctuating parts) was abandoned in favor of a triple decomposition (mean, large-scale fluctuations, and small-scale fluctuations). The latter distinguishes between the large turbulence scales, which are responsible for large-scale mixing and which ultimately set the dissipation rate of the turbulent kinetic energy, and the small (dissipative) scales, which mostly react to the energy sent down to the small scales from the large scales.

The evolution equation for the turbulent kinetic energy is not much different from standard forms used in the literature. The greatest difference is the estimation of the dissipation in terms of the large scale enstrophy of the turbulence. The evolution equation is

$$\frac{\partial k}{\partial t} + \bar{u}_j \frac{\partial k}{\partial x_j} = -R_{ij}\frac{\partial \bar{u}_i}{\partial x_j} - \varepsilon + \frac{\partial}{\partial x_j}\left(\left[\nu\delta_{jk} + \frac{\alpha_k}{\sigma_k} r_{jk}\frac{\sqrt{k}\,l}{F_\varepsilon}\right]\frac{\partial k}{\partial x_k}\right), \tag{4.76}$$

where $\varepsilon$, the dissipation rate of turbulent kinetic energy, is

$$\varepsilon = F_\varepsilon k\frac{\sqrt{k}}{l} + \nu\tilde{\omega}^2, \qquad F_\varepsilon = C_\varepsilon(3\overline{\text{fd}}), \qquad \overline{\text{fd}} = f_{ij}^{cc} d_{ji}^{cc}. \tag{4.77}$$

The large-scale turbulent enstrophy equation is the recent novelty that incorporates a more fundamental basis. It is given by

$$\frac{\partial \tilde{\omega}^2/2}{\partial t} + \bar{u}_j \frac{\partial \tilde{\omega}^2/2}{\partial x_j} = \tilde{\omega}^2 f_{ij}^{cc} \frac{\partial \bar{u}_i}{\partial x_j} - \left[C_{\tilde{\omega}^2 T} - (9\overline{\mathrm{rdf}}) C_{\tilde{\omega}^2 P}\right] \tilde{\omega}^2 \frac{\sqrt{k}}{l} - C_{\tilde{\omega}^2 \nu}\, \nu \frac{\tilde{\omega}^2}{l^2} + \frac{\partial}{\partial x_j}\left(\left[\nu \delta_{jk} + \frac{\alpha_k}{\sigma_{\tilde{\omega}^2}} r_{jk} \frac{\sqrt{k}\, l}{F_\varepsilon}\right] \frac{\partial \tilde{\omega}^2/2}{\partial x_k}\right), \tag{4.78}$$

where $\overline{\mathrm{rdf}} = r_{ij} d_{jk}^{cc} f_{ki}^{cc}$ .

The length scale is evaluated from

$$l^2 = \frac{l_h^2}{1 + C_{l1}} \left[1 + \frac{C_{l1}}{(1 - B_{kk})^2}\right] \left[1 + C_{l2} \frac{\partial l_h}{\partial x_k} \frac{\partial l_h}{\partial x_k}\right], \qquad l_h^2 = \frac{k}{\tilde{\omega}^2}. \tag{4.10}$$

The model constants for the scale equations were optimized as in RLK02, and for matching the channel DNS database of Moser, Kim, and Mansour (1999).

$$\begin{aligned} &C_\varepsilon = 0.3, \quad C_{\tilde{\omega}^2 T}/C_\varepsilon = 2.56, \quad C_{\tilde{\omega}^2 P}/C_\varepsilon = 1.73, \quad C_{\tilde{\omega}^2 \nu} = 5/6, \\ &C_{l1} = 0.1, \quad C_{l2} = 20, \quad \alpha_k = 0.25, \quad \sigma_k = 1, \quad \sigma_{\tilde{\omega}^2} = 1.45. \end{aligned} \tag{4.79}$$

The algebraic equations developed in Chapter 3 respond to the mean deformation normalized with a turbulence time scale, $\tau$, defined as

$$\tau^2 = \left(\frac{k}{\varepsilon}\right)^2 + \left(C_\tau \sqrt{\frac{\nu}{\varepsilon}}\right)^2, \tag{4.8}$$

where $C_\tau = 2.0$ (strictly $\tau$ is needed only for normalizing the mean strain rate in Equation 3.15 — it cancels out in other places where a mean-velocity gradient or a frame rotation-rate appears).

At a solid wall, the scale equations are subjected to the boundary conditions

$$k = 0, \qquad \frac{\partial k}{\partial x_n} = 0, \tag{4.80}$$

where $x_n$ is the direction normal to the wall.

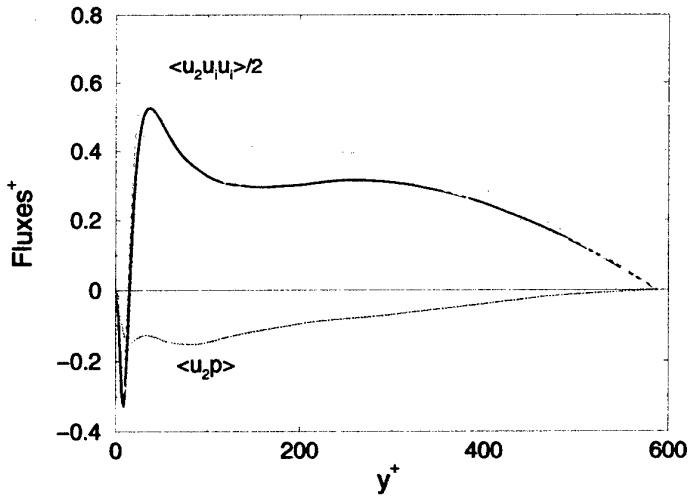


Figure 4.1: Turbulent kinetic energy fluxes in fully-developed channel-flow at $Re_\tau = 590$ (DNS by Moser *et al.* 1999). Dotted line: $(1/\rho)\overline{p'u_2'}$. Dashed line: $\overline{u_2'u_i'u_i'}/2$. Solid line: sum, $(1/\rho)\overline{p'u_2'} + \overline{u_2'u_i'u_i'}/2$. Dot-dashed line: model, $-0.25R_{22}(k/\varepsilon)(dk/dy)$.

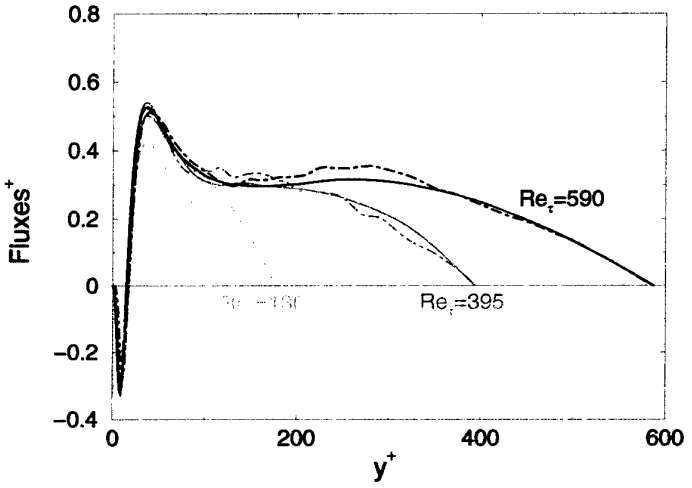


Figure 4.2: Comparison of DNS and modeled turbulent kinetic energy fluxes in fully-developed channel-flow at $Re_\tau = 180$, 395, and 590. Solid line: DNS by Moser *et al.* (1999). Line: model approximation, $\alpha_k/\sigma_k = 0.25$.

# Chapter 5

# Model Results

Chapter 3 explored the response of the algebraic structure equations (uncoupled from the turbulence) to different homogeneous normalized deformation rates. This chapter explores the complete ASBM with emphasis on inhomogeneous flow conditions. The algebraic description of the turbulence stresses and structure, given in Chapter 3, is now combined with the scale equations introduced in Chapter 4 to form a complete set of equations amenable to numerical integration.

Initially the equilibrium response of the full set of model equations to homogeneous shear flow in a rotating frame is analyzed. Pettersson Reif, Durbin, and Ooi (1999) explored this flow using it as a guide to calibrate model constants and to ensure a physically realistic model. The behavior of the ASBM is assessed for the same flow to help further guide the choice of model constants.

Later the ASBM is assessed/optimized in a set of inhomogeneous flows. These correspond to a family of pressure-driven fully-developed channel flows, in presence of distinct directions of frame rotation; spanwise frame rotation aligned with the mean flow rotation, and streamwise frame rotation aligned with the principal flow direction (that of the pressure gradient).

The channel flow may seem deceptively simple. However it is a stringent test to evaluate the model capability to cope with the integration of the complete model equations through the buffer layer to the wall. It is already a challenge to propose a physically acceptable and realizable turbulence model, adequate for high-Reynolds-number flows. Proposing a realizable structure model adequate for integration through wall-affected low-Reynolds-number regions proved to be quite difficult.

Furthermore, the presence of the distinct modes of frame rotation allows the investigation of the model's response to rotation in perhaps the most critical fashion, when all secondary effects are solely due to the turbulence. In more complex flows, other terms representative of the mean motion (convective, Coriolis, body force, and especially pressure gradient terms) can also be active in the momentum equations, sharing some of the job of representing distinct physical phenomena. Then inaccuracies in the turbulence model itself

may be overshadowed due to smaller importance of the Reynolds stress in the momentum equations.

## 5.1 Homogeneous Shear in a Rotating Frame

Homogeneous turbulence subjected to shear in a spanwise-rotating frame continuously evolves in time. Nevertheless there exists an equilibrium limiting state for appropriately normalized variables such as the energy-normalized Reynolds stress and structure-dimensionality tensors, as well as the ratio of the mean to turbulence time scales and the ratio of production to dissipation of the turbulent kinetic energy (see for example Speziale and Mac Giolla Mhuiris 1989).

The turbulence grows or decays depending on the value of the parameter $\eta_f \equiv -2\Omega_3^f/S$, the ratio of frame vorticity to mean flow vorticity. When the mean flow rotation is in the same direction as the frame rotation, $\eta_f < 0$, the turbulence experiences decay whenever the magnitude of $\eta_f$ is larger than some small threshold. In the counter-rotating case, when the mean flow rotation is opposite to the mean flow rotation, the turbulence first experiences more vigorous growth in the range $0 < \eta_f < 1$, and then again it experiences decay when $\eta_f$ grows somewhat larger than 1. This coincides with the behavior of the 2D RDT solution for the same flow given in Chapter 3.

Second-moment closure models display a bifurcation between two stable equilibrium states. The bifurcation corresponds to a change between exponential and algebraic time dependent growth of the turbulence. Pettersson Reif, Durbin, and Ooi (1999) introduced the use of this bifurcation diagram for the improvement of turbulence models, both as a guide to calibrate model constants and to ensure a physically realistic model.

The equilibrium response of the full set of model equations from the ASBM will be investigated now. The mean flow is given by $U_i = \{U(y), 0, 0\}$ in a coordinate system $x_i = \{x, y, z\}$, and the frame rotation rate vector is given by $\Omega_i^f = \{0, 0, \Omega_3^f\}$. In the following the notation $S \equiv dU/dy$ is used often.

As the turbulence is homogeneous, gradients of the Reynolds stresses vanish, and the mean flow remains constant, while the turbulence scales evolve in time. For the scales used

with the ASBM the time evolution equations are

$$\frac{dk}{dt} = -R_{12}\frac{dU}{dy} - \varepsilon, \tag{5.1}$$

$$\frac{d\tilde{\omega}^2/2}{dt} = \tilde{\omega}^2 f_{12}\frac{dU}{dy} - [C_{\tilde{\omega}^2 T} - (9r_{ik}f_{kj}d_{ji})C_{\tilde{\omega}^2 P}]\,\tilde{\omega}^2\frac{\sqrt{k}}{l}, \tag{5.2}$$

where $\varepsilon$ and $l$, respectively the dissipation rate of turbulent kinetic energy and the length scale, are

$$\varepsilon = C_\varepsilon(3f_{ij}d_{ji})k\frac{\sqrt{k}}{l}, \qquad l^2 = \frac{k}{\tilde{\omega}^2}, \tag{5.3}$$

and the model constants are

$$C_\varepsilon = 0.3, \qquad C_{\tilde{\omega}^2 T}/C_\varepsilon = 2.56, \qquad C_{\tilde{\omega}^2 P}/C_\varepsilon = 1.73. \tag{5.4}$$

The time scale used to normalize the mean deformation and provide input to the ASBM is defined as

$$\tau = \frac{k}{\varepsilon}. \tag{5.5}$$

The Reynolds stresses and the turbulence structure are then computed with the algebraic equations summarized in Section 3.11.

Pettersson Reif *et al.* looked at two different measures of model response. A bifurcation of the time scale ratio $\varepsilon/(Sk)$ in $\eta_f$ space, and the behavior of the ratio of production to dissipation of the turbulent kinetic energy. The existence of the bifurcation point depends on a specific model predicting $r_{12} \propto O((Sk/\varepsilon)^{-1})$ as $Sk/\varepsilon \to \infty$. The ASBM however predicts $r_{12} \propto O((Sk/\varepsilon)^{-1/2})$ so it does not predict a bifurcation. This is not necessarily bad, as the bifurcation is really a feature of turbulence models; there is no evidence to what should be the behavior of real turbulence. Thus the most critical parameter should be the ratio of production to dissipation of the turbulent kinetic energy, $P/\varepsilon$, as that dictates if the turbulence is able to sustain itself or not.

The ASBM has this turbulence growth or decay dependence on $\eta_f$ built into it, as the structure parameters were set in Chapter 3 to mimic RDT behavior (when applicable). RDT predicts turbulence growth when $0 \leq \eta_f \leq 1$, and turbulence decay otherwise.

Figure 5.1 shows $P/\varepsilon$ for the complete ASBM model. If $P/\varepsilon > 1$ there is turbulence growth, otherwise if $P/\varepsilon < 1$ the turbulence decays. The ASBM prediction for the threshold between growth and decay, $\eta_f = \{-0.27, 1.96\}$ happens at values slightly further away from

the region $0 < \eta_f < 1$ than suggested by Pettersson Reif *et al.*, who quote the quasi-linear SSG model (Speziale, Sarkar, and Gatski 1991) to have $P/\varepsilon = 1$ at $\eta_f = \{-0.19, 1.08\}$. If the ASBM constants were chosen so as to have $P/\varepsilon = 1$ at $\eta_f$ closer to 1, the slope of the mean velocity for the case ($Re_\tau = 180$, $Ro = 0.77$) would have improved somewhat (see Section 5.4), however the magnitude of the turbulent intensities for all rotating cases would degrade significantly.

## 5.2 Channel Flow Equations

In the sequence the mean-flow and turbulence-evolution equations are particularized for the channel flow in a (possibly) rotating frame. The equations are then integrated and the resulting variables are plotted for a plain fixed frame channel flow, a spanwise-rotating channel flow, and a streamwise-rotating channel flow.

The mean flow is given by $U_i = \{U(y), 0, W(y)\}$ in a coordinate system $x_i = \{x, y, z\}$ where $y$ is the wall normal direction (the sole direction of inhomogeneity), $x$ is the streamwise direction with associated velocity $U$, and $z$ is the spanwise direction with associated velocity $W$. The frame rotation rate vector is given by $\Omega_i^f = \{\Omega_1^f, 0, \Omega_3^f\}$. The wall-normal mean velocity necessarily vanishes by continuity for a fully developed channel flow with zero velocity at the walls.

The mean momentum equation in the streamwise direction ($P^*$ as given by Equation 4.13 encompasses the centripetal acceleration),

$$\frac{dU}{dt} = -\frac{dP^*}{dx} + \nu\frac{d^2U}{dy^2} - \frac{dR_{12}}{dy} = 0,$$

can be integrated from the wall at $y = 0$ to the wall at $y = 2h$, where $h$ is the half channel height, to yield ($R_{12}$ vanishes at both walls),

$$\begin{aligned} -\frac{dP^*}{dx}(2h) &= -\nu\frac{dU}{dy}\bigg|_{y=0} + \nu\frac{dU}{dy}\bigg|_{y=2h} = \frac{\tau_w}{\rho}\bigg|_{y=0} + \frac{\tau_w}{\rho}\bigg|_{y=2h}, \\ &= u_\tau^2|_{y=0} + u_\tau^2|_{y=2h} \equiv 2u_\tau^2, \\ -\frac{dP^*}{dx} &= \frac{u_\tau^2}{h}, \end{aligned}$$

where $\tau_w$ represents a wall shear stress, and the friction velocity, $u_\tau = \sqrt{\tau_w/\rho}$, may be different on different walls, as is the case in the spanwise-rotating channel. In wall coordinates,

$$-\frac{dP^+}{dx^+} = \frac{1}{h^+} = \frac{1}{Re_\tau}, \tag{5.6}$$

where $P^+ = P^*/u_\tau^2$, $x^+ = u_\tau x/\nu$, and $Re_\tau = h^+ = u_\tau h/\nu$.

The complete equations for the mean flow and for the turbulence are

$$\frac{dU}{dt} = 0 = -\frac{dP^*}{dx} + \nu\frac{d^2U}{dy^2} - \frac{dR_{12}}{dy}, \tag{5.7}$$

$$\frac{dW}{dt} = 0 = \nu\frac{d^2W}{dy^2} - \frac{dR_{23}}{dy}, \tag{5.8}$$

$$\frac{dk}{dt} = 0 = -R_{12}\frac{dU}{dy} - R_{23}\frac{dW}{dy} - \varepsilon + \frac{d}{dy}\left(\left[\nu + \frac{\alpha_k}{\sigma_k} r_{22}\frac{\sqrt{k}\,l}{F_\varepsilon}\right]\frac{dk}{dy}\right), \tag{5.9}$$

$$\begin{aligned}\frac{d\tilde{\omega}^2/2}{dt} = 0 = \tilde{\omega}^2\left(f_{12}^{cc}\frac{dU}{dy} + f_{23}^{cc}\frac{dW}{dy}\right) - \left[C_{\tilde{\omega}^2 T} - (9\overline{\mathrm{rdf}})C_{\tilde{\omega}^2 P}\right]\tilde{\omega}^2\frac{\sqrt{k}}{l} - C_{\tilde{\omega}^2\nu}\,\nu\frac{\tilde{\omega}^2}{l^2} \\ + \frac{d}{dy}\left(\left[\nu + \frac{\alpha_k}{\sigma_{\tilde{\omega}^2}} r_{22}\frac{\sqrt{k}\,l}{F_\varepsilon}\right]\frac{d\tilde{\omega}^2/2}{dy}\right),\end{aligned} \tag{5.10}$$

where $\overline{\mathrm{rdf}} = r_{ij} d_{jk}^{cc} f_{ki}^{cc}$, and $\varepsilon$ and $l$, respectively the dissipation rate of turbulent kinetic energy and the length scale, are

$$\varepsilon = C_\varepsilon(3\overline{\mathrm{fd}})k\frac{\sqrt{k}}{l} + \nu\tilde{\omega}^2, \qquad \overline{\mathrm{fd}} = f_{ij}^{cc} d_{ji}^{cc}, \tag{4.77}$$

$$l^2 = \frac{(k/\tilde{\omega}^2)}{1 + C_{l1}}\left[1 + \frac{C_{l1}}{(1 - B_{ii})^2}\right]\left[1 + C_{l2}\left(\frac{d\sqrt{k/\tilde{\omega}^2}}{dy}\right)^2\right], \tag{4.10}$$

and the blockage is given by

$$B_{ij} = \delta_{i2}\delta_{j2}\Phi, \tag{5.11}$$

$$L^2\frac{d^2\Phi}{dy^2} = \Phi. \tag{5.12}$$

The time scale used to normalize the mean deformation and provide input to the ASBM is defined as

$$\tau^2 = \left(\frac{k}{\varepsilon}\right)^2 + \left(C_\tau\sqrt{\frac{\nu}{\varepsilon}}\right)^2, \tag{4.8}$$

with $C_\tau = 2.0$. The Reynolds stresses and the turbulence structure are then computed with the algebraic equations summarized in Section 3.11.

The remaining model constants are posted here again for completeness,

$$\begin{aligned} &C_\varepsilon = 0.3, \quad C_{\tilde{\omega}^2 T} = 2.56, \quad C_{\tilde{\omega}^2 P} = 1.73, \quad C_{\tilde{\omega}^2\nu} = 5/6, \\ &C_{l1} = 0.1, \quad C_{l2} = 20, \quad \alpha_k = 0.25, \quad \sigma_k = 1, \quad \sigma_{\tilde{\omega}^2} = 1.45, \end{aligned} \tag{4.79}$$

and $Lu_\tau/\nu = 23$.

The model equations are subjected to the wall boundary-conditions

$$U = 0, \qquad k = 0, \qquad \frac{\partial k}{\partial y} = 0, \qquad \Phi = 1. \tag{5.13}$$

Combining the scale equations with the algebraic equations for the turbulence structure given in Section 3.11 gives the complete set of equations solved to obtain the results presented in this chapter. The solutions depend on two parameters that completely characterize these fully developed channel flows; the friction Reynolds number, $Re_\tau$,

$$Re_\tau = \frac{u_\tau h}{\nu}. \tag{5.14}$$

and a rotation number, defined differently for the spanwise-rotating cases and for the streamwise-rotating cases.

## 5.3 Fixed Frame Channel Flow

Here $\Omega_1^f = \Omega_3^f \equiv 0$. Figure 5.2 shows mean velocity profiles in wall coordinates (normalized by the wall shear stress and viscosity) for a series of friction Reynolds numbers in a fixed frame channel flow. Comparisons are made with the DNS of Moser, Kim, and Mansour (1999) at $Re_\tau = \{180, 395, 590\}$. Two distinct log laws are also shown. The traditional one given by Coles and Hirst (1969), and the revised one given by Österlund, Johansson, Nagib, and Hites (2000). The ASBM constants $C_\varepsilon$, $C_{l2}$, and $L$ were optimized for matching the DNS at $Re_\tau = \{395, 590\}$ ($C_\varepsilon$ are $C_{l2}$ not really independent — given one there is a single value for the other that optimizes the mean velocity profile). The end result is that the DNS at $Re_\tau = 180$ is somewhat underpredicted while the log law is slightly overpredicted.

Figure 5.3 shows the turbulence intensities for the fixed frame channel at $Re_\tau = 590$. The peak kinetic energy near the wall, which can be inferred from the intensities, is also optimized by the selection of the model constants $C_\varepsilon$, $C_{l2}$, and $L$. The anisotropy predicted in the log region is a testament to the accuracy of the ASBM in this case. As the centerline is approached, a degradation of the results is seen: while the DNS still predicts some anisotropy there, the ASBM predicts isotropy as a result of the zero deformation rate at the centerline. This is a flaw with the equilibrium approach. Near the centerline the diffusion of these quantities becomes important and the local equilibrium assumption embedded in the model no longer applies. In fact the balance in the evolution equations for structure quantities

(*e.g.* Reynolds stresses or structure dimensionalities) near the centerline lies in dissipation and turbulent transport. However this region should not play a major role in the dynamics of the complete flow.

Figure 5.4 shows assorted model variables for the $Re_\tau = 395$ case.

Figure 5.4(a) shows the normalized Reynolds stress tensor, again displaying the proper anisotropy in the log region and near the wall and the lack of anisotropy near the centerline. Notice also that the normalized shear stress $r_{12}$ and the wall-normal Reynolds-stress component $r_{22}$ do behave according to their expected asymptotic behavior, $O(y)$ and $O(y^2)$ respectively.

Figure 5.4(b) shows the structure-dimensionality components for this case. Of note is the $d_{11}^{cc}$ component. It is the smaller component indicating structures preferentially aligned with the $x$-direction. Furthermore it shows a minimum near the wall, where near-wall streaks aligned with the flow direction have come to be expected.

Figure 5.4(c) shows the eddy-axis tensor components. In the log region, in locally homogeneous shear flow, the transverse components $a_{22}$ and $a_{33}$ coincide (as in plain homogeneous shear flow), whereas near the wall $a_{22}$ is forced to vanish by the wall-blocking applied.

Finally Figure 5.4(d) displays the structure parameters used in the model. Note that for the particular case of no frame rotation $\beta$ is modeled as unity throughout the flow region (in this shear flow situation), and that $\phi$ grows large near the wall, indicating that the near-wall streaks are mostly of a jetal nature. Thus enforcing $\phi = 1$ at the wall as required by the asymptotic behavior of the Reynolds stress is consistent with its near-wall behavior without blocking.

## 5.4 Channel Flow with Spanwise Frame Rotation

Here $\Omega_1^f \equiv 0$ and the frame rotation is aligned with the mean flow rotation. The ASBM will be compared against the DNS of Alvelius (1999). This database consists of two friction Reynolds numbers, $Re_\tau = \{180, 360\}$. For $Re_\tau = 360$ there are results for the fixed frame and for a rotation number $Ro = 0.22$. For the lower Reynolds number, $Re_\tau = 180$, results are available for a fixed frame and for several rotation numbers, $Ro = \{0.055, 0.11, 0.22, 0.43, 0.77\}$. First the results for the larger Reynolds number are investigated. Then the smaller $Re_\tau$, and finally skin friction coefficients and mass flow rates

are compared. Here in the spanwise-rotating frame case the rotation number is defined as

$$Ro = \frac{\Omega^f 2h}{U_b}, \tag{5.15}$$

where $\Omega^f$ is the magnitude of the frame rotation rate, $h$ is the half height of the channel and $U_b$ is the bulk velocity in the channel. To match the DNS $\Omega_3^f < 0$ was used.

Figure 5.5 shows mean velocity profiles normalized by the bulk velocity at $Re_\tau = 360$. The fixed-frame result is similar to that reported previously with the database of Moser *et al.* Adding frame rotation, $Ro = 0.22$, the velocity profile becomes asymmetric about the centerline of the channel. In spanwise frame rotation, the Coriolis terms drop out of the mean flow equations making them insensitive to direct effects of frame rotation. The mean flow asymmetry is then a secondary effect due to the effect of the frame rotation on the Reynolds stresses and turbulence structure. The ASBM does capture the asymmetry of the velocity profile.

In Figure 5.6 the ASBM turbulence intensities are compared to the DNS results. Once again the ASBM captures the anisotropy of the Reynolds stresses and its dependence on frame rotation. Notice in particular the fact that the wall-normal intensity, $v'$, outgrows the streamwise intensity $u'$ in the core region of the channel.

Figure 5.7 shows profiles of the structure dimensionality tensor for the rotating case. Comparing with Figure 5.4(b) it is clear that the dimensionality is little affected by the frame rotation. It does display an asymmetry, but this results directly from the asymmetry in the mean velocity gradient. There are no dramatic changes as in the Reynolds stresses.

The lower Reynolds number case, $Re_\tau = 180$, is less enticing for model development because it may still be contaminated by low Reynolds number effects. In particular the wall region is felt across much of the domain. Nevertheless it is rich in different rotation numbers available.

Figure 5.8 displays mean velocity profiles, normalized by the bulk velocity, for several rotation numbers, at $Re_\tau = 180$. The fixed frame result is again similar to that explored previously with the database of Moser *et al.* With increasing frame rotation rate, the velocity profile becomes more asymmetric about the centerline of the channel. The DNS displays a region of the flow with a nearly linear velocity profile, which is not clearly captured by the ASBM. This might be the result of low Reynolds number effects creeping into the model results.

Figures 5.9(a–d) present the turbulence intensities for the higher rotation numbers.

Along with the anisotropy of the stresses it is interesting to observe the increasing separation between the $v'$ and the $u'$ intensities in the core region of the channel.

The structure dimensionality is explored for the same four rotation numbers in Figures 5.10(a–d). It is still remarkably insensitive to the rotation rate, except for the larger rotation rates where $d_{11}^{cc}$ becomes smaller, indicating elongated structures in the streamwise direction, and $d_{33}^{cc}$ becomes increasingly larger, indicating also a growing effect of flattening of most structures in the mean and frame-rotation directions.

Figure 5.11 displays wall friction velocities for all the Reynolds numbers and rotation numbers investigated so far, normalized by the wall friction velocity for the fixed frame case. The stable suction side experiences turbulence decay, as evident in the left hand side of the mean velocity and turbulence intensities profiles shown earlier (see Figures 5.8 and 5.9 for example). The unstable pressure side experiences turbulence growth as evident in the same figures. This is again evident here in the form of lower friction velocities in the stable side and larger friction velocities in the unstable side. The ASBM predicts a more gradual growth of the skin friction asymmetry, compared to the DNS which seems more abrupt.

Figure 5.12 shows the bulk Reynolds number, $Re_b = U_b h/\nu$, where $U_b$ is the bulk velocity. Evidently there is a mass flow increase with the friction Reynolds number. A more subtle effect is the mass flow rate growth with increasing rotation number. For the higher $Re_\tau = 360$, the ASBM seems to capture the DNS trend. For the smaller Reynolds number, the ASBM seems slightly over-sensitive to the rotation number, perhaps due to excessive near wall influence (low Reynolds number effects).

## 5.5 Channel Flow with Streamwise Frame Rotation

Here $\Omega_3^f \equiv 0$ and the frame rotation is aligned with the mean flow direction. The flow and the turbulence respond symmetrically or anti-symmetrically to the direction of the rotation applied (anti-clockwise or clockwise), depending on if the quantities vanish for no frame rotation or not. The ASBM will be compared against the DNS of Oberlack, Cabot, and Rogers (1998). This database consists of a channel flow at a friction Reynolds number $Re_\tau = 180$ at two rotation numbers, $Ro = \{3.2, 10\}$. Here in the case of a streamwise-rotating frame the rotation number is defined as

$$Ro = \frac{\Omega^f 2h}{u_\tau}, \tag{5.16}$$

where $\Omega^f$ is the magnitude of the frame rotation rate, $h$ is the half height of the channel and $u_\tau$ is the friction velocity in the channel. In the DNS $\Omega_1^f > 0$ was explored.

This is a severe test for the ASBM as the model was not optimized for this flow, and furthermore, the rotation is not in the plane of the flow, making this a three-dimensional problem. The model responds to rotation in a way determined by the optimization for the case of spanwise frame rotation. As the flow physics are not the same in the present case, the ASBM will not perform as nicely, as already predicted when analyzing the behavior of the algebraic structure equations to different normalized deformation rates of streamwise frame rotation (see Section 3.12.4). Because the effects of frame rotation are parameterized by a scalar, it cannot distinguish the presence of a different mode of rotation.

Figure 5.13(a) shows the streamwise mean velocity $U$ normalized by the friction velocity for the different rotation numbers. The DNS shows very little sensitivity to the frame rotation. In fact the centerline velocity even decreases for the larger rotation rate. In contrast the ASBM displays a monotonic growth of the centerline velocity with rotation number, indicating the stabilizing effect the rotation has on the model. Smaller turbulent levels imply less friction velocity and therefore higher centerline velocities. The problem is more evident for the higher rotation rate, and is similar to the one found by Oberlack *et al.* exploring differential second moment models.

Figure 5.13(b) shows the spanwise mean velocity $W$ resulting from the frame rotation rate. The presence of the frame rotation excites Reynolds stress components that normally do not exist. These components in turn are responsible for the appearance of the spanwise velocity. Again as in the differential model explored in Oberlack *et al.*, the ASBM underpredicts the DNS results.

Figures 5.14(a) and 5.14(b) show the normal Reynolds stresses for the two different rotation numbers. The stresses from the DNS are hardly affected by the rotation, while a somewhat increased effect can be seen in the ASBM.

Figures 5.14(c) and 5.14(d) show the shear stresses for the same flows. Here the DNS shear stresses $R_{13}$ and $R_{23}$ become quite energized as the rotation number is increased, while the ASBM stresses do not grow at the same rate. Nevertheless it can be seen that the model predicts the correct sign for the shear stresses.

Figures 5.15(a) and 5.15(b) show the structure-dimensionality tensor components for the rotation rates of 3.2 and 10, respectively. Again the dimensionality tensor is relatively insensitive to the frame rotation. Nonetheless a reduction of $d_{11}^{cc}$ is observed, indicating

an elongation of the structures in the streamwise direction. The off-plane dimensionality components $d_{13}^{cc}$ and $d_{23}^{cc}$ have been activated, but they are just barely evident.

## 5.6 Summary and Model Assessment

This chapter explored the complete algebraic structure-based model, consisting of the algebraic equations for the turbulence structure laid down in Chapter 3 were coupled to the scale evolution equations from Chapter 4. The chapter concentrated on the exploration of wall-bounded channel flows, under different imposed modes of frame rotation.

The homogeneous structure based models have proved capable of giving realistic representations for the Reynolds stresses and structure dimensionality tensors for different mean deformations with or without frame rotation (see Chapter 3, and/or previous algebraic structure based models, Reynolds *et al.* 2000 and Haire 2003).

This was the first time the full model was implemented in a wall-bounded flow, integrating all model equations through the viscous sublayer (say $y^+ < 30$). A set of fixed frame channel flows was explored to investigate the model performance when dealing with near wall regions. The results are encouraging as good log laws were achieved, as well as proper anisotropies for the Reynolds stress and dimensionality tensors in the log region. However near the centerline, when the mean deformation vanishes, the model fails to predict any anisotropy, contrary to DNS results. This is a feature common to all algebraic models, reflecting the local nature of their formulation.

Model predictions for the spanwise-rotating frame again did not show any spurious effect of the integration through either viscous sublayer: the stable side can be quite challenging, with its small levels of turbulence activity. The model did display asymmetric mean velocity profiles and proper anisotropy levels, including the cross over of the normal stresses. The qualitative comparison with DNS reflects the adequacy of the choices for the structure parameters made in Chapter 3.

The model's response to increased frame rotation rate in terms of wall skin friction is a little too gradual at first, but then saturates as in the DNS. The mass-flow rate grows a little faster than the DNS. It is not clear however what effect the low Reynolds number of the simulations might have on these results.

Model predictions for the streamwise-rotating frame again show adequate behavior as the viscous sublayer is bridged. This time however the model did display an oversensitivity

to the rate of frame rotation. A stabilizing effect of rotation on the turbulence is observed in the model results, opposite to the rather insensitive character of the DNS results. This fact is blamed in the fact that the model (i) was optimized for the case of spanwise frame rotation, which required a rather large parameter sensitivity to frame rotation, and (ii) the scalar parameterization chosen cannot transmit information about the direction of frame rotation back to the model for obvious reasons. Also surprising is the fact that the secondary flow generated is much weaker than predicted by DNS, perhaps a casualty of the excessive stabilization driven by the frame rotation.

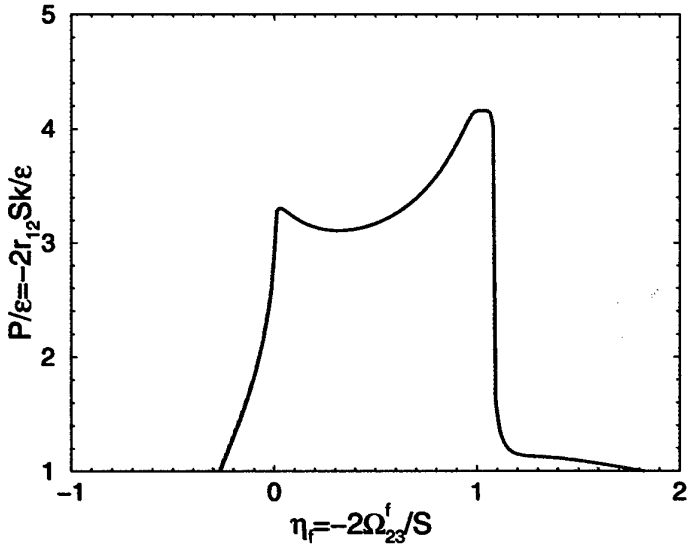


Figure 5.1: Equilibrium ratio of production to dissipation of turbulent kinetic energy for homogeneous shear in a rotating frame

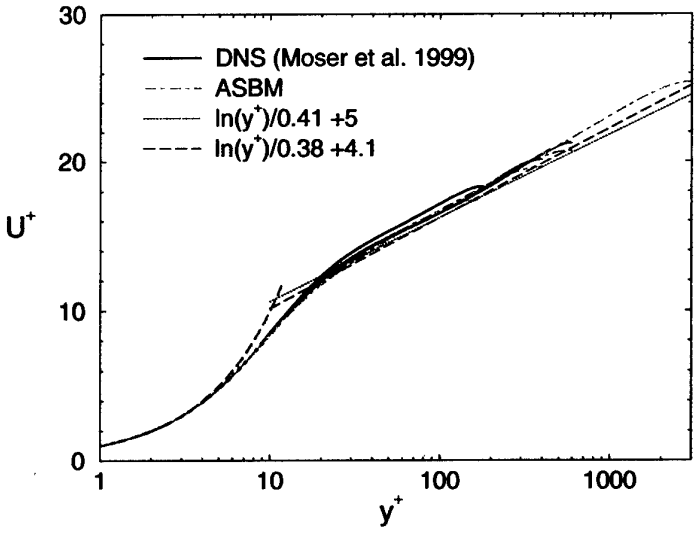


Figure 5.2: Mean velocity for the fixed-frame channel at $Re_\tau = \{180, 395, 590, 3000\}$. Solid lines: DNS. Dotted line: $\log y^+/0.41 + 5$. Dashed line: $y^+$ and $\log y^+/0.38 + 4.1$. Dot-dashed line: ASBM.

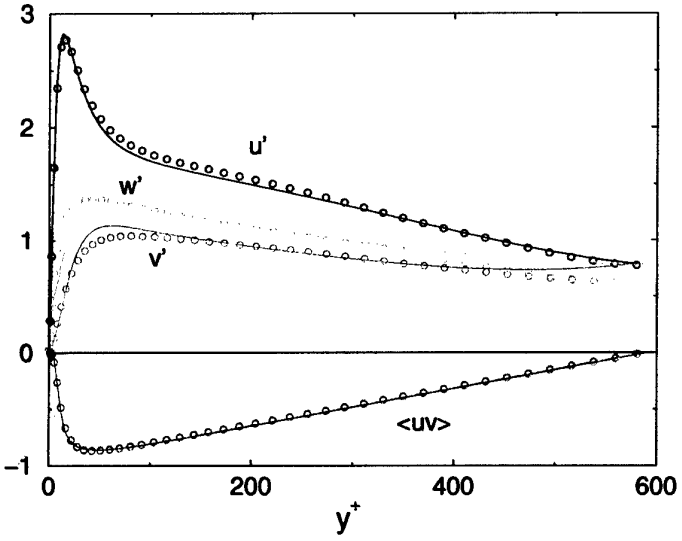


Figure 5.3: Turbulence intensities and shear stress for fixed-frame channel at $Re_\tau = 590$. Symbols: DNS (Moser *et al.* 1999). Solid line: ASBM.

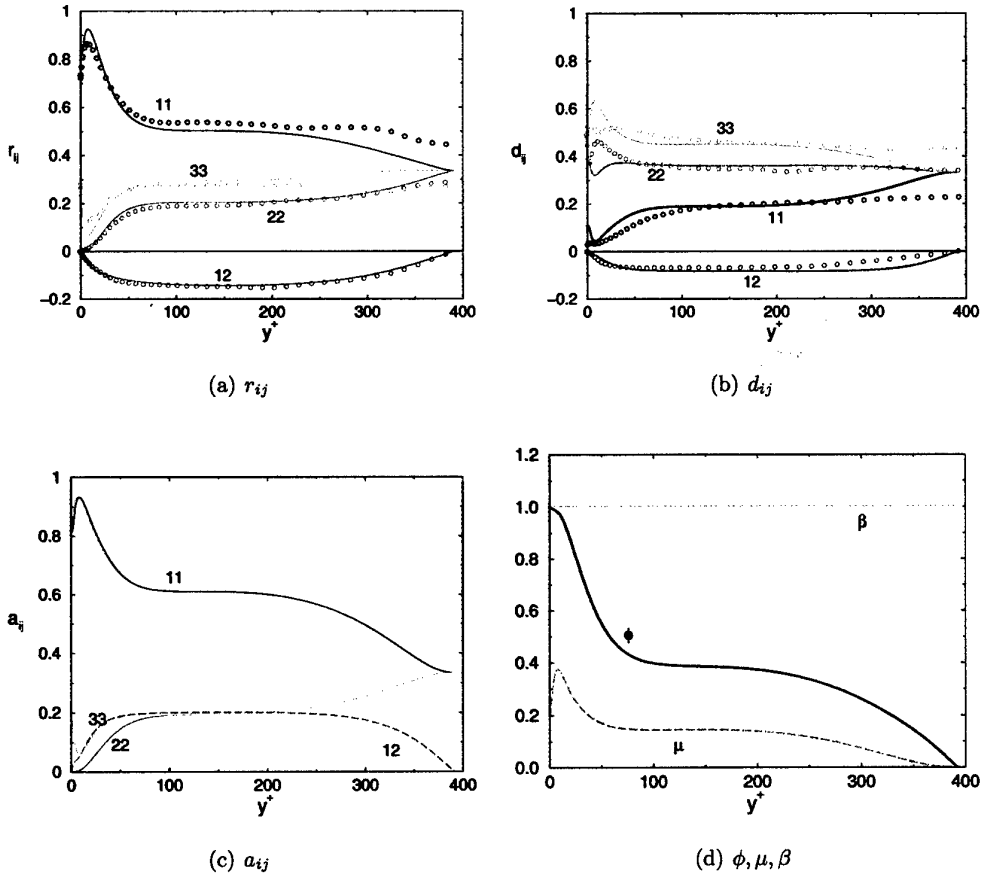


(a) $r_{ij}$ (b) $d_{ij}$

(c) $a_{ij}$ (d) $\phi, \mu, \beta$

Figure 5.4: Turbulence structure and model parameters in fixed-frame channel-flow at $Re_\tau = 385$. Symbols: DNS (Kim 1992). Solid lines: ASBM.

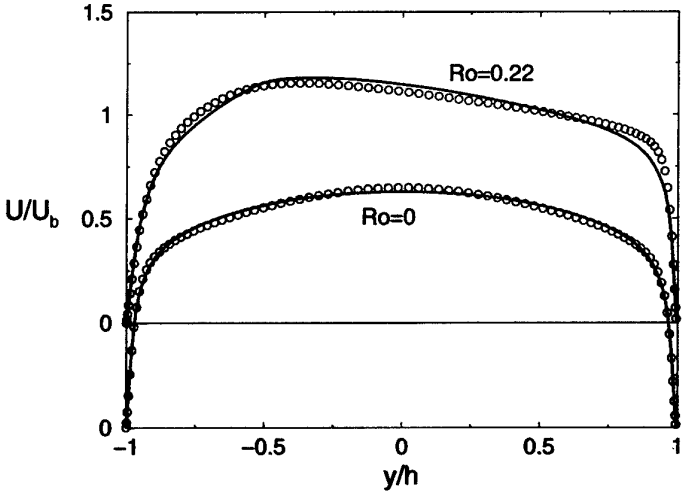


Figure 5.5: Mean-velocity normalized by bulk-velocity for the spanwise-rotating channel at $Re_\tau = 360$ and $Ro = \{0, 0.22\}$. Symbols: DNS (Alvelius 1999). Solid lines: ASBM.

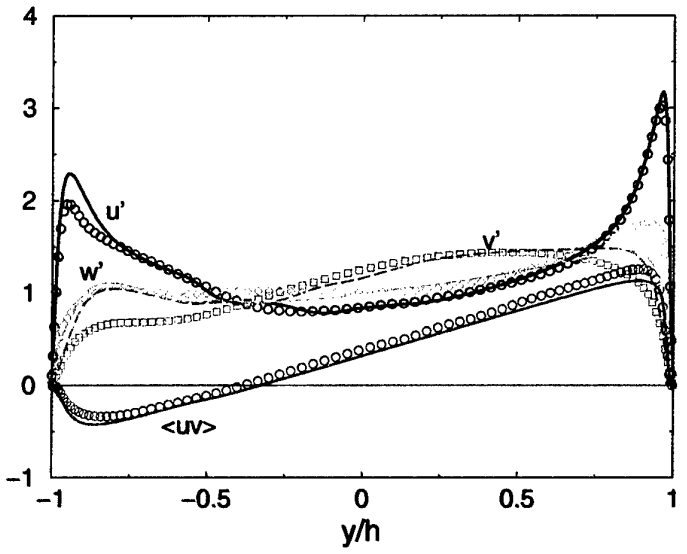


Figure 5.6: Turbulence intensities and shear stress for the spanwise-rotating channel at $Re_\tau = 360$, and $Ro = 0.22$. Symbols: DNS (Alvelius 1999). Solid lines: ASBM.

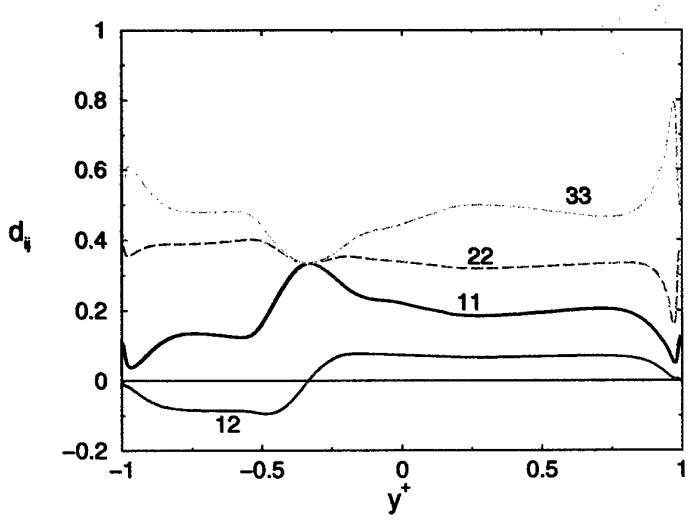


Figure 5.7: Turbulence structure-dimensionality for the spanwise-rotating channel at $Re_\tau = 360$ and $Ro = 0.22$. Solid lines: ASBM.

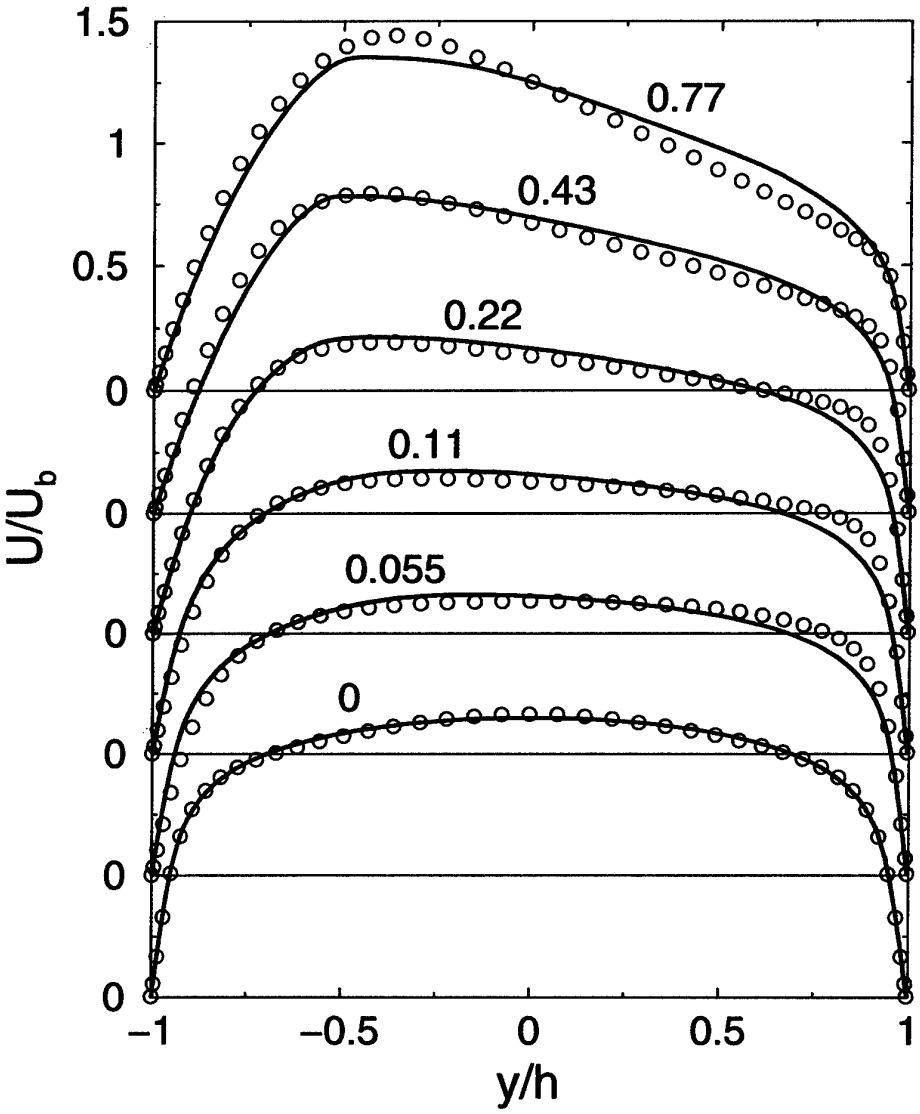


Figure 5.8: Mean-velocity normalized by bulk-velocity for the spanwise-rotating channel at $Re_\tau = 180$ and $Ro = \{0.11, 0.22, 0.43, 0.77\}$. Symbols: DNS (Alvelius 1999). Solid line: ASBM.

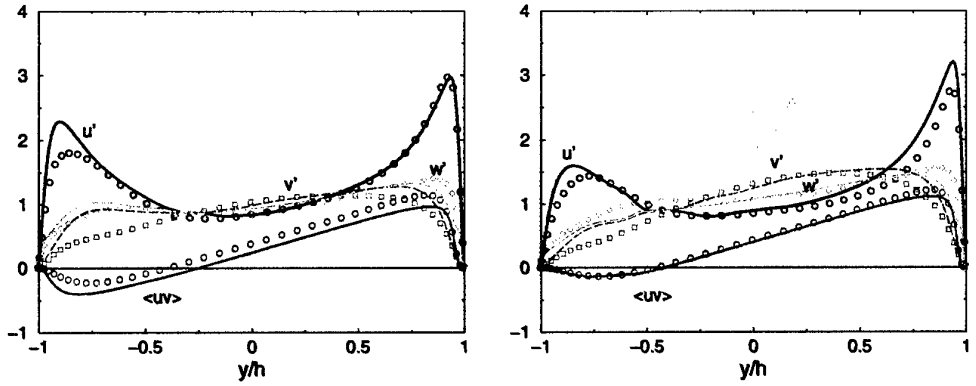


(a) $Ro = 0.11$ (b) $Ro = 0.22$

(c) $Ro = 0.43$ (d) $Ro = 0.77$

Figure 5.9: Turbulence intensities and shear stress for spanwise-rotating channel at $Re_\tau = 180$ and $Ro = \{0.11, 0.22, 0.43, 0.77\}$. Symbols: DNS (Alvelius 1999). Solid lines: ASBM.

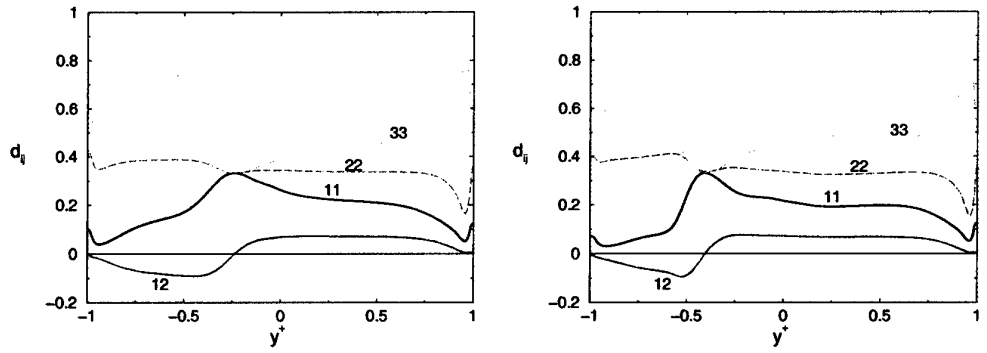


(a) $Ro = 0.11$




(b) $Ro = 0.22$

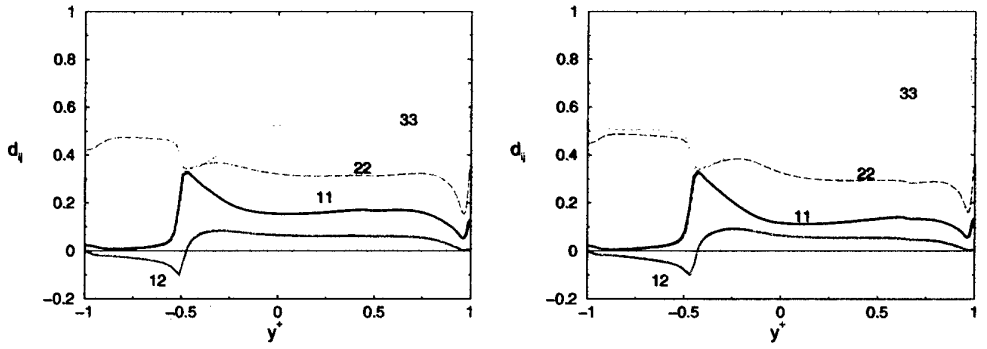


(c) $Ro = 0.43$




(d) $Ro = 0.77$

Figure 5.10: Turbulence structure-dimensionality for the spanwise-rotating channel at $Re_\tau = 180$ and $Ro = \{0.11, 0.22, 0.43, 0.77\}$. Solid lines: ASBM.

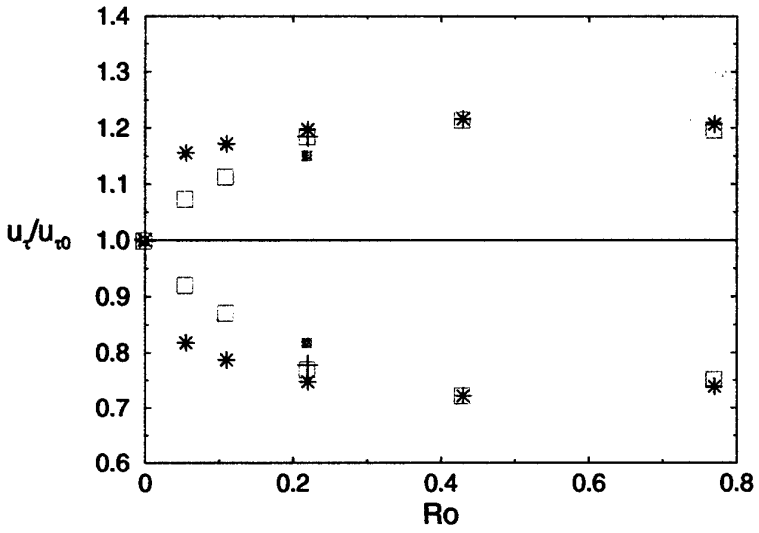


Figure 5.11: Friction velocity vs. rotation number. $*$, $+$: DNS (Alvelius 1999). $\square$, $\blacksquare$: ASBM. Spanwise-rotating channel at $Re_\tau = \{180, 360\}$ respectively.

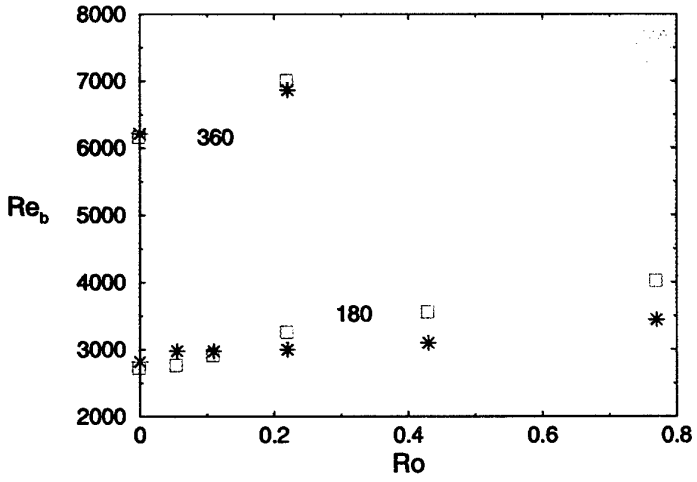


Figure 5.12: Bulk-velocity Reynolds-number vs. rotation number. $*$: DNS (Alvelius 1999). $\square$: ASBM. Spanwise-rotating channel at $Re_\tau = \{180, 360\}$ respectively.

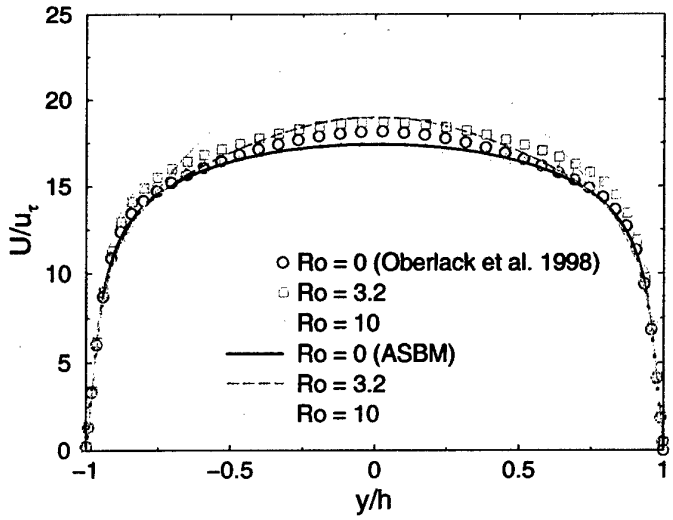


(a) $U^+$

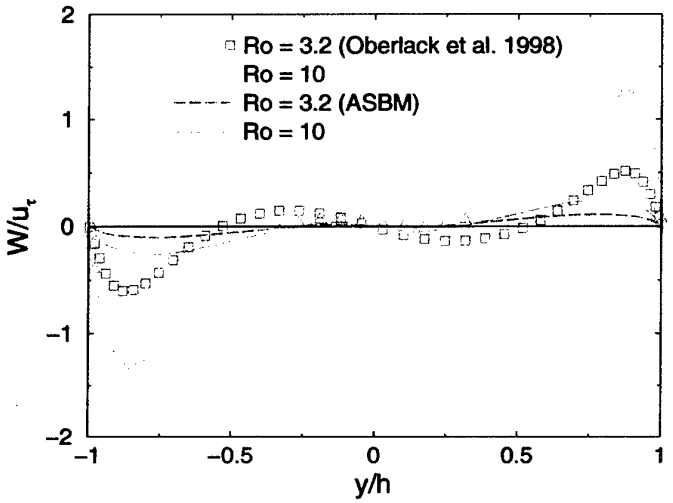


(b) $W^+$

Figure 5.13: Mean streamwise-velocity, $U^+$, and spanwise-velocity, $W^+$, for streamwise-rotating channel at $Re_\tau = 180$ and $Ro = \{3.2, 10\}$. Symbols: DNS (Oberlack *et al.* 1998). Lines: ASBM.

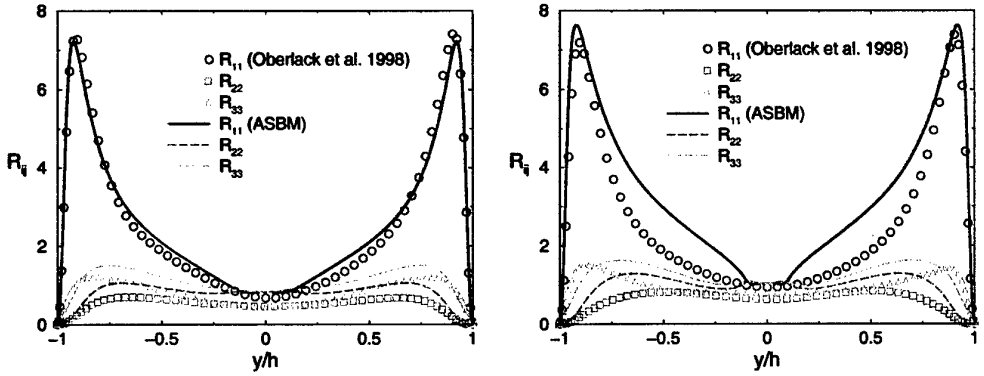


(a) $R_{\alpha\alpha}$, $Ro = 3.2$




(b) $R_{\alpha\alpha}$, $Ro = 10$

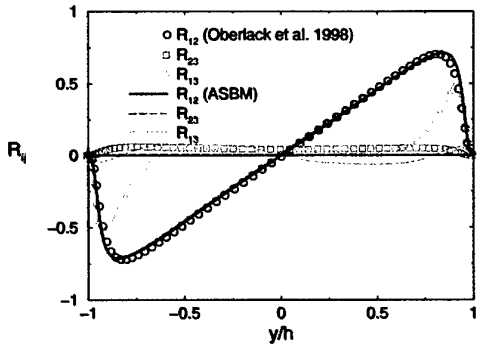


(c) $R_{\alpha\beta}$, $Ro = 3.2$

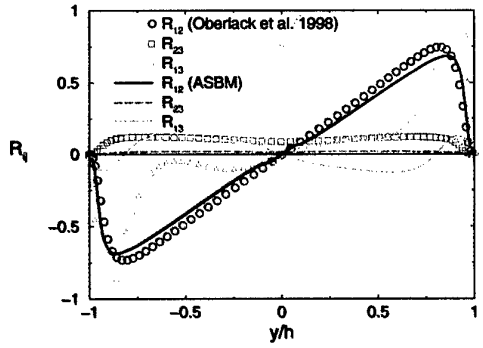


(d) $R_{\alpha\beta}$, $Ro = 10$

Figure 5.14: Reynolds stresses for streamwise-rotating channel at $Re_\tau = 180$ and $Ro = \{3.2, 10\}$. Symbols: DNS (Oberlack *et al.* 1998). Lines: ASBM.

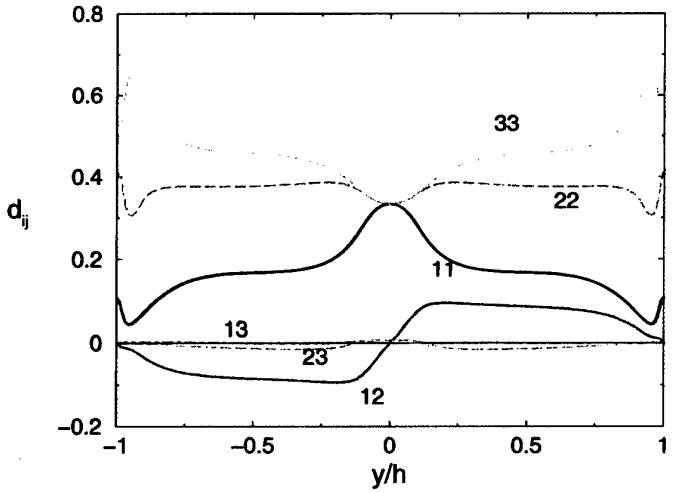


(a) $U^+$

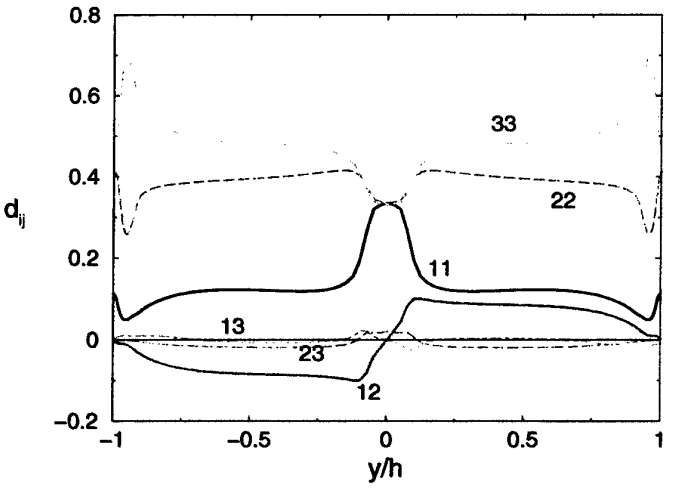


(b) $W^+$

Figure 5.15: Turbulence structure-dimensionality for the streamwise-rotating channel at $Re_\tau = 180$ and $Ro = \{3.2, 10\}$. Lines: ASBM.

# Chapter 6

# Conclusions and Recommendations

## 6.1 Summary and Conclusions

The starting point of this work is the appreciation that there is more than one independent tensor variable describing a turbulence state. For instance, the Reynolds stress tensor and the structure dimensionality tensor carry independent information. With mean and/or frame rotation both are important. Structure information is brought into the proposed turbulent model through the use of hypothetical turbulent eddies, each assigned a set of properties. Averaging over an ensemble of eddies produces eddy statistics, and constitutive relations between these statistics and the Reynolds stress and dimensionality tensors.

The proposed model uses an algebraic approximation for the eddy statistics. This implicitly assumes the existence of an analysis frame where the turbulence is locally in (or near) equilibrium with the mean flow. The farther away from equilibrium, the worse the algebraic approximation will be. The algebraic model produces physically consistent turbulence states for different combinations of normalized mean strain and mean or frame rotation rates, and displays the property of material indifference of 2D turbulence to rotation aligned with its direction of independence. A weakness appears for the case of shear in presence of streamwise frame rotation. Here the principal shear stress is too sensitive to the frame rotation, while the secondary stresses are underpredicted.

The algebraic equations for the turbulence structure are complemented by a set of scale equations for the turbulent kinetic energy and the large-scale enstrophy, originally developed for homogeneous flows by Reynolds, Langer, and Kassinos (2002). Exact terms in the evolution equations represent large scale processes, leaving the modeled equations with a more solid basis than traditional choices, especially for the second scale.

Both the algebraic equations and the scale equations are sensitized to the presence of a wall in a way that preserves proper asymptotic behavior for different quantities in the vicinity of a wall. The essence of the idea is to get the relative magnitude of different quantities properly. For example, in the linear sublayer (say $y^+ < 5$) molecular transport should dominate over turbulent transport.

The complete model — evolution equations for the turbulent scales, and algebraic equations for the energy-normalized turbulence structure — was investigated and optimized for a set of channel flows in fixed and rotating frames of reference. This is the first time a complete algebraic structure based model has been applied to the solution of a wall bounded flow. For fully developed channel flow, using a single set of model coefficients, it was found that:

- the near-wall modifications successfully allowed the integration of the model equations through the viscous sublayer (say $y^+ < 30$) without indication of any spurious effects;
- in the fixed-frame case, the mean velocity and the Reynolds stresses compare favorably with DNS, near the wall and in the logarithmic region;
- the model responded favorably to spanwise frame rotation, displaying an increased asymmetry of the velocity profile with rotation number, similar to the DNS results. The Reynolds stresses are roughly in agreement with the DNS, with particular mention to the crossover of the normal stresses in the unstable side of the channel;
- in a streamwise-rotating frame, the model displayed excessive turbulent stabilization for large rotation numbers while underpredicting the secondary motion resulting from the frame rotation (reminiscent of second moment model results reported along with the DNS results),
- in all flows, when the mean deformation vanishes, the model predicts an isotropic state, in contrast to DNS results, due to the inability of the algebraic model to deal with non-equilibrium situations.

## 6.2 Recommendations for Future Work

This work primarily addressed model development for diverse deformation rates with and without frame rotation, and model development for compliance with near-wall regions. There remain areas that need further exploratory work.

- The algebraic model for the eddy-axis tensor needs to be revisited for compliance with required behavior near the edge of a shear layer (turbulent/non-turbulent interface), as suggested in Equation (4.64) for example.

- The model needs to be assessed in increasingly complex flows, culminating with the evaluation of its performance in rotating machinery configurations.
- Explore some analytical approximation to incorporate non-local effects when the mean deformation vanishes.
- Revisit the algebraic equations to address the excessive turbulence stabilization that develops for shear in streamwise-rotating frame.

When the structure approach is deemed robust and tractable enough for complex engineering flows, a structure-based extension for the energy equation should be pursued. This might for example involve assigning an additional temperature property to the individual eddies, in the same way other eddy properties were assigned in Section 3.3, and then analyzing how averaged eddy properties combine to produce structure-based statistics, useful for the averaged mean flow and energy equations.

# Appendix A

# Flattened Eddy-Axis Model

This appendix details the construction of the structure model, following Reynolds (personal communication).

In the eddy-axis model, a turbulence field is described in terms of an ensemble of hypothetical eddies. Each eddy is described in terms of an eddy-axis unit vector, $\vec{a}$, and an eddy-flattening unit vector, $\vec{b}$, that gives a non-axisymmetric form to the eddy. Given an eddy-axis vector and a flattening direction, the turbulence structure is expressed in terms of moments conditioned on both vectors, and this is used as basis for model statistics. The first step is developing an expression for the conditioned dimensionality tensor. This is then later used in the development of the conditioned Reynolds-stress tensor.

## A.1 Conditioned Dimensionality Tensor

The conditioned dimensionality tensor represents an average over all eddies that share the same direction, with same flattening orientation. It is first written as the most general function of the two vectors, $\vec{a}$ and $\vec{b}$. Appropriate constraints will then determine the free coefficients.

The most general form, given two vectors, is

$$\langle V^2 n_i n_j | \vec{a}, \vec{b} \rangle / \tilde{V}^2 = C_1 \delta_{ij} + C_2 a_i a_j + C_3 b_i b_j + C_4 (a_i b_j + a_j b_i) + C_5 (\epsilon_{ipq} a_p b_q b_j + \epsilon_{jpq} a_p b_q b_i) + C_6 (\epsilon_{ipq} a_p b_q a_j + \epsilon_{jpq} a_p b_q a_i), \tag{3.3}$$

where $\tilde{V}^2 = \langle V^2 | \vec{a}, \vec{b} \rangle$.

The orthogonality between the eddy-axis tensor and the normal vector is expressed by the constraint

$$a_j n_j = 0. \tag{A.8}$$

Multiplying Equation (3.3) by $a_j$ gives relations between constants (recall $a_j a_j = 1$)

$$a_j \langle V^2 n_i n_j | \vec{a}, \vec{b} \rangle / \tilde{V}^2 = 0 = C_1 a_i + C_2 a_i + C_3 (a_n b_n) b_i + C_4 [(a_n b_n) a_i + b_i] + C_5 (a_n b_n) \epsilon_{ipq} a_p b_q + C_6 \epsilon_{ipq} a_p b_q. \tag{A.9}$$

Equating coefficients of like terms gives

$$C_1 + C_2 + (a_n b_n)C_4 = 0, \qquad (a_n b_n)C_3 + C_4 = 0, \qquad (a_n b_n)C_5 + C_6 = 0,$$

or

$$C_6 = -(a_n b_n)C_5, \qquad C_4 = -(a_n b_n)C_3, \qquad C_2 = -C_1 + (a_n b_n)^2 C_3. \tag{A.10}$$

The next constraint is the unit trace (normalization) requirement,

$$\langle V^2 n_i n_i | \vec{a}, \vec{b} \rangle / \tilde{V}^2 = 1 = 3C_1 + C_2 + C_3 + 2C_4(a_n b_n). \tag{A.11}$$

Substituting Equations (A.10) the normalization condition becomes

$$2C_1 + [1 - (a_n b_n)^2]C_3 = 1. \tag{A.12}$$

Defining

$$C_3 \equiv \tilde{\chi}, \qquad C_5 \equiv \tilde{\zeta}, \tag{A.13}$$

the other constants can be represented by

$$C_1 = \tfrac{1}{2}\{1 - \tilde{\chi}[1 - (a_n b_n)^2]\}, \tag{A.14}$$

$$C_2 = -\tfrac{1}{2}\{1 - \tilde{\chi}[1 + (a_n b_n)^2]\}, \tag{A.15}$$

$$C_4 = -(a_n b_n)\tilde{\chi}, \tag{A.16}$$

$$C_6 = -(a_n b_n)\tilde{\zeta}. \tag{A.17}$$

Hence

$$\begin{aligned} \langle V^2 n_i n_j | \vec{a}, \vec{b} \rangle / \tilde{V}^2 = {} & \tfrac{1}{2}\{1 - \tilde{\chi}[1 - (a_n b_n)^2]\}\delta_{ij} - \tfrac{1}{2}\{1 - \tilde{\chi}[1 + (a_n b_n)^2]\}a_i a_j \\ & + \tilde{\chi} b_i b_j - (a_n b_n)\tilde{\chi}(a_i b_j + a_j b_i) \\ & + \tilde{\zeta}(\epsilon_{ipq} a_p b_q b_j + \epsilon_{jpq} a_p b_q b_i) - (a_n b_n)\tilde{\zeta}(\epsilon_{ipq} a_p b_q a_j + \epsilon_{jpq} a_p b_q a_i). \end{aligned} \tag{A.18}$$

The most basic eddy-axis model is an axisymmetric model which does not include any flattening effects, *i.e.* $\tilde{\chi} = \tilde{\zeta} = 0$. It seems only natural to start analyzing flattening by adding one perturbation at a time. That is achieved by allowing a nonzero $\tilde{\chi}$ and taking $\tilde{\zeta} = 0$,

$$\begin{aligned} \langle V^2 n_i n_j | \vec{a}, \vec{b} \rangle / \tilde{V}^2 = {} & \tfrac{1}{2}\{1 - \tilde{\chi}[1 - (a_n b_n)^2]\}\delta_{ij} - \tfrac{1}{2}\{1 - \tilde{\chi}[1 + (a_n b_n)^2]\}a_i a_j \\ & + \tilde{\chi} b_i b_j - (a_n b_n)\tilde{\chi}(a_i b_j + a_j b_i). \end{aligned} \tag{3.4}$$

### A.1.1 Special Cases

If $\tilde{\chi} = 0$ the axisymmetric limit is obtained,

$$\langle V^2 n_i n_j | \vec{a}, \vec{b} \rangle / \tilde{V}^2 = \tfrac{1}{2}(\delta_{ij} - a_i a_j). \tag{A.19}$$

If $a_n b_n = 0$, the eddy-axes are all perpendicular to the vector that organizes the flattening, and

$$\langle V^2 n_i n_j | \vec{a}, \vec{b} \rangle / \tilde{V}^2 = \tfrac{1}{2}(1 - \tilde{\chi})(\delta_{ij} - a_i a_j) + \tilde{\chi} b_i b_j.$$

Furthermore, if $\tilde{\chi} = 1$, the eddies are fully flattened in the direction of the $\vec{b}$ vector,

$$\langle V^2 n_i n_j | \vec{a}, \vec{b} \rangle / \tilde{V}^2 = b_i b_j.$$

## A.2 Conditioned Reynolds-Stress Tensor

Following Kassinos and Reynolds (1994), hereafter referred to as TF-61, the velocity vector is written in an eddy coordinate system, with a component normal to the eddy and a component aligned with the eddy-axis direction,

$$V_i = V(v_m a_m) a_i + V(\epsilon_{rst} v_r n_s a_t) \epsilon_{ipq} a_p n_q. \tag{3.5}$$

Taking the second moment of the velocity gives an expression for the conditioned stresses in terms of the eddy-axis vector and the conditioned dimensionality tensor,

$$\begin{aligned} R_{ij}^{|\vec{a},\vec{b}} = \langle V_i V_j | \vec{a}, \vec{b} \rangle = & \langle (v_m a_m)^2 V^2 a_i a_j | \vec{a}, \vec{b} \rangle \\ & + \langle (v_m a_m)(\epsilon_{rst} v_r n_s a_t) V^2 (\epsilon_{ipq} a_p a_j n_q + \epsilon_{jpq} a_p a_i n_q) | \vec{a}, \vec{b} \rangle \\ & + \langle (\epsilon_{rst} v_r n_s a_t)^2 V^2 \epsilon_{ipq} \epsilon_{jkl} a_p n_q a_k n_l | \vec{a}, \vec{b} \rangle. \end{aligned} \tag{3.6}$$

To simplify Equation (3.6), the identity

$$\epsilon_{rst}\epsilon_{opq} = \delta_{ro}\delta_{sp}\delta_{tq} + \delta_{rp}\delta_{sq}\delta_{to} + \delta_{rq}\delta_{so}\delta_{tp} - \delta_{ro}\delta_{sq}\delta_{tp} - \delta_{rp}\delta_{so}\delta_{tq} - \delta_{rq}\delta_{sp}\delta_{to} \tag{2.11}$$

is used. Then the coefficient of the third term in Equation (3.6) simplifies to

$$\begin{aligned} (\epsilon_{rst} v_r n_s a_t)^2 &= (\epsilon_{rst} v_r n_s a_t)(\epsilon_{opq} v_o n_p a_q), \\ &= 1 - (v_m a_m)^2. \end{aligned} \tag{A.20}$$

Next $\tilde{\phi}$ and $\tilde{\gamma}_s$ are defined as

$$\tilde{\phi} \equiv (v_m a_m)^2, \tag{3.7}$$

$$\tilde{\gamma}_s n_s \equiv (\epsilon_{rst} v_r a_t)(v_m a_m) n_s. \tag{3.8}$$

Finally, part of the third term in Equation (3.6) can be simplified as

$$\epsilon_{ipq}\epsilon_{jkl} a_p n_q a_k n_l = \delta_{ij} - a_i a_j - n_i n_j. \tag{A.21}$$

Substituting Equations (A.20), (3.7), (3.8), and (A.21) into Equation (3.6) gives

$$\begin{aligned} R_{ij}^{|\vec{a},\vec{b}} = & \langle \tilde{\phi} V^2 a_i a_j | \vec{a}, \vec{b} \rangle \\ & + \langle \tilde{\gamma}_s V^2 (\epsilon_{ipq} a_p a_j n_q n_s + \epsilon_{jpq} a_p a_i n_q n_s) | \vec{a}, \vec{b} \rangle \\ & + \langle (1 - \tilde{\phi}) V^2 (\delta_{ij} - a_i a_j - n_i n_j) | \vec{a}, \vec{b} \rangle. \end{aligned} \tag{A.22}$$

Substituting the conditioned dimensionality tensor, Equation (3.4), into Equation (A.22) produces

$$\begin{aligned} R_{ij}^{|\vec{a},\vec{b}} = & \langle V^2 \tilde{\phi} a_i a_j \rangle + \langle V^2 (1 - \tilde{\phi}) [\tfrac{1}{2}(\delta_{ij} - a_i a_j) + \tilde{\chi} \{ \tfrac{1}{2}[1 - (a_n b_n)^2] \delta_{ij} \\ & - \tfrac{1}{2}[1 + (a_n b_n)^2] a_i a_j - b_i b_j + (a_n b_n)(a_i b_j + a_j b_i) \}] \rangle \\ & + \langle V^2 \tilde{\gamma}_s (\epsilon_{ipq} a_p a_j + \epsilon_{jpq} a_p a_i) [\tfrac{1}{2} \{ 1 - \tilde{\chi}[1 - (a_n b_n)^2] \} \delta_{qs} + \tilde{\chi} b_q b_s - \tilde{\chi}(a_n b_n)(a_s b_q)] \rangle. \end{aligned} \tag{3.9}$$

The final step in the modeling process requires taking the ensemble average over all eddies (eddy-axis orientations and flattening directions, $\vec{a}$ and $\vec{b}$). TF-61 introduces the definitions

$$q^2 r_{ij} \equiv \langle V_i V_j \rangle, \qquad q^2 d_{ij}^{cc} \equiv \langle V^2 n_i n_j \rangle, \qquad q^2 a_{ij} \equiv \langle V^2 a_i a_j \rangle, \qquad q^2 b_{ij} \equiv \langle V^2 b_i b_j \rangle, \tag{3.10}$$

$$q^2 \phi \equiv \langle V^2 \tilde{\phi} \rangle, \qquad q^2 \gamma_k \equiv \langle V^2 \tilde{\gamma}_k \rangle, \qquad q^2 \chi \equiv \langle V^2 \tilde{\chi} \rangle, \tag{3.11}$$

respectively the energy-weighted normalized Reynolds stress tensor, eddy-axis tensor, eddy-flattening tensor, and the energy-weighted structure jetal parameter, structure helix vector, and structure flattening parameter.

Higher moments also appear during the averaging of Equation (3.9). Among others, $\langle V^2 \tilde{\phi} a_i a_j \rangle$ and $\langle V^2 \tilde{\gamma}_s \epsilon_{ipq} a_p a_j \tilde{\chi} (a_n b_n)(a_s b_q) \rangle$. These are modeled as if the scalars were independent from the tensorial forms, and with special care to keep some of the traces correct.

In the two examples mentioned the results are

$$\begin{aligned}\langle V^2\tilde{\phi}a_i a_j\rangle &= q^2\phi\, a_{ij},\\ \langle V^2\tilde{\gamma}_s\epsilon_{ipq}a_p a_j\tilde{\chi}(a_n b_n)(a_s b_q)\rangle &= \langle V^2\tilde{\gamma}_s\epsilon_{ipq}a_p a_j\tilde{\chi}(a_s a_n b_n b_q)\rangle,\\ &= q^2\gamma_s\,\epsilon_{ipq}\,a_{pj}\,\chi\,(a_{sn}b_{nq}).\end{aligned}$$

The approximation is exact for some limiting cases. In irrotational flow in a fixed frame of reference, $\phi = \gamma_t = 0$, and both sides are zero. The case of no mean flow deformation is a subset of the one just mentioned. On the other side of the spectrum, in rapidly deformed flows in which the eddy-axis tensor approaches the 1C state the approximations again apply.

With this approximation, and definitions given by Equations (3.10) and (3.11), the ensemble averaged normalized structure tensors become

$$\begin{aligned}d_{ij} =&\tfrac{1}{2}[1-\chi(1-a_{nm}b_{mn})]\delta_{ij} \qquad (3.12)\\ &-\tfrac{1}{2}[1-\chi(1+a_{nm}b_{mn})]a_{ij}+\chi b_{ij}-\chi(a_{in}b_{nj}+a_{jn}b_{ni}),\\ r_{ij} =&(1-\phi)\tfrac{1}{2}(\delta_{ij}-a_{ij})+\phi a_{ij} \qquad (3.13)\\ &+(1-\phi)\chi\,[\tfrac{1}{2}(1-a_{nm}b_{mn})\delta_{ij}-\tfrac{1}{2}(1+a_{nm}b_{mn})a_{ij}-b_{ij}+a_{in}b_{nj}+a_{jn}b_{ni}]\\ &+(-\gamma\Omega_k^T/\Omega^T)(\epsilon_{ipr}a_{pj}+\epsilon_{jpr}a_{pi})\{\tfrac{1}{2}[1-\chi(1-a_{nm}b_{mn})]\delta_{kr}+\chi b_{kr}-\chi a_{kn}b_{nr}\}.\end{aligned}$$

$f_{ij}$ is not an independent quantity. It can be obtained through the relation

$$r_{ij}+d_{ij}+f_{ij}=\delta_{ij}. \qquad (2.19)$$

# Appendix B

# Algebraic Model for the Eddy-Axis Tensor

This appendix details basic thoughts involved in the construction of the model for the eddy-axis tensor, as it appears in Reynolds, Kassinos, Langer, and Haire (2000). Initial attempts at writing down a model for $a_{ij}$ as a single expression in terms of the mean strain and mean rotation always showed the undesirable feature of producing unrealizable eddy-axis tensor states for some combinations of mean strain and mean rotation. To overcome this issue, the computation of the eddy-axis tensor was separated in two parts. First a model that takes into consideration only the mean strain of the flow is proposed. This form is found to produce realizable states. In a second step the eddy-axis tensor is sensitized to rotation through a rotation operation, function of the mean rotation, which preserves the realizability characteristic of the initially strained eddy-axis tensor.

## B.1 Eddy-Axis Tensor Under Pure Strain

The first part of the model deals only with pure strain, using the simple eddy-axis model

$$a_{ij} = \frac{1}{3}\delta_{ij} + \frac{(S^*_{ik}a_{kj} + S^*_{jk}a_{ki} - \frac{2}{3}S^*_{mn}a_{nm}\delta_{ij})\tau}{a_0 + a_1\sqrt{\tau^2 S^*_{kp}S^*_{kq}a_{pq}}}.$$

In the principal coordinates of the anisotropic strain-rate tensor $S^*_{ij} = S_{ij} - S_{kk}\delta_{ij}/3$, where $S_{ij} = \frac{1}{2}(G_{ij} + G_{ji})$, take

$$S^*_{ij} = \frac{1}{2}\begin{pmatrix} \Gamma & 0 & 0 \\ 0 & -\frac{1}{2}(\Gamma+\alpha) & 0 \\ 0 & 0 & -\frac{1}{2}(\Gamma-\alpha) \end{pmatrix}.$$

For $\Gamma > 0$ and $\alpha < 2$, $S^*_{11}$ dominates and in the RDT limit when $\Gamma\tau >> 1$,

$$a_{ij} = \begin{pmatrix} 1 & 0 & 0 \\ 0 & 0 & 0 \\ 0 & 0 & 0 \end{pmatrix} \qquad S^*_{nm}a_{mn} = \Gamma.$$

The component equations are

$$a_{11} = 1 = \frac{1}{3} + \frac{(2\Gamma - \frac{2}{3}\Gamma)\tau}{a_1\Gamma\tau} = \frac{1}{3} + \frac{\frac{4}{3}}{a_1}, \qquad a_{22} = 0 = \frac{1}{3} + \frac{(-\frac{2}{3}\Gamma)\tau}{a_1\Gamma\tau} = \frac{1}{3} - \frac{\frac{2}{3}}{a_1}.$$

Note that these two equations are the same, and both produce $a_1 = 2$. This includes all cases of pure strain except axisymmetric contraction, which for $\Gamma > 0$ corresponds to $\alpha = 2$. For axisymmetric expansion the strain rate can be recasted as

$$S^*_{ij} = \begin{pmatrix} -\Gamma & 0 & 0 \\ 0 & \frac{1}{2}\Gamma & 0 \\ 0 & 0 & \frac{1}{2}\Gamma \end{pmatrix},$$

and then the RDT limit for $\Gamma\tau >> 1$ must be

$$a_{ij} = \begin{pmatrix} 0 & 0 & 0 \\ 0 & \frac{1}{2} & 0 \\ 0 & 0 & \frac{1}{2} \end{pmatrix}, \qquad S^*_{nm}a_{mn} = \tfrac{1}{2}\Gamma.$$

The component equations are

$$a_{11} = 0 = \frac{1}{3} + \frac{(-\frac{1}{3}\Gamma)\tau}{a_1\frac{1}{2}\Gamma\tau} = \frac{1}{3} - \frac{\frac{2}{3}}{a_1}, \qquad a_{22} = \frac{1}{2} = \frac{1}{3} + \frac{(\frac{1}{2}\Gamma - \frac{1}{3}\Gamma)\tau}{a_1\frac{1}{2}\Gamma\tau} = \frac{1}{3} + \frac{\frac{1}{3}}{a_1}.$$

Note that these two equations are the same, and that both produce $a_1 = 2$. The conclusion is that $a_1 = 2$ will produce the correct RDT limit state for all forms of pure strain.

## B.2 Effect of Mean Rotation

Suppose there is a combination of strain and rotation. The eddy-axis tensor is first calculated just considering strain, denoted by $a^s_{ij}$.

$$a^s_{ij} = \frac{1}{3}\delta_{ij} + \frac{(S^*_{ik}a^s_{kj} + S^*_{jk}a^s_{ki} - \frac{2}{3}S^*_{mn}a^s_{nm}\delta_{ij})\tau}{a_0 + 2\sqrt{\tau^2 S^*_{kp}S^*_{kq}a^s_{pq}}}. \tag{3.15}$$

In order to generate a realizable $a_{ij}$ including effects of rotation, a rotation operation is performed on $a^s_{ij}$,

$$a_{ij} = H_{ik}H_{jl}a^s_{kl}. \tag{3.16}$$

where the rotation tensor $H_{ij}$ must satisfy the orthonormal conditions

$$H_{ik}H_{jk} = \delta_{ij}, \qquad H_{ki}H_{kj} = \delta_{ij}.$$

$H_{ij}$ is modeled as a function of the mean rotation-rate tensor $\Omega_{ij}$,

$$H_{ij} = C_1\delta_{ij} + h_1C_2\Omega_{ij} + C_3\Omega_{ik}\Omega_{kj}.$$

The coefficients are determined by the orthonormal condition,

$$H_{ik}H_{jk} = \delta_{ij} = C_1^2\delta_{ij} + 2C_1C_3\Omega_{ij}^2 - C_2^2\Omega_{ij}^2 + C_3^2\Omega_{in}\Omega_{nj}^3,$$

where $\Omega_{ij}^2 = \Omega_{ik}\Omega_{kj}$. Now a Cayley-Hamilton result is needed:

$$\Omega_{12}^3 = \Omega_{12}\Omega_{21}\Omega_{12} + \Omega_{12}\Omega_{23}\Omega_{32} + \Omega_{13}\Omega_{31}\Omega_{12} = -\Omega_{12}(\Omega_{12}^2 + \Omega_{13}^2 + \Omega_{23}^2) = -\frac{1}{2}\Omega^2\Omega_{12},$$

where $\Omega^2 = \Omega_{nk}\Omega_{nk}$. Also,

$$\Omega_{11}^3 = \Omega_{12}\Omega_{23}\Omega_{31} + \Omega_{13}\Omega_{32}\Omega_{21} = 0.$$

Hence the Cayley-Hamilton result is $\Omega_{ij}^3 = -\frac{1}{2}\Omega^2\Omega_{ij}$, and the orthonormality condition gives

$$H_{ik}H_{jk} = \delta_{ij} = C_1^2\delta_{ij} + 2C_1C_3\Omega_{ij}^2 - C_2^2\Omega_{ij}^2 - \tfrac{1}{2}C_3^2\Omega^2\Omega_{ij}^2.$$

Matching the tensors,

$$C_1 = 1, \qquad 2C_1C_3 - C_2^2 - \tfrac{1}{2}C_3^2\Omega^2 = 0,$$

$$C_2 = \pm\sqrt{2C_3 - C_3^2\Omega^2/2}.$$

Letting

$$C_2 = \frac{\alpha}{\Omega}, \qquad C_3 = \frac{\beta}{\Omega^2},$$

then

$$C_2 = \pm\frac{1}{}\Omega\sqrt{2\beta - \tfrac{1}{2}\beta}.$$

The parameter $\beta$ will be set by reference to RDT for combined plane strain and rotation, where

$$S^*_{ij} = \begin{pmatrix} 0 & e & 0 \\ e & 0 & 0 \\ 0 & 0 & 0 \end{pmatrix}, \qquad \Omega_{ij} = \begin{pmatrix} 0 & \omega & 0 \\ -\omega & 0 & 0 \\ 0 & 0 & 0 \end{pmatrix}.$$

The equations for a material line element $L$ in the mean flow are

$$\dot{L}_1 = G_{12}L_2 = (e+\omega)L_2, \qquad \dot{L}_2 = G_{21}L_1 = (e-\omega)L_1.$$

These produce

$$\frac{d}{dt}\left(\frac{L_1}{L_2}\right) = (e+\omega) - \left(\frac{L_1}{L_2}\right)^2 (e-\omega).$$

The fixed point solution gives

$$a_{11} = \frac{L_1^2}{L^2} = \frac{e+\omega}{2e}, \quad a_{22} = \frac{L_1^2}{L^2} = \frac{e-\omega}{2e}, \quad a_{12} = \frac{L_1 L_2}{L^2} = \frac{\sqrt{e^2-\omega^2}}{2e}, \quad \text{for } (e)-\omega \geq 0.$$

For this case

$$\Omega^2 = 2\omega^2, \qquad C_3 = \frac{\beta}{2\omega^2}, \qquad C_2 = \pm\frac{1}{\omega}\sqrt{\beta - \beta^2/4},$$

so the rotation matrix is

$$H_{11} = H_{22} = 1 - \beta/2, \qquad H_{12} = -H_{21} = \pm\sqrt{\beta - \beta^2/4}.$$

Then

$$a_{11} = H_{1k}H_{1l}a^s_{kl} = \tfrac{1}{2} \pm (1-\beta/2)\sqrt{\beta - \beta^2/4},$$

$$a_{22} = \tfrac{1}{2} \mp (1-\beta/2)\sqrt{\beta - \beta^2/4},$$

$$a_{12} = \tfrac{1}{2} - \beta + \beta^2/4.$$

Note that $a_{11} + a_{22} = 1$ for any $\beta$. Let $r = \omega^2/e^2$. Then from the RDT limit solution

$$a_{12} = \tfrac{1}{2}\sqrt{1-r} = \tfrac{1}{2} - \beta + \beta^2/4.$$

Solving for $\beta$,

$$\beta = 2 \pm 2\sqrt{\tfrac{1}{2} + \tfrac{1}{2}\sqrt{1-r}}.$$

The minus sign is taken in order that $\beta = 0$ when $r = 0$ (no rotation),

$$\beta = 2 - 2\sqrt{\tfrac{1}{2} + \tfrac{1}{2}\sqrt{1-r}}.$$

$a_{11} - a_{22}$ gives

$$a_{11} - a_{22} = \pm\sqrt{r} = \pm 2(1 - \beta/2)\sqrt{\beta - \beta^2/4}.$$

Using the $\beta$ solution,

$$1 - \beta/2 = \sqrt{\tfrac{1}{2}[1 + \sqrt{1-r}]},$$

$$\beta - \beta^2/4 = \tfrac{1}{2}[1 - \sqrt{1-r}].$$

Hence

$$a_{11} - a_{22} = \pm\sqrt{r} = \pm 2\sqrt{\tfrac{1}{2}[1 + \sqrt{1-r}]}\sqrt{\tfrac{1}{2}[1 - \sqrt{1-r}]} = \pm\sqrt{r},$$

so the analysis checks. Hence for $r < 1$

$$\beta = 2 - 2\sqrt{\tfrac{1}{2}[1 + \sqrt{1-r}]}, \qquad r \leq 1.$$

The sign ambiguity in $C_2$ is resolved by looking at $a_{11}$

$$a_{11} = \tfrac{1}{2}(1 + r) = \tfrac{1}{2} \pm (1 - \beta/2)\sqrt{\beta - \beta^2/4} = \tfrac{1}{2} \pm \tfrac{1}{2}r,$$

so the $+$ sign is required. The two coefficients are therefore

$$C_2 = \frac{1}{\Omega}\sqrt{2\beta - \beta^2}, \qquad C_3 = \frac{\beta}{\Omega^2}.$$

Now a generalization is made replacing $r$ by

$$r = \frac{a_{pq}\Omega_{qr}S^*_{rp}}{S^*_{kn}S^*_{nm}a_{mk}}.$$

In the RDT limit used above, this definition gives the same value for $r$ used above, $r = \omega^2/e^2$. This definition of $r$ allows the model to be extended to elliptic streamline flows, where

$|\omega| > e$, and to rotations in other planes. It also produces material indifference when the rotation is about an axis of independence. Apparently $r \geq 0$[1].

Consider what happens when $\omega^2 >> e^2$ (elliptic mean streamlines). If $\beta = 2$ is chosen for large $r$, then $H_{11} = H_{22} = 0$, $H_{21} = 1$, and $H_{12} = -1$, which produces $a_{11} = a_{22} = \frac{1}{2}$ and $a_{12} = -\frac{1}{2}$. This says that the dominant (most energetic eddies) are at right angles to the axis of principal strain rate, which at first glance may seem unreasonable. However, the rate of energy input to the eddy varies as $\cos(\omega t)$, where $t = 0$ corresponds to the time at which the eddy axis is aligned with the axis of principal strain rate. Hence

$$\frac{dk}{dt} = A\cos(\omega t) \qquad k = B\sin(\omega t)$$

so it is indeed reasonable that in these strongly elliptic flows the most energetic eddies lag the angle of maximum straining of the eddies by $\pi/2$.

Guided by the discussion above the following generalization is proposed

$$\beta = \begin{cases} 2 - 2\sqrt{\frac{1}{2}(1+\sqrt{1-r})} & \text{if } r \leq 1, \\ 2 - 2\sqrt{\frac{1}{2}(1-\sqrt{1-1/r})} & \text{if } r \geq 1. \end{cases}$$

Using $\alpha = \sqrt{2\beta - \beta^2/2}$,

$$\alpha = \begin{cases} \sqrt{1-\sqrt{1-r}} & \text{if } r \leq 1, \\ \sqrt{1+\sqrt{1-1/r}} & \text{if } r \geq 1. \end{cases}$$

The model described above is used to generate the eddy-axis tensor, $a_{ij}$, *in the frame for which the mean deformation-rate is constant.* The argument for this is that the evolution of the eddy-axis tensor is kinematic, and since the algebraic model is an equilibrium model it should be applied in the frame for which the mean deformation rate is essentially steady. Hence for shear in a rotating frame (turbomachinery) we apply the model above in the frame of the rotor or stator. However, in the Reynolds stress model the parameters are based on the *total* rotation rate (frame rotation rate plus mean rotation rate relative to the frame) because the dynamics of the velocity in a given eddy is determined by the absolute rotation rate.

[1]WCR has found $r > 0$ for all cases. However, during the iteration for the solution $r < 0$ can be encountered. The program uses a smooth continuation of the functions to negative $r$ in order to achieve a convergent iteration, and returns an error flag if the final $r$ is negative

# References


Alvelius, K. (1999). *Studies of Turbulence and its Modelling through Large Eddy- and Direct Numerical Simulation.* Ph. D. thesis, Department of Mechanics, KTH, Stockholm, Sweden.

Bernard, P. S. (1990). Turbulent vorticity transport in three dimensions. *Theor. and Comp. Fluid Dyn. 2*, 165–183.

Blaisdell, G. A. and K. Shariff (1996). Simulation and modeling of the elliptic streamline flow. In *Studying Turbulence Using Numerical Simulation Databases VI. Proceedings of the 1996 Summer Program*, pp. 433–446. NASA Ames/Stanford Center for Turbulence Research.

Cazalbou, J. B. and P. Bradshaw (1993). Turbulent transport in wall-bounded flows. Evaluation of model coefficients using direct numerical simulation. *Phys. Fluids 5*(12), 3233–3239.

Cazalbou, J. B. and P. Chassaing (2002). The structure of the solution obtained with Reynolds-stress-transport models at the free-stream edges of turbulent flows. *Phys. Fluids 14*(2), 597–611.

Cazalbou, J. B., P. R. Spalart, and P. Bradshaw (1994). On the behavior of two-equation models at the edge of a turbulent region. *Phys. Fluids 6*(5), 1797–1804.

Coles, D. E. and E. A. Hirst (1969). Memorandum on data selection. In D. E. Coles and E. A. Hirst (Eds.), *Proceedings of the 1968 AFOSR-IFP-Stanford Conference on Computation of Turbulent Boundary Layers*, Volume II, Stanford, CA, pp. 47–54.

Durbin, P. A. and B. A. Pettersson Reif (2002). The elliptic relaxation method. In B. Launder and N. Sandham (Eds.), *Closure Strategies for Turbulent and Transitional Flows*, pp. 127–152. Cambridge University Press.

Greenspan, H. P. (1968). *The Theory of Rotating Fluids.* Cambridge University Press.

Haire, S. L. (2003). *Toward An Affordable Two-Equation, Structure-Based Turbulence Model.* Ph. D. thesis, Mechanical Engineering Department, Stanford University.

Jeffreys, H. (1931). *Cartesian Tensors.* Cambridge University Press.

Kassinos, S. C. and W. C. Reynolds (1994). A structure-based model for the rapid distortion of homogeneous turbulence. Technical Report TF-61, Mechanical Engineering Department, Stanford University.

Kassinos, S. C., W. C. Reynolds, and M. M. Rogers (2001). One-point turbulence structure tensors. *J. Fluid Mech. 428*, 213–248.

Kim, J. (1992). Turbulence structure database in channel flow at $Re_\tau = 385$. Unpublished.

Mansour, N. N., T.-H. Shih, and W. C. Reynolds (1991). The effects of rotation on initially anisotropic homogeneous flows. *Phys. Fluids 3*(10), 2421–2425.

Moser, R. D., J. Kim, and N. N. Mansour (1999). Direct numerical simulation of turbulent channel flow up to $Re_\tau = 590$. *Phys. Fluids 11*(4), 943–945.

Oberlack, M., W. Cabot, and M. M. Rogers (1998). Group analysis, DNS and modeling of turbulent channel flow with streamwise rotation. In *Studying Turbulence Using Numerical Simulation Databases VII. Proceedings of the 1998 Summer Program*, pp. 221–242. NASA Ames/Stanford Center for Turbulence Research.

Obukhov, A. M. (1941). On the energy distribution in the spectrum of a turbulent flow. *Dokl. Akad. Nauk SSSR 32*, 22–24. As reprinted in C. R. (Dokl.) Acad. Sci. URSS **32**, 19–21 (1963).

Österlund, J. M., A. V. Johansson, H. M. Nagib, and M. H. Hites (2000). A note on the overlap region in turbulent boundary layers. *Phys. Fluids 12*(1), 1–4.

Parneix, S., P. A. Durbin, and M. Behnia (1998). Computation of 3-D turbulent boundary layers using the V2F model. *Flow, Turbulence and Combustion 60*, 19–46.

Paullay, A. J., R. E. Melnik, A. Rubel, S. Rudman, and M. J. Siclari (1985). Similarity solutions for plane and radial jets using a $k$-$\varepsilon$ turbulence model. *J. Fluids Engg. 107*, 79–85.

Pettersson Reif, B. A., P. A. Durbin, and A. Ooi (1999). Modeling rotational effects in eddy-viscosity closures. *Int. J. Heat Fluid Flow 20*, 563–573.

Reynolds, W. C. (1991). Towards a structure-based turbulence model. In T. B. Gatski, S. Sarkar, and C. G. Speziale (Eds.), *Studies in Turbulence*, Lumley 60th birthday Symposium, pp. 76–80. Springer-Verlag, New York.

Reynolds, W. C. and A. K. M. F. Hussain (1972). The mechanics of an organized wave in

turbulent shear flow. Part 3. Theoretical models and comparisons with experiments. *J. Fluid Mech. 54*(2), 263–288.

Reynolds, W. C. and S. C. Kassinos (1995). One-point modelling of rapidly deformed homogeneous turbulence. *Proc. Roy. Soc. London A 451*, 87–104. Osborne Reynolds Centenary Volume.

Reynolds, W. C., S. C. Kassinos, C. A. Langer, and S. L. Haire (2000). New directions in turbulence modeling. Presented at the *Third International Symposium on Turbulence, Heat, and Mass Transfer*. Nagoya, Japan April 3–6.

Reynolds, W. C., C. A. Langer, and S. C. Kassinos (2002). Structure and scales in turbulence modeling. *Phys. Fluids 14*(7), 2485–2492.

Ristorcelli, J. R., J. L. Lumley, and R. Abid (1995). A rapid-pressure covariance representation consistent with the Taylor-Proudman theorem materially frame indifferent in the two-dimensional limit. *J. Fluid Mech. 292*, 111–152.

Robinson, D. F., J. E. Harris, and H. A. Hassan (1995). Unified turbulence closure model for axisymmetric and planar free shear flows. *AIAA J. 33*(12), 2325–2331.

Singh, K. and J. L. Lumley (1971). Extension of Heisenberg's model for spectral transfer to second-order fluids in turbulent flow. *Appl. Sci. Res. 24*(2–3), 187–202.

Speziale, C. G. (1981). Some interesting properties of two-dimensional turbulence. *Phys. Fluids 24*(8), 1425–1427.

Speziale, C. G. and N. Mac Giolla Mhuiris (1989). On the prediction of equilibrium states in homogeneous turbulence. *J. Fluid Mech. 209*, 591–615.

Speziale, C. G., S. Sarkar, and T. B. Gatski (1991). Modelling the pressure-strain correlation of turbulence - an invariant dynamical systems approach. *J. Fluid Mech. 227*, 245–272.

Strang, G. (1993). *Introduction to Linear Algebra*. Wellesley-Cambridge Press.